AD-A106 770 MAX-PLANCK-INST FUER AERONOMIE LINDAU-UEBER-NORTHEIM --ETC F/G 20/14
HIGH ALTITUDE ATMOSPHERIC INVESTIGATIONS. PART II. DEVELOPMENT --ETC(U)
JUN 81 H WIDDEL DA-ERO-76-G-076

UNCLASSIFIED NL

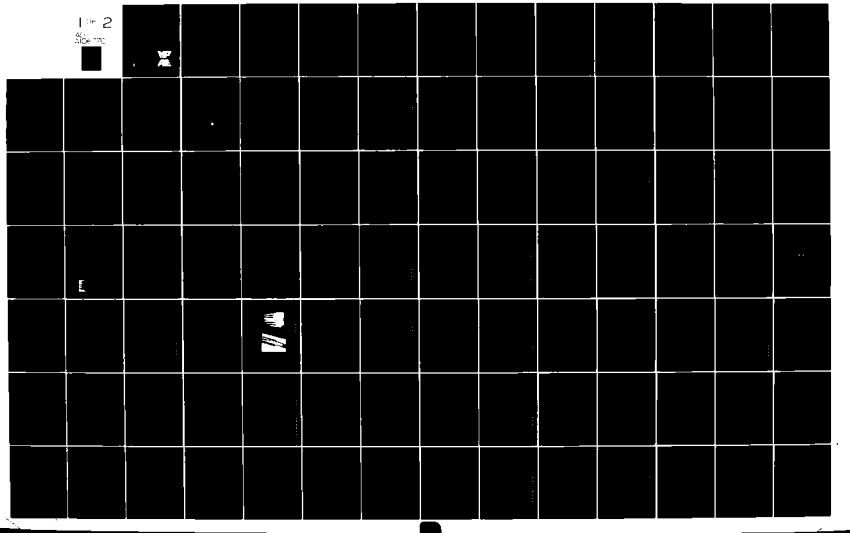

LEVEL II

(4)

AD A106770

MAX-PLANCK-INSTITUT FÜR AERONOMIE

MPAE

DEVELOPMENT OF IN-SITU EXPERIMENTS FOR MEASUREMENTS IN THE D-REGION OF THE IONOSPHERE AND THEIR RESULTS

BY

HANS-ULRICH WIDDEL
MAX-PLANCK-INSTITUT FÜR AERONOMIE
D-3411 KATLENBURG-LINDAU 3
FEDERAL REPUBLIC OF GERMANY

UNCLASSIFIED

SECURITY CLASSIFICATION OF THIS PAGE (When Data Entered)

R&D 2246-EN

REPORT DOCUMENTATION PAGE	READ INSTRUCTIONS BEFORE COMPLETING FORM
1. REPORT NUMBER	2. GOVT ACCESSION NO. AD-A106 770 (1)	3. RECIPIENT'S CATALOG NUMBER
4. TITLE (and Subtitle) High Altitude Atmospheric Investigations. Part II, Development of In-Situ Experiments for Measurements in the D-Region of the Ionosphere and their Results.	5. TYPE OF REPORT & PERIOD COVERED Final Report, Part II 1 Aug 75 — 1 Aug 80
	6. PERFORMING ORG. REPORT NUMBER
7. AUTHOR(s) Hans-Ulrich Widdel (12)	8. CONTRACT OR GRANT NUMBER(s) DAER075-G-076
9. PERFORMING ORGANIZATION NAME AND ADDRESS Max Planck Institut für Aeronomie D-3411 Katlenburg-Lindau 3 West Germany (14)	10. PROGRAM ELEMENT, PROJECT, TASK AREA & WORK UNIT NUMBERS 61102A (11) 1T161102BH57 01
11. CONTROLLING OFFICE NAME AND ADDRESS USARDSG-UK Box 65, FPO NY 09510 (11)	12. REPORT DATE 3 Jun 81 (12) 112
	13. NUMBER OF PAGES 111
14. MONITORING AGENCY NAME & ADDRESS (If different from Controlling Office)	15. SECURITY CLASS. (of this report) Unclassified
	15a. DECLASSIFICATION/DOWNGRADING SCHEDULE

16. DISTRIBUTION STATEMENT (of this Report)

Approved for Public Release - Distribution Unlimited

17. DISTRIBUTION STATEMENT (of the abstract entered in Block 20, If different from Report)

18. SUPPLEMENTARY NOTES

19. KEY WORDS (Continue on reverse side if necessary and identify by block number)

Absorption, Radio Wave, A3 Method, South-West-Europe Diurnal Variations, Seasonal Variations, Absolute Measurement, Winter Anomaly, in-situ experiments, wind measurements, foil cloud experiment, guardring probe, electron density distribution, small sounding rockets.

20. ABSTRACT (Continue on reverse side if necessary and identify by block number)

Results of A3 absorption. Radio absorption measured from the ground is determined by the integral over the electron density weighted with the collision frequency of the electrons with the ambient neutral gas. The boundaries of the relevant conditions are difficult to establish. Absorption is also affected by properties of the ionosphere, and these properties change with seasons, sun position, and other factors. These multiple effectors make unambiguous interpretation impossible. The report describes →

DD FORM 1 JAN 73 1473 EDITION OF 1 NOV 65 IS OBSOLETE

UNCLASSIFIED

SECURITY CLASSIFICATION OF THIS PAGE (When Data Entered)

20. Cont./

attempts to select and describe parameters that might most strongly influence radio wave absorption. Technical details of in-situ experiments to measure wind and electron density are communicated and some results obtained with these instruments are presented. It was found that the ratio between the positive ion current and the electron current measured with the guardring probe experiment is affected by both, the ion composition in the ion sheath and by neutral air temperature. This might explain the ambiguities found when a direct comparison of results obtained with "Langmuir" probes and wave propagation experiments is attempted. The effect might be used to derive local air temperatures provided that the ion composition of the ion sheath is known and that a quantitative theoretical description can be established.

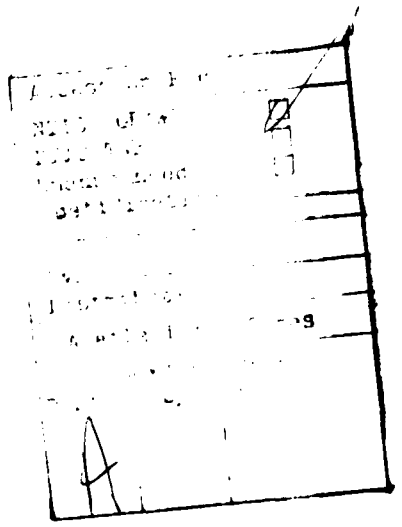

C O N T E N T

INTRODUCTION

The first part of this final report (1) has shown that ground-based measurements of radio wave absorption can be used to monitor certain changes of the state of the D-region of the ionosphere provided that the measurements are executed with care. The advantage of absorption measurements is their relative simplicity. The accuracy of measurement can well exceed 1 dB when reliable equipment is available which is frequently calibrated.

The interpretation of the results in terms of atmospheric physics turns out to be extremely difficult. This is mainly caused by the fact that the radio wave absorption measured from the ground is determined by the integral over the electron density weighted with the collision frequency of the electrons with the ambient neutral gas. The boundaries of this integral are not a priori known in any specific cases. The amount of radio wave absorption is further affected by the properties of the ionospheric reflector of the wave which turns back the probing wave to ground. These properties change with season and with the diurnal variation of the sun's zenith angle. Therefore, any attempt to relate the change of radio wave absorption to changes of electron density or electron collision frequency at certain heights remains ambiguous unless the interpretation to supported by measurements of other kind than radio wave absorption.

The selection of parameters which might affect most strongly radio wave absorption is a difficult task. As the results of ground-based absorption measurements seem to suggest that meteorological events strongly affect the morphology of radio wave absorption especially during winter a measurement of meteorological parameters like winds, temperature, pressure and density seems to be a good choice for a first approach. Because temperature influences strongly the composition of minor constituents, its measurement appears to be most important. But, unfortunately, no simple and reliable means to measure temperature in the height region of interest has been developed yet, and it seems doubtful if a simple method of measurement can ever be found.

Besides of the necessity to measure simultaneously a larger number of different parameters other than meteorological ones like electron density, number density of minor constituents and their composition , the meteorological hypothesis has some unpleasant consequences for the practical execution of measurements: Meteorological events contain a considerable amount of unpredictability which is caused by lack of knowledge of all parameters which influence the development of effects observed locally. Measurements of the kind described and suggested here must remain local measurements for just plain practical reasons: Most of the parameters mentioned here can be measured reliably in situ only. This calls for the use of measurement devices carried by sounding rockets. The locations on which sounding rockets can be launched are, for obvious reasons, limited in number and of geographical distribution. This means that even a world-wide effort would supply only a fairly wide grid of observations. Fortunately, the results of ground-based work (the most recent one see (2)) show that the widely-meshed grid seems not to be a serious handicap because, for example, winter ancmaly extends over fairly large areas simultaneously. These areas seem to be larger than tropospheric meteorological events cover. The relatively small number of places from which sounding rockets can be launched seems therefore not to be a very serious handicap for in-situ investigations.

Forecast of radio wave absorption

The inherent unpredictability of the amount of radio wave absorptions however may cause quite some discomfort if a measurement campaign is aimed for a special event. This may be illustrated by the results of an analysis performed for planning our own campaigns and that of the Western European Winter anomaly campaign 1975/76 (3). (The results of the Western European Winter anomaly campaign were published in special issues of (4) and (5)).

The methods applied in this analysis (3) and (6) were quite straightforward. Using data collected in Southern Spain between 1967 and 1975, it was at first investigated if the amount of absorption (mean noon value and parameter L_D) could be forecasted with some accuracy for the following

day by using data of the key day or days before key day. The answer was that no relation exists which allows to forecast the absorption conditions following the key day with any degree of accuracy.

On the other hand, the fairly long observation period on which the analysis was based allowed to specify the month in which the probability to find winter anomaly is highest (100 %) and, further, to forecast within an accuracy of about 3 days the date on which the first group of winter-anomaly days started. Also the length of the winter-anomaly period was correctly predicted. Such forecasts are, however, only possible when data from a longer period of continuous measurements are available. Further it turned out that the amount of near-noon and afternoon radio wave absorption can be forecasted with rather high accuracy from data collected during morning and forenoon hours of the same day. These results of long and short term forcecasts were used to advantage during the Western European Winter Anomaly Campaign 1975/76 to decide if and when to launch the rocket "salvoes" described in (4) and (5).

The failure of the attempt to forecast absorption conditions from trend data of absorption found on the preceding day means that important changes in the D-region of the ionosphere take place over night and that dynamic processes which change composition and/or number density of certain minor constituents play an important role for the development of excessive radio wave absorption during winter which is called winter-anomaly.

Required number of measurements

The great variability of conditions found in the D-region which is indicated by the large day-to-day variation of absorption, and, especially during winter, by its regular and irregular diurnal variations clearly disproves the concept that a limited number of in-situ measurements would be sufficient to obtain a reasonably clear set of data which would allow to establish a model of what causes the winter-anomaly absorption. A fairly large number of individual experiments turns out to be necessary instead. Constraints of financial resources, however, then call for the use of simple and inexpensive experiments and payloads. A reduction of costs can also be achieved by using small rockets which are relatively inexpensive and do not need elaborate ground handling equipment and crew.

A program based on this concept was executed during the past years by the Max-Planck-Institut für Aeronomie. An European launch facility for small sounding rockets (El Arenosillo, South West Spain) was used. Radio wave absorption and ionosonde measurements were performed continuously at and (on a second circuit) near the launching site. These data supplied the base of judgement for planning campaigns and for the criteria to launch the rockets.

This report describes technical details of payloads which were developed and their results.

NUMBER OF EXPERIMENTS REQUIRED TO ACHIEVE AT A SIGNIFICANT RESULT, AND CHOICE OF VEHICLES:

It may become clear from the introduction that a successful approach to resolve even simple relations between physical parameters of the atmosphere at D-region heights of the ionosphere requires a fairly large number of individual measurements until the result may be considered significant. For obvious reasons, not too much attention seem to have paid to this - admittedly - uncomfortable aspect of atmospheric research when in-situ experiments carried out by rockets were involved. To the knowledge of the author, the first attempt to take this aspect under consideration was published in (7) and (8). In these papers, the relation between change of absorption and changes of wind (wind speed and wind direction) and air density of the neutral atmosphere was investigated.

If it is possible to estimate from a model the correlation coefficient between two parameters, a figure for the minimum number of experiments can be derived by considering the significance. This number of individual experiments might yield a significant result. This heuristic approach yields however only an estimate about the minimum effort which is necessary to achieve at a significant result. A certain proof of its validity was a result obtained during the Western European Winter Anomaly Campaign 1975/76. 15 wind finding experiments were launched then. The results were correlated with changes of absorption (this was a repetition of experiments performed earlier (7), (8), (9), (10), and in turned out (as was expected) that the number of launched were slightly too small to obtain a better significance than 90% for the correlation coefficients. The correlation coefficients obtained during this

campaign were of same order found during earlier experiments. The significance w (n,r) (the probability that r is not caused just by accident) can be calculated for a given correlation coefficient by the following formulas:
(n: number of experiments)

$$w(n,r) = \frac{2}{\pi}\left[\arcsin r + r\sqrt{1-r^2}\left(1 + \frac{2}{3}r^2 + \frac{2\cdot 4}{3\cdot 5}r^4 + \ldots + \frac{2\cdot 4\cdot 6\cdots(n-3)}{3\cdot 5\cdot 7\cdots(n-2)}r^{n-3}\right)\right] \quad (1)$$

$$w(n,r) = \left[1 - \frac{1}{2}\left(1 + r^2 + \frac{1\cdot 3}{2\cdot 4}r^4 + \ldots + \frac{1\cdot 3\cdot 5\cdots(n-3)}{2\cdot 4\cdot 6\cdots(n-2)}r^{n-3}\right)\right] \quad (2)$$

Because the expected correlation coefficients for the relation between wind and absorption are not very high, a fairly large number of individual experiments n may be required. This calls for simple payloads and for small rockets, preferably for those used for meteorological experiments. When our first project was in the planning stage, the choice of suitable rockets was rather limited but an apogee of 90-95 km (preferably 100 km) was desired. Even today rather few meteorological rockets can meet this requirement. One of these rockets is the "Super Loki Dart" vehicle. The payload capacity of this rocket is however rather limited and it was not sufficiently large to carry the instrument package intended to be developed. (This situation is by far much better now because of advances in the design of electronic components.) It was therefore decided to improve an European rocket system (SKUA) which has been used successfully by the British Meteorological Office and to develop it into a vehicle which can carry 7.5 kg up to a height of 90-95 km (SKUA II and further developments).

After some minor teething troubles, the vehicle turned out to be very reliable and a success rate of the experiment (payload and rocket) of over 95 % was achieved. The rocket has a diameter of 13 cm. This diameter offers enough space to accomodate a number of experiments to be flown on the same payload. Most of the results communicated here were obtained with this kind of vehicle.

The foil cloud experiment

The shape of diurnal variation of absorption, the quasi-irregularity of occurrence of winter-anomalous absorption and their tendency of reoccurrence and persistence described in part I of this report suggests that meteorological phenomena play an important role for the morphology of winter anomaly. If meteorological events do affect winter anomaly absorption, one should expect a correlation between wind and absorption. The wind profile however has to be measured with a good resolution of height because one can expect that more than one height level becomes affected. Until recently, ground-based methods could not supply data with the required resolution of height. The obvious way-out is to use a target which is deployed at apogee of a rocket trajectory and is tracked by radar from the ground on its descend. This concept has the advantage that this experiment is independent of weather conditions and can therefore be used at any time which permits a launch of a rocket. This is not the case for an alternative in which a luminous trail is ejected from the rocket during ascent which can be observed from the ground. This method is confined more or less to twilight or night conditions and requires clear sky over the optical observation sites which have to be at least some 40 km apart in order to yield useful resolution.

The principal disadvantage of these kinds of in-situ measurements lies in its sampling nature. The time of measurement extends only over a few minutes. This means that local measurements are made and no conclusions can be drawn about the magnitude of tides etc. unless a close sequence of launches is performed. This, however, turns out to be rather costly. Nevertheless, if all launches in a series are performed at the same local time and if a separation between prevailing winds and tidal winds is not necessary a series of local measurement retains its value.

Besides measuring wind, falling targets can be used also to determine other important meteorological parameters of the atmosphere.

Measurement of air density and air temperature with falling bodies

Provided the aerodynamic flow around the body is known, atmospheric density and temperature can be derived from the descend velocity of the body. This is used extensively in the "falling sphere"-experiment of which several versions became known. The movement of the body is described by the equation:

$$(3) \qquad m \cdot \dot{v} = -mg - C_D \cdot A \cdot \frac{\rho}{2} v^2$$

m denotes the mass of the body, v the velocity, $\dot{v}$ the acceleration, g the gravitational acceleration, g the ambient density, A the cross section area of the body exposed to the air-flow and C_D the drag coefficient. C_D can be considered as being constant only when certain flow conditions are present. Otherwise it is a more or less complicated function of Reynolds number, of Mach-number and of Knudsen number λ/L = kn. (ratio between mean free path length of a molecule and the characteristic length of the body)

Provided the variations of air density with height, ρ (h), is known between h = z and h = z_o, one obtains the temperature profile by integrating the hydrostatic equation when temperature and density at height 70 is known either by direct independent measurements, from reference atmospheres or by estimates.

$$T = \frac{m}{\rho k} \int_{z}^{z_o} \rho g \, dz + \frac{\rho_o}{\rho} T_o$$

(h = Boltzmann constant, ρ_o, T_o density and temperature at reference height h_o, m mass of air molecule). When doing this, one tacitly assumes that the atmosphere is at rest. This means that no vertical movements of air, permanent or transient, are present during the descend of the falling body. This restriction is inherent to all experiments which use falling objects as sensors. Recent observations (Sidi and Teitelbaum (12) (13)) have shown without doubt that rather violent vertical movements do exist in the atmosphere of the ionospheric D-region and have by this confirmed an earlier result of Rose and Widdel (14) who derived an updraught of short lifetime of about 5-10 ms^{-1} at a height

of 80 km. An observed change of descend speed of a falling object can therefore either be caused by a change of air density or by vertical gusts. A priori it is not possible to decide if an observed change of descend speed was caused by a change of air density (caused by a change of temperature) or by a vertical lift or downwind. Some examples of measurement of vertical movements which show unusual changes of descend velocity are shown in Fig. 1 (taken from (15)).

Foil clouds versus falling spheres: Merits and deficiencies

In order to achieve at a high accuracy of measurement of the trajectory of the falling object, a low descend speed is desirable. A low descend speed results in a good response of the falling object to changes of wind direction with height but increases the sensitivity against transient vertical gusts which may affect the result of density and temperature measurement. One is however allowed to assume that vertical gusts occur mainly in heights in which turbulence is present. Turbulence may be present in strong wind shears which extend over a limited range of altitude. A slow descend speed increases also the number of trajectory data points which can be collected by the radar in unit time. This allows data smoothing which reduces random error and increases overall accuracy.

Solid sensors like falling spheres have the advantage that they remain "point targets" for the radar all the time but physical and technological reasons do not allow to produce solid targets which have a sufficiently small weight-to-area ratio to keep the descend velocity low enough (well below 100 ms^{-1}) to allow a good response to change of winds at heights above about 85 km. The rather high descend speed of solid objects however has an advantage when air density and temperature profiles are to be determined because the influence of vertical gusts on the descend speed remains small. However, the short time during which the object passes the higher levels above about 85 km calls for very precise radar tracking devices. Such devices are available only on a few launch facilities. Solid targets are therefore well suited to measure density and temperature but are less good when the wind profile should be measured with good accuracy and good height resolution at heights above 85 km.

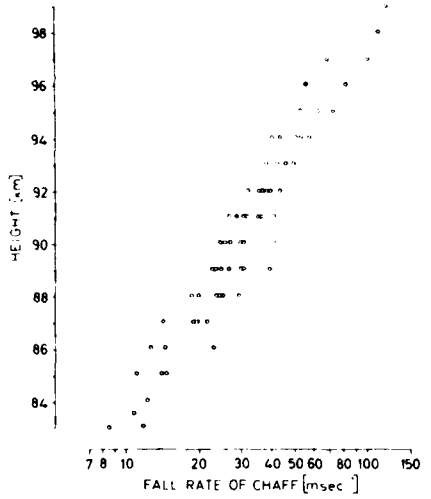

Fig. 1: Measured descend speed of foil clouds which can be interpreted as being affected by vertical gusts.

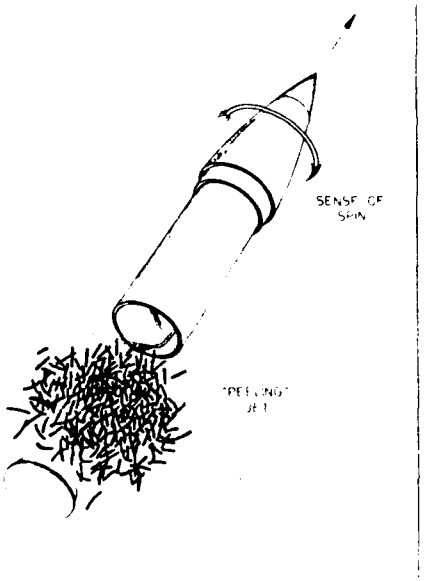

Fig. 2: Principle of foil cloud generation:
The payload is separated from the rocket motor near apogee. By this, the rear end of the canister which contains the loosely-packed foils is exposed. After a short delay an overpressure is generated in the canister which causes the lid to move. The expanding gas (nitrogen) carriers the foils with it. Simultaneously two (in the latest version: four) jets produce a veil of gas which acts as a wall: momentum is taken from the foils, the size of the cloud is confined and the foils are separated from each other.

Foil cloud experiments avoid the disadvantage of a restricted weight-to-area ratio. Because the target is no more solid, the elements from which the cloud is formed can be made as light as materials will allow. Weight-to-area ratios of order of 2 gm^{-2} can be realized with ease. One obtains then a descend velocity which remains well below 80-100 ms^{-1} at heights near 95 km. This yields a good response to changes of wind and a good accuracy of measurement.

But this advantage has to be bought in by some trade-offs: The low descend velocity results in a fairly high sensitivity to turbulent motions and vertical gusts. Further, and more serious, the target does not remain a point target on its descend. Diffusion spreads out the foil elements and enlarges the diameter of the cloud. When the size of the cloud approaches the aperture angle of the radar (which uses in most cases conical scan tracking to derive azimuth and elevation) random fluctuations of the density of the foil cloud cause random variation of the radar brightness of the cloud. This in turn may cause the radar to "hunt" and precise measurements are then no more possible. Further, turbulences often present in strong windshears tear the cloud into several smaller clouds. This has about the same effect upon the radar tracking. It well may happen that useful tracking of the descending cloud is possible only over a relatively narrow height interval because turbulences have dissolved the foil cloud.

Further, if the descend speed is low and the horizontal wind velocity is high, it may happen that the cloud drifts out of the useful range of the radar. This may limit the usefulness of foil cloud sensors in applications in which measurements over a pre-determined height interval are desired or mandatory. Such constraints do not hold when solid targets are used because their descend is much faster.

By principle, it should be possible to derive density and temperature from the descend velocity of foil clouds also. The practical feasibility, however, has to be investigated and established by comparisons with results obtained with establishment methods. The results of an attempt of this kind will be described in this report.

The Lindau foil cloud experiment

A foil cloud experiment was developed at the Max-Planck-Institut für Aeronomie which was designed to measure wind speed and wind direction in the height range between 95 und 80 km. Very thin plastic (polyphterephtalate) foils, 2.5 micrometers thick, were used. The plastic foils were aluminized from all sides. in order to keep the weight low, the thickness of metallization corresponded to only a few skin depths of the radar wave (S-band) used to track the target. The foils were 50 mm long (this corresponds to half a wave length of the tracking radar (MPS-19). The width of the foils was 9 mm. Such thin foils have a strong tendency to stick to each other and certain means have to be taken to overcome this problem. The tendency for bird's nesting of these plastic foils is, however, by far much lower than was found for conventional needle-type "chaff" used for military ECM purposes. All attempts to get this needle-type chaff separated did fail, while this problem was relatively easy solved for foils as will be shown soon.

In order to get a good response to winds and little distortion, the foil cloud should be generated in such a way that its relative motion to the surrounding air is as close to zero as possible. This calls for an ejection of the foil cloud backwards to the direction of flight short before apogee of the rocket's trajectory is reached. In this case, the vertical and part of the horizontal component of the rocket's trajectory speed is compensated and the cloud can be considered as being generated at rest in relation to the ambient air. The foil cloud enlarges during descend due to diffusion and under the influence of centrifugal forces because the rocket spins at a rate of about 14 rev sec^{-1}. Up to a certain degree the effects of centrifugal forces and diffusion can be compensated by two or more gas jets which are operated during expulsion of the foil packet. These gas jets are mounted at the rear end of the canister. They are orientated against the direction of the rocket's spin under a certain angle (30°). The nozzles of the jet pipes are slightly bent inwards. These jets form a "veil" which takes off the kinetic energy of the foils gained by centrifugal forces. The jets cause also an increase of the foil density towards the centre of the cloud. This increase of foil density compensates to a certain degree the effects of diffusion and the radar sees then for a longer time a point-like target. The beneficial effects of these provisions are, however, offset when the cloud passes a strong wind shear. In such a case distortion of the cloud cannot be avoided.

The principle of operation of the payload is shown in Fig. 2. The payload front end is separated from the rocket by igniting a separation charge which acclerates the payload section to a relative speed between payload and motor of about 25-50 m/s. The foils are stored (loosely packed) in a cylindrical canister which is part of payload. 1.6 - 2.2 sec later the separation between motor and payload is then of order 50-100 m. The pyrotechnic valves which seal three small storage containers of nitrogen are then activated by an electric timer. This timer is energized by a microswitch which is mounted at the rear end of the canister. This microswitch connects the timer with a battery. Nickel-cadmium batteries have been used but for applications were a long "shelf life", for example, a long stand-by of the rocket on the launch pad is required, dry batteries of the silver-oxyde type with an additional storage capacitor is recommended. Lithium batteries may also be used but no practical experience was obtained with them up to now.

Response of the foil cloud to wind and air density

In order to estimate the actual response of the foil cloud to winds, some information about the drag coefficient has to be obtained. The width of the foil elements (9mm) are much smaller than the mean free path at the height in which the cloud is generated. It is clear then that the aerodynamic flow is ruled by Knudsen flow and by Reynolds numbers. This means that C_D is not a constant. Fig. 3 shows the result of descend velocity measurements obtained on 13 rocket flights. It follows from these data (and from results of other flights) that the deceleration of the foil elements is of order 0.1 g at a height of 95 km and decreases rapidly with decreasing height provided that the cloud was created above 95 km where a quasi-equilibrium descend velocity was achieved. We can therefore neglect the term $m\dot{v}$ in eq. 3 and obtain the simplified equation of motion; eq 5.

$$(5)\quad mg = C_D \cdot A \cdot \frac{\rho}{2} v^2$$

The gravity forces (left side of eq 5) can be assumed as being nearly independent of height. We should then expect, if the air density varies exponentially with height (this is a good approximation) and if the drag coefficient C_D is a constant, that v^2 varies proportional to . The data, however, show that this is not the case but suggest that the descend velocity is described by

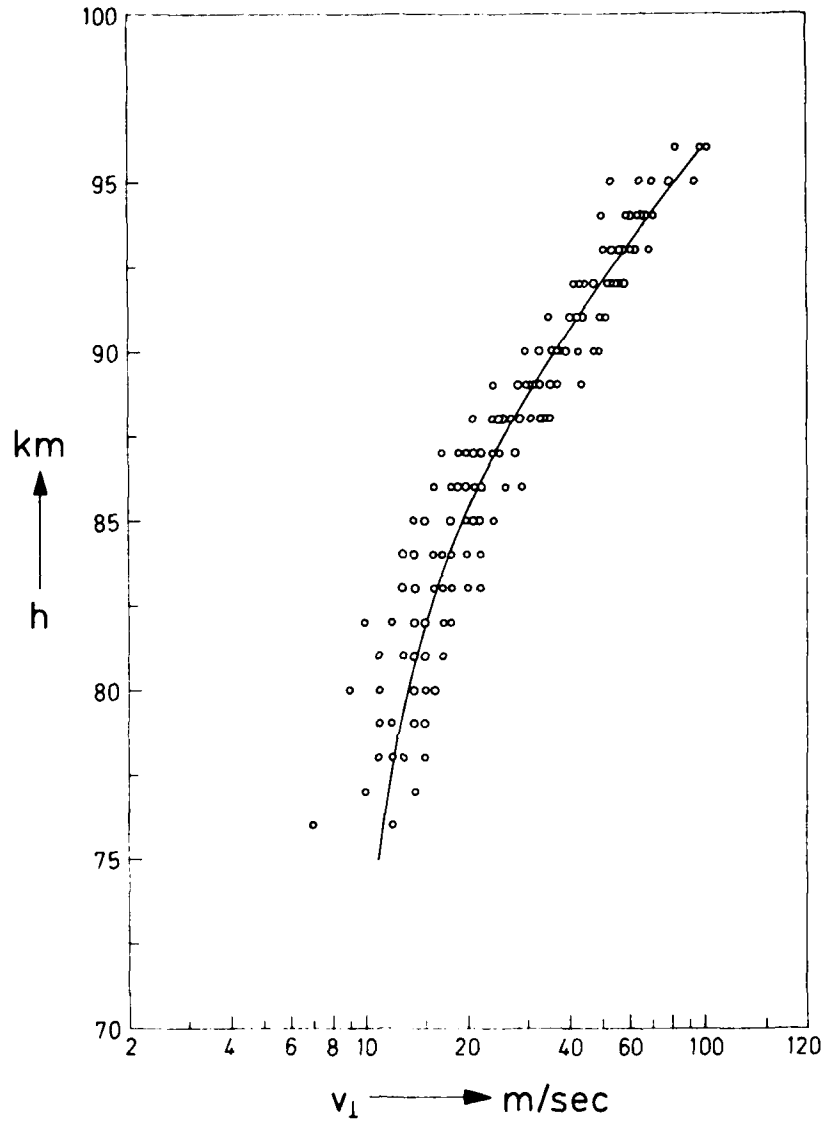

Fig. 3: Measured descend velocity of foil clouds flown on 13 rocket launches.

between an altitude of 83 and 95 km.

A rigid calculation of the drag coefficient appeared to be hopelessly complicated. Even the falling sphere-experiment relies upon empirically determined drag coefficients.

Assuming that the vertical movement of the foils is governed by (a modified) viscous flow, which means that the frictional forces dominate the inertial forces, and that the drag force varies proportional to $1/\varrho$; one can formally write for the drag coefficient

$$C_D = C \cdot \varrho^{\gamma} V^{\Theta} \quad ; \quad \frac{1+\gamma}{2+\varrho} = 0.76.$$

with $\Theta = -1$.

This yields:

This procedure follows standard practice in that the formal relation: "Drag force proportional density" is kept and that the variation of the drag force is described by a variation of C_D. For viscous flow, the movement of the foils is governed by small Reynolds numbers Re < 1. Experiments show that the drag coefficient C_D is then inversely proportional to the Reynolds number for all kinds of bodies, so for rectangular and circular disks (c.f. Hoerner (16)) when the flow is perpendicular to the body's surface. C_D is then:

$$C_D = \text{Const.} Re^{-1} = \text{Const.} \frac{\eta}{v.\varrho.L}$$

η is the viscosity, L the characteristic length of the body. This holds true for continuum flow but the foils are not in an environment in which continuum flow is present. The viscosity η has to be corrected by a term which takes into account the relation between the mean free path of the air molecules λ and the characteristic length (width) of the foil elements L.

This effective viscosity η_{eff} can be written as:

$$\eta_{eff} = \frac{\eta_o}{1+\lambda/L}$$

in which η_o is the continuous flow viscosity

$$\eta_0 = \frac{1}{3} \rho \bar{u} \lambda$$

(ρ = air density, $\bar{u}$ = mean velocity of the air molecules = $\sqrt{\frac{3kT}{\pi \cdot m}}$.
Eq. (8) can then be written as:

$$c_D = \text{Const.} \cdot Re^{-1} = \text{const.} \cdot \frac{\bar{u}}{1+\rho \cdot L/a} \cdot v^{-1}$$

the proportionality constant a relates the density ρ to the mean free path length λ:

$$a = \left(4\sqrt{2}\, \pi r^2 N\right)^{-1} \approx 1.2 \cdot 10^{-7} \text{kg} \cdot \bar{u}^2$$

Finally, one obtains for the equilibrium descend velocity $v_\perp$:

$$v_\perp = \frac{6g}{C\bar{u}} \cdot w^* \left(\frac{L}{a} + \frac{1}{\rho}\right)$$

w* is the mass per unit area (weight-to-area-ratio) of the foil elements. The constant C has still to be determined.

Eq. (8) and (13) explain the experimental result why the descend velocity of the foils tends to vary little with height when a certain height is reached: The equilibrium descend velocity is (after an initial acceleration phase which is difficult to observe) to a very good approximation proportional to ambient viscosity and inversely proportional to density. When the mean free path becomes smaller than the characteristic length of the foil element, the effective viscosity becomes independent of gas density and the remaining dependence of $v_\perp$ from $1/\rho$ is partially offset by the (exponential) increase of density ρ when going to lower height. This results in only a slight dependence of descend velocity of height. At greater heights, when the mean free path is larger than the characteristic length of the elements, the descend velocity becomes proportional to the mean free path of the molecules of the surrounding gas and the descend velocity becomes by this inversely proportional to density. Because the density varies exponentially with height, the descend velocity varies also to a good approximation with ambient pressure but only in the upper part of the trajectory. This can be seen in Fig. 3.

Useful range of density measurement

These results show that foil clouds can be used for density (pressure) measurements only over a limited height range. The range over which foils can be used for this purpose is determined by the mass to area ratio w* and by the characteristic length L (width) of the elements. For use at lower heights, one has to increase the mass of the elements and to decrease the width. However, it turned out (17) that the temperature and density range over which a measurement is possible becomes narrower and narrower with decreasing height. Below about 65-70 km, foils or chaff fails to provide such measurements whatever design one chooses. The ability to measure winds however remains, at all heights, but other methods (inflated spheres for example) are superior to the chaff method below about 70-75 km and should be preferred at these heights.

Response of the foil cloud to horizontal changes of wind

Using targets as sensors for wind finding one is always faced with the problem how fast the target responds to changes of wind speed and wind direction and how large the slip between true wind speed and that attained by the sensor is.

The results presented in the preceding paragraph allowed an estimate how fast the foil clouds could respond to sudden changes of wind. The result of this estimate is shown in Fig. 4. It was assumed for this calculation that the cloud was deployed into calm air and that the wind starts to blow at $t = 0$ with a velocity v_o. Fig. 4 shows the time needed for the cloud to attain a certain percentage of the wind speed v_o in three different heights, 95, 90 and 85 km. The figures given as parameters indicate the height interval which the cloud has to pass until it has attained the relevant percentage of the ambient wind speed. These estimates represent a "worst case" condition. One may expect that the actual response of the foil cloud to winds is somewhat faster. Nevertheless the result of this estimate lets one expect that a good height resolution can be obtained with light-weight sensors at D-region heights of the ionosphere but an experimental verification remains necessary.

EXPERIMENTAL VERIFICATION

Wind measurements

An experimental verification of response of the foil cloud and of measurement accuracy seemed to be difficult because no other sensor of known accuracy was available. Therefore, indirect methods had to be used instead. The most obvious method for a check is to track the foil cloud on its descend with two independent radars simultaneously, preferably with radars of the same type or of same performance. Such experiments were possible at the launching site "El Arenosillo" southern Spain) were two NASA-modified MPS 19 tracking radars were available. Both radars were located close to each other at a distance of not more than 50 m. The two radars observed therefore the cloud under the same angle of view. It was found that the tracking results obtained with both radars were about the same unless a large windshear occurred. The cloud was distorted in this shear and often turn into several smaller clouds. When this happened, the spread of the cloud was so large that the conical-scan radar sometimes lost the target by "hunting". If the trajectory of the cloud can be further tracked by the radar depends then upon the degree of distortion of the cloud. During these experiments, the same procedure of evaluation and the same type of (analog) computer was used.

The results were less satisfactory when two radars of the same type were used but put about 1 km apart and a different type of data aquisition was used. This is seen in the following Figures 5 and 6 in which the wind direction and wind speed determined by the two radars were correlated. Both radars, "X" and "Y" were MPS-19 but radar "X" processed its data on an analog computer and recorded the results on a strip chart recorder while radar "Y" digitized the aquisition dates and recorded the momentary values once per second on punched tape. The recorded analog data contained already some data smoothing which was improved during data read-out by hand by fitting appropriate lines through the "wiggles" when present. As expected, the largest differences between the two radar measurements of both, wind speed and wind direction, are found at the beginning of tracking (apogee) and at the end at low heights when the cloud has passed one or more wind shears. This series of measurement was selected because the foil clouds were deployed at heights between 97 and 100 km. This height is far in excess of the optimum height of about 93-95 km. While the average of

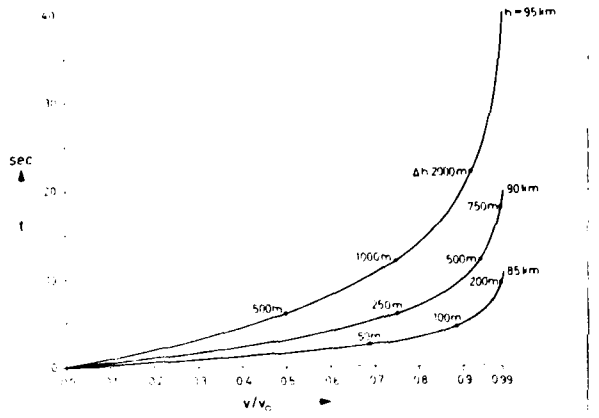

Fig. 4: Calculated response of a foil cloud to a sudden change of horizontal wind. Experimental evidences suggest that the response of the foils to wind shears is faster than indicated by calculation. Calculation is based upon the assumption that the foils are at rest and that a wind of windspeed suddenly starts to blow.

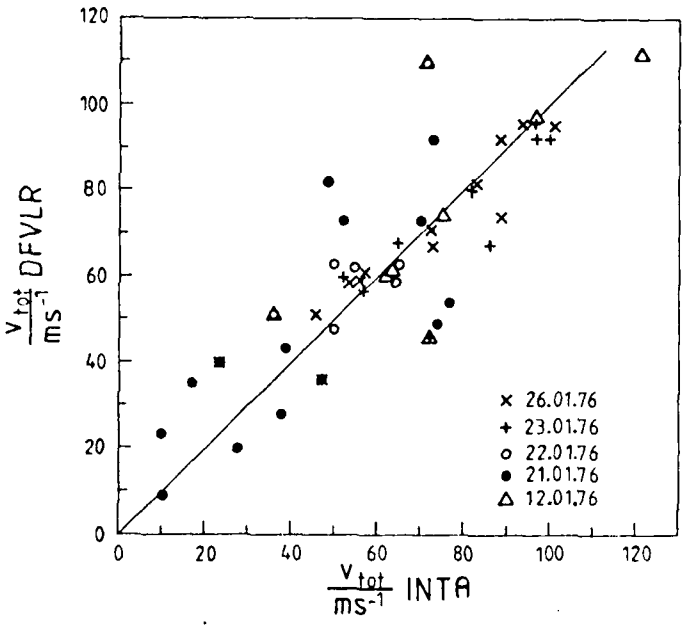

Fig. 5: Correlation of tracking data of two radar sets of same type located 1 km apart using different types of data evaluation. Measurement of vector wind speed. Ejection of foil cloud was between 97 and 100 km. (Design height: 93 - 94 km).

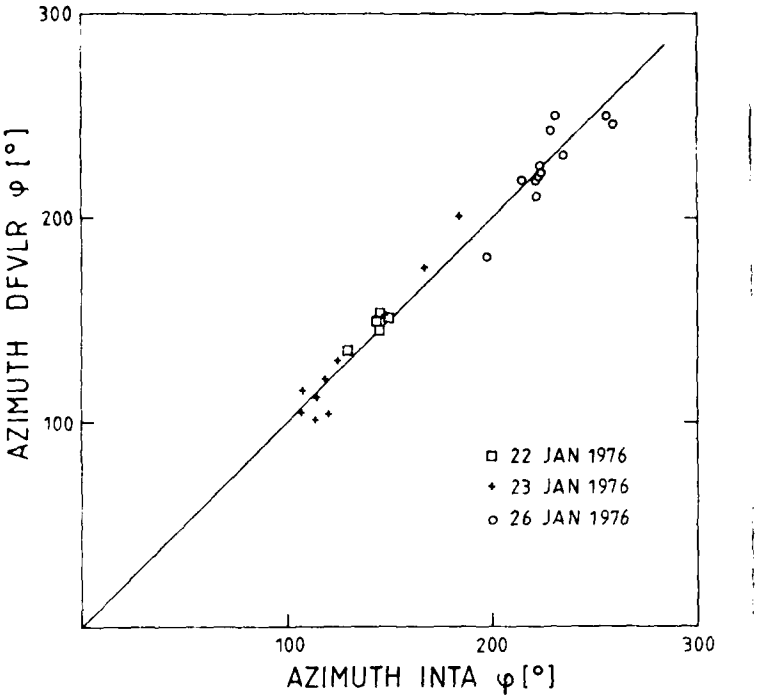

Fig. 6: Same as fig. 5, Measurement of wind direction.

all deviations turns out to be quite small, the individual deviations are quite large and become larger when the foil cloud was deployed too high. That these large deviations are caused by wind shears was proved in this program by the results of lithium trails (11) which were launched somewhat later after the launch of the foilclouds: wind shears were observed by this experiment of same direction and magnitude near 90-92 km as was found by the foil cloud experiment. Further, Meteor radar data taken in Southern France (18) showed also wind shears at the same height and of similar magnitude as was seen by the rocket experiment. This proves that this shear region is not a local feature but extends over very large areas simultaneously.

A similar experiment was performed in White Sands in which foil clouds were launched on ARCAS vehicles. The foil clouds were tracked by precision radars. These radars used fast digital data aquisition and recording. The high sequence of data allowed a good data averaging. The result of these experiments are shown in Fig. 7 and Fig. 8. The deviations between the tracking data of the two radars are rather small and notable only in those parts of the trajectory where the foil cloud has passed a wind shear in which a considerable distortion of the foil cloud had occurred. This result suggests that good wind data can be obtained when good radars are available and when the recording sequence of tracking data is high enough to allow averaging.

Two foil cloud experiment

The experiments described so far yield some indirect evidence about the response time to changes of wind in that the differences of results obtained with two radars which track the same foil cloud are largest after generation of the foil cloud. A further experiment yielded some proof of the theoretical considerations presented before. During this experiment two foil clouds were ejected at the same height. One foil cloud consisted of light foils (9 mm wide, 2.5 μm thick, index "L" in the following figures). The other cloud was made of heavier foils (3 mm wide, 10 μm thick, indexed "H"). The latter type of foils was designed to match conditions found below about 83-85 km in order to yield density data from fall rates. Two MPS-19 radars were available for tracking. Each radar tracked one cloud. Vector wind speed, wind direction and descend velocity measured by these radars were correlated with each other. The result is shown in Fig. 9, 10 and Fig. 11.

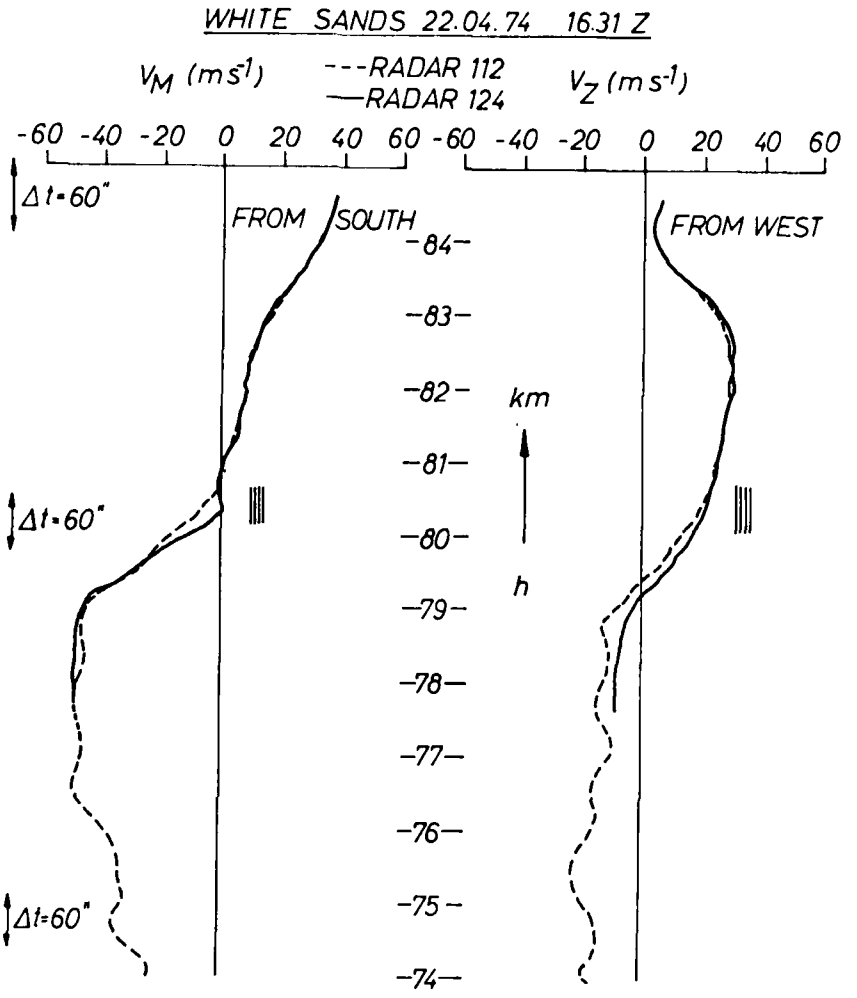

Fig. 7 and 8: Result of foil cloud tracking with two different precision radars after data smoothing (smoothing interval indicated). Bars indicate region of wind shear.

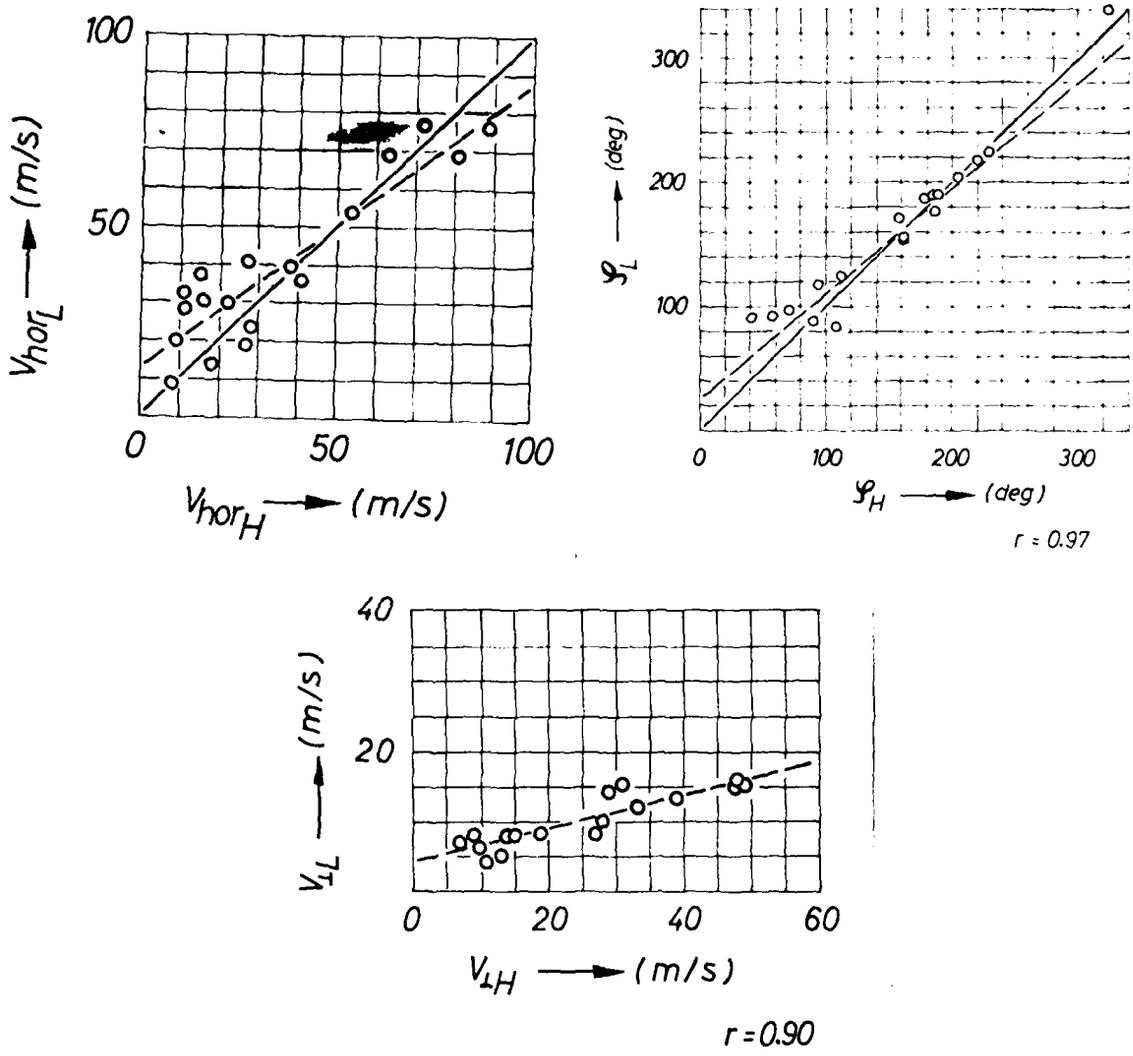

Fig. 9,10,11: Correlation of tracking data for vector wind speed v_{tot}, wind direction φ, and descend velocity $v_{\perp}$, of two foil clouds having different area to mass ratio. (Index L = "light", H = "heavy" indicates area to mass ratio). Both clouds were generated simultaneously at the same height and each cloud was tracked by a radar MSP19.

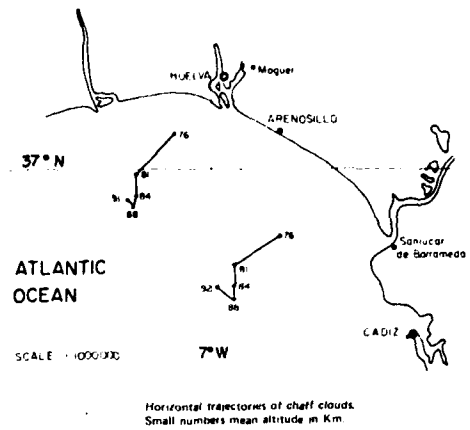

Fig. 12: Spacial validity of measurements. Two foil clouds were generated almost simultaneously about 50 km apart and tracked with the same type of radar (MPS19). Projection of trajectory.

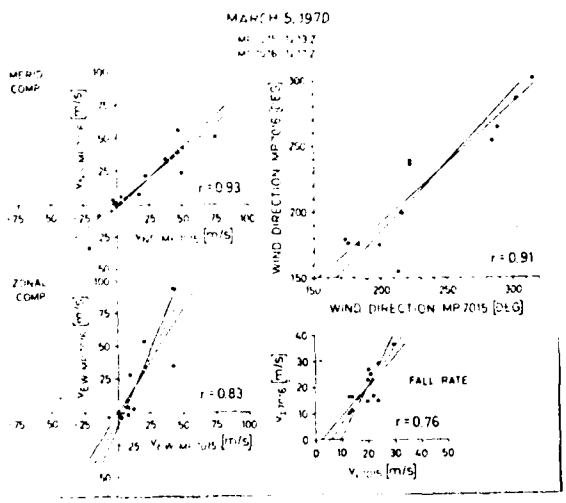

Fig. 13: Correlograms of meridional wind, zonal wind, wind direction and descend velocity.

As was expected, the largest deviations of measured wind speed were found at heights were the cloud of "heavy" foils did respond slower to changes of winds. The same holds true for wind direction. The ratio between the descend velocities corresponded to that what was expected. The results indicate that the response of the cloud to changes of wind is somewhat faster than the estimate. This means that a good height resolution of wind measurements can be obtained.

Spatial validity of measurement

One concern about the significance of the wind data obtained with foil cloud experiments is that these measurements are local measurements of the sampling type, and it is known that local changes of winds may occur within a very short time. There are many indications for that.
In order to obtain an estimate, two clouds were produced almost simultaneously (time difference: 5 min) at a horizontal distance of about 50 km. The result of this experiment is shown in Fig. 12 and Fig. 13. Fig. 12 shows the projection of the foil cloud trajectory on a map and Fig. 13 the correlograms for meridional and zonal wind component, wind direction and descend velocity (fall rate). The agreement of data is not perfect but shows that the wind profile measured with the foil cloud may be taken as representative for a larger area.

Comparison of foil cloud wind measurements with wind data derived from falling spheres.

In the preceding paragraphs, comparisons were made between results obtained with foil clouds of the same type. It may be of interest to compare results of foil cloud measurements with those gathered with other type of falling body sensors. This opportunity was given in experiments performed over White Sands, New Mexico during a joint ASL-MPAE program. Inflated plastic spheres of about 1 m diameter (Robin spheres) were used which were launched almost simultaneously with the chaff cloud experiments. Robin spheres are known to be less suitable for wind measurements at greater heights due to their high descend speed which yields a slow response to winds. Their primary use for is air density and air temperature measurement. Both type of experiments were tracked simultaneously with two precision radars. The result is shown in Fig. 14. It shows clearly that the errors of wind measurement are fairly large. The corresponding results of foil

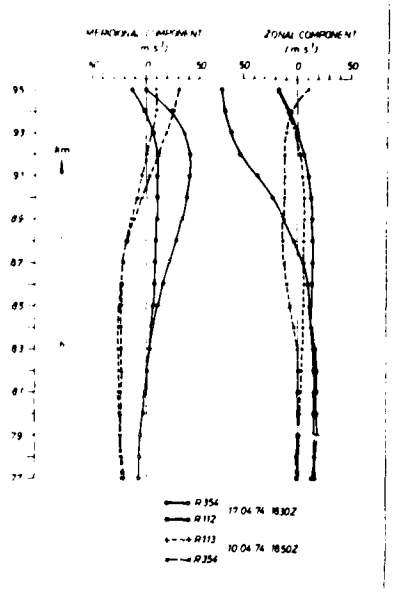

Fig. 14: Wind profiles derived from radar tracking of falling spheres ("ROBIN"-spheres). Each sphere was tracked simultaneously by two radars. Divergence in tracking results above about 83 km indicates that falling spheres (Robinspheres) are not very suitable for wind measurements at greater heights.

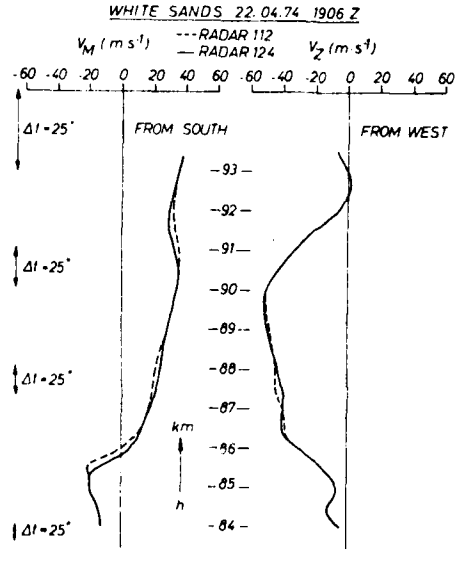

Fig. 15: Result of a simultaneous tracking of a foil cloud by two independent precision radars.

cloud measurements tracked with the same type of radar is shown in Fig. 15. Below about 84 km the agreement between the two radars becomes very good. Falling spheres of the Robin type can therefore be used to advantage below this height, while foil clouds hold an advantage at heights between 95 and 85 km.

Density measurements

The problems involved when air density is to be derived from the descend rate of falling objects have been discussed before. Because the descend rate of the foil cloud is well below the speed of sound, it is easily affected by vertical gusts. This was noted already during the first launches of the experiment that the then very small foil cloud was lifted with a speed of about 10 m s^{-1} at a height which later turned out to be the seat of rather permanent wind shears (14). Examples of rather unusual variations of the descend velocity are shown in Fig. 16. These samples were selected from a data set of about 120 individual measurements. This means that such events which obviously persist over a longer period of time (some ten minutes) are comparatively rare. Nevertheless they are present and there are indications that small, transient vertical movements of air are nearly always present at certain height intervals. This was confirmed recently for European latitudes by VHF radar measurements performed near Lindau. One has therefore to keep in mind that density values derived from changes of descend velocities of foil clouds might be contaminated by effects of vertical gusts which might have lasted during the time of measurement and remained undetected.

A means to decide if "good" uncontaminated foil cloud descend data can be used to derive air densities is to compare data obtained with foil clouds with those gathered by established methods. Such an opportunity was also had during a joint ASL-MPAE campaign performed at White Sands. Unfortunate events however prevented to gather data from simultaneous launches of foil clouds and Robin spheres but reference could be made to Robin data obtained some days before and after the launch. Density was determined for the height range between 87 and 92 km assuming an isothermal atmosphere. The result is shown in Fig. 17. The densities derived from the descend velocity of the foil cloud follows the density variation derived from Robin sphere / Datasonde measurements

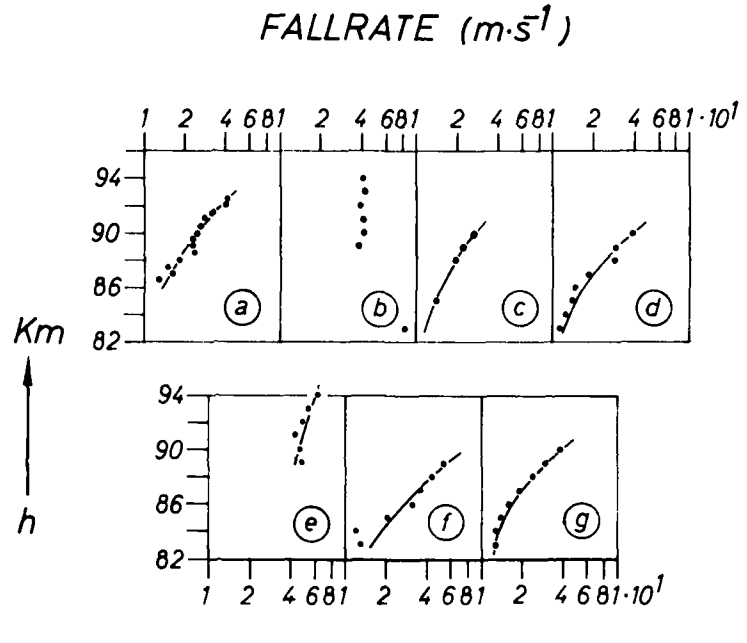

Fig. 16: Unusual descend velocities of foil clouds observed near noon during winter over South West Spain. Selected from a collective of 120 individual experiments.

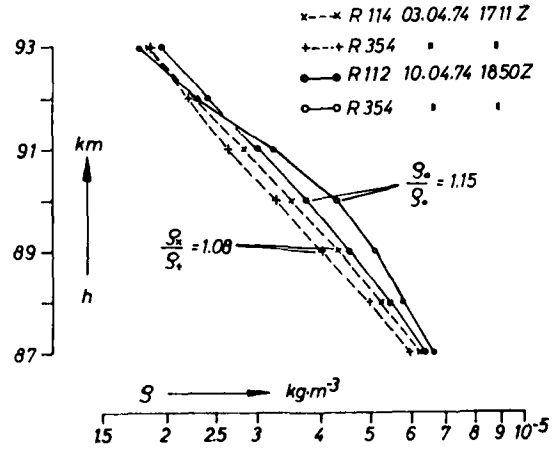

Fig. 17: Comparison between air densities derived from falling sphere and from foil cloud experiments. Descend trajectory of both experiments was measured simultaneously by two radars. The ratios quoted in the figure refer to the ratio of densities derived from the trajectory data of each radar assigned to the relevant experiment. For deriving densities from the foil cloud experiments an isothermal atmosphere has to be assumed. If this assumption does not meet reality, the method fails.

quite closely. Fig. 17 shows the ratio between Robin sphere data and foil cloud results. The deviation is of same order of that shown by the results of the individual Robin sphere measurements. The result of this experiment was taken as a proof that the approximation used to derive density from descend velocity data of the foil cloud was permissible for this height region. But one should expect that this approach fails when the atmosphere is not isothermal.

RESULTS OF EXPERIMENTS

Correlations between changes of radio wave absorption and of winds:

The hypothesis that the winter anomaly of radio wave absorption is caused (at least partly) by advection of minor constituents like nitric oxyde and possibly $O_2^1 \Delta g$ (both constituents have a low ionization potential and can be ionized by wavelengths near 1000-2300 nm) involves that significant correlations between wind and absorption may be expected. The irregularity of this effect (occurrence and diurnal variation which follow rarely the variation of the sun's zenith angle) supports the meteorological concept and encourages investigations in this direction.

At first sight, a serious objection against the attempt to correlate winds with absorption is that it is not possible to separate the influence of tides from the prevailing wind when only a single measurement per day is made. Data from meteor wind measurements show that strong tides do exist in the 90-100 km level and there is no sound reason why such tides should not be present at lower heights. However, if the meteorological hypothesis contains some truth, both, tides and prevailing wind, work together. From this point of view it is not necessary to separate the two components if relations between wind and absorption are sought for, but a fairly large set of data is necessary to achieve at a significant result. In order to obtain significant results the launches should take place at or near the same phase of diurnal variation. For practical reasons it is advisable to choose noon because absorption is then normally at maximum and does not change too much with time. The same is true for the phase of wind. This allows to shift the launch time a little bit if a hold in the launch procedure turns out to be necessary without serious impairing the scientific value of the experiment.

Such measurements have been carried out between 1968 until 1976 (with some interruptions) during winter. The observed wind profile was correlated with absorption measured at time of launch in order to find out "sensitive" height levels in which absorption correlates significantly with changes of wind. Because the results of ground-based measurements indicate that more than one height level might be involved, the correlation coefficients between wind and absorption for a specific height may become numerically small. This is one of reasons why a fairly large number of individual measurements is needed to obtain results which can be considered as significant.

"Beam correlations"

It is common practice to describe the vector wind by components of a Cartesian coordinate system which is orientated south-north (meridional component) and west-east (zonal component). It seems worthwhile to mention that a different notation exists for both components which can easily become a reliable source of misunderstandings and of discussion. Meteorologists consider the direction from where the wind is coming. A westerly wind is therefore a wind coming from the West and going to the East, and is counted as positive. Ionospheric physicists count the same wind as being easterly because the wind is blowing from the West to the East. This difference of notation has to be kept in mind.

The separation into two components is of cause very convenient but it does not fit our purposes when we attempt correlations between wind and absorption, because we get the correct (largest) correlation coefficient only when we look into the direction φ_{max} of the wind component which causes the correlation. This direction φ_{max} is a priori unknown. In order to find out this direction, we have to go around the compass card and have to calculate the wind component pointing to each direction φ. For this, we use the original zonal and meridional components Z_i and M_i (i = relevant number of measurement) and correlate these values with absorption. When we plot the correlation coefficients $r(\varphi)$ on a polar diagram, we will find a maximum for a certain angle φ_{max}. This is then the direction of the wind for which correlation between absorption and wind change exists. An ambiguity however remains: the wind can increase from this direction or can decrease from the opposite. Both cases are equivalent and yield an increase

or decrease of absorption. This method was described first in (7) and has turned out to be useful (20). The method has been checked before application in model calculations. Details of this model calculation have been described in (7). The quantitative formulation is as follows (7): We designate the meridional wind components by M_i , the accompanying zonal component by Z_i (M_i is positive for winds going to the north, Z_i for winds going to the east) and the absorption values which were measured at the same time by y_i. The correlation coefficient $r(\varphi)$ between the wind components going towards the direction φ (φ being measured clockwise from the north) and the absorption values is then described by

$$r(\alpha_j) = \frac{A\cos\alpha + B\sin\alpha}{\sqrt{(C\cos^2\alpha + D\sin^2\alpha - 2E\sin\alpha\cos\alpha)}\sqrt{F}}$$

with

$$A = \Sigma M_i y_i - (1/n)\,\Sigma M_i \Sigma y_i, \qquad D = \Sigma Z_i^2 - (1/n)\,(\Sigma Z_i)^2,$$
$$B = \Sigma Z_i y_i - (1/n)\,\Sigma Z_i \Sigma y_i, \qquad E = \Sigma M_i Z_i - (1/n)\,\Sigma M_i \Sigma Z_i,$$
$$C = \Sigma M_i - (1/n)\,(\Sigma M_i)^2, \qquad F = \Sigma y_i^2 - (1/n)\,(\Sigma y_i)^2.$$

n is the number of data pairs to be correlated. The correlation coefficients so obtained have, however, little meaning unless their significance is established. (This was outlined before in 2.) The formula (equ. (1) and (2) were given which yield the significance of the correlation coefficient r.) This "beam" correlation was calculated for all sets of data which were available.

Results

A fairly large number of individual measurements were carried out during the winter season between 1968 until 1976. This time interval covers a period in which the solar activity delined from rather high (1968/1970) to extremely low values (1973/76). The number of measurements were large enough to consider the two states (high and low solar activity) separately. Beam correlation was applied to all data.

The result is shown in Fig. 18. It shows that significant correlations between absorption and changes of wind were found in periods of low and of high activity of the sun at well defined height levels, but these levels were found in different heights for the different periods. Taking the direction of the wind as a guide, we find that the levels in which correlations with changes of the wind coming from the same direction with absorption were by about half a

Fig. 18:

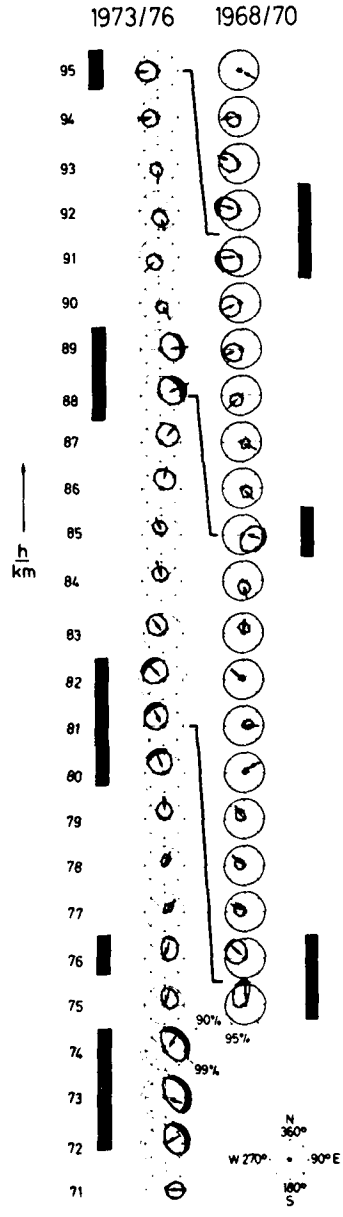

Beam correlation diagram: Correlation between radio wave absorption at time of launch of the foil cloud experiment and wind measured in different heights. The parameter which contains the required information if correlation between winds and absorption exists is not contained in the numerical value of the correlation coefficient but in its significance, the circles indicate significance levels of 90 %, 95 % and 99 % probability of not beeing generated by accident. Distinct levels were found in which a change of wind correlates with changes of absorption. These levels were further identified as the seat of fairly permanent windshears. The height of these levels vary with solar activity: When solar activity is low (left), the levels are found at greater heights than is the case when solar activity is high (right). The reason for this is a change of air density which is caused by a change of solar heat input into the upper atmosphere. The change of density was seen also as a change of descend rate of foil cloud at relevant heights.

TABLE 1:

1969/70 Dez/Jan (R = 104.6)			1973/74 Dez/Jan (R = 26.65)			Ser.Progr.Jan 1976 (R = 8.5)		
Datum	h =90 km	h = 88 km	Datum	h =90 km	h = 88 km	Datum	h= 90 km	h = 88 km
09.12.69	42	34	03.12.73	-	38	02.01.76	50	32
10.12.69	30	28	07.12.73	-	27	04.01.76	29	28
12.12.69	36	25	11.12.73	-	24	06.01.76	34	29
16.12.69	53	33	12.12.73	-	29	09.01.76	32	28
17.12.69	30	33	16.12.73	-	32	12.01.76	34	33
18.12.69	57	31	10.01.74	45	38	22.01.76	38	29
15.01.70	47	48	19.01.74	50	43	23.01.76	34	29
16.01.70	56	30	21.01.74	33	29	28.01.76	41	29
16.02.70	39	33	23.01.74	40	43	05.02.76	38	34
			25.01.74	41	26			
Mean	43,3	32,7	Mean	41,8	32,9	Mean	36,6	30,1
Standard deviat:	10,5	6,4	Standard deviat:	6,3	7,0	Standard deviat:	6,1	2.26
Standard error	3,5	2,1	Standard error	2,8	2,2	Standard error	2,0	0,75
Median	42	33	Median	41	32	Median	34	29
						26.01.76	67	67
						17.12.75	41	25
						Mean *	39,8	33
						Stand-dev *	10,6	11,5
						Stand.err *	3,2	3,5
						Median *	38	29
						Mean **	37	29,6
						Stand-dev **	6,0	2,7
						Stand.err **	1,9	0,9
						Median **	3,4	2,9

* 26.01.76 und 17.12.75 included

** without 26.01.76

[illegible] end velocity of foil cloud in m/s, measured at [illegible] km and 88 km during winter 1969/70, 1973/74 and 1976.

scale height (3 km) lower when the activity of the sun was high.

This difference of height for which correlations between wind and absorption changes were found could be caused by the change of solar activity. Air density changes parallel to solar activity as the result of decreased radiation of the sun at certain wavelengths (21). This causes a reduction of energy input into the upper atmosphere. One should expect that this change of air density causes a change (decrease) of the descend velocity of the foil cloud when the solar activity becomes low. This, however, turned out to be difficult to prove for several reasons. One cause is the limited accuracy to which the descend velocity of the foil cloud can be measured. Transient vertical movements (as was mentioned before) affect the measurement and the individual measurements display a fairly large scatter. Finally, the number of measurements performed during each period was limited and the sensitivity of the descend velocity to density changes becomes less at lower height. (The reason for this was outlined before.) From this, one might expect an observable effect only for greater heights above about 87-88 km. Table 1 shows the result of this investigation. Because the number of measurements performed during January 1976 was not very large, an about equal number of consecutive measurements covering the winter period were selected from the previous campaigns (1969/70 and 1973/74) in order to give all three samples the same statistical weight. All launches of the first two campaigns took place near local noon while the launches of January 1976 took place during afternoon (around 1600 UT). The latter deserves some cautious consideration when these data are compared with those obtained during the previous campaigns. Fortunately, some data were available from a tide program which was executed during January/February 1970 (22). During this program, measurements of wind were performed on several days at about the same local time as the launch time of the rockets which were flown during the Aeronomy program. These data were used for comparison: The descend velocity of the foil cloud at 90 km was then measured as 41 ± 1.5 ms^{-1} (Standard deviation $S = 2.65$ ms^{-1}). The sunspot number declined from R = 104 (1968/69) to R = 8.5 (1976) during the observation period. Table 1 shows that the trend of data follows expectation but the differences are still within the error bars of the mean. A better result is obtained when the median value is considered which is known to be less sensitive to data excursions. The result is plausible if one remembers that a (however, loose) connection between the "intensity" of winter anomaly and sunspot activity exists and that the height of the E-layer changes with solar activity (23). A quantitative evaluation has, however, still to be made.

Correlation between changes of wind and of absorption and its relation to wind shears.

While it was shown that correlation between wind changes and changes of absorption do exist, the question remains what these correlations physically mean. If these correlations would solely mirror advection, and by this, transport, one should expect significant correlations in much wider height intervals than found. Indeed, an attempt to derive horizontal transport velocity and direction of transport by analyzing absorption data obtained on observations (either relatively close-spaced (of order 350 km) or 1000-1500 km apart) did suggest some movement from northwest to south-east (3) (24). The actual direction varied from one winter to another, but the north-south component remained. The result remained somewhat uncertain because a considerable amount of data filtering had to be applied in order to achieve at a significant result.This fact suggests that the effects of transport of minor constituents from their place of origin might be superimposed by effects caused by "local" phenomena (which might well extend over an area of some 10.000 km² or be confined to smaller scales) like gravity waves or turbulence. Transport however must be present anyway because large-scale pressure systems with their associated winds do exist in the D-region of the ionosphere and they are moving. Further, some important minor constituents like nitric oxyde have a long life time against photolysis and can survive several days in the winter atmosphere of the D-region.

A probable seat of turbulence are wind shears when they exceed a certain magnitude which depends upon temperature. The smaller height intervals in which correlations between wind and absorption changes were found suggest that these levels might coincide with the location of windshears. Wind shears can admit or inhibit vertical transport and mixing.

The data set which gave the most significant correlations between wind and absorption was that of the period 1973/76 (low solar activity). This data set was therefore analyzed using the definition of a shear:

$$S = \sqrt{\left(\frac{\Delta v_m}{\Delta h}\right)^2 + \left(\frac{\Delta v_z}{\Delta h}\right)^2}$$

v_m = meridional, v_z = zonal component of the vector wind. Considering the D-region of the ionosphere as a whole (72-95 km) a characteristic distribution of abundance of shears was found. This distribution is shown in Fig. 19. The abundance shown in this figure are normalized in order to compensate for the different number of observations available for the different height intervals. Fig. 19 shows that

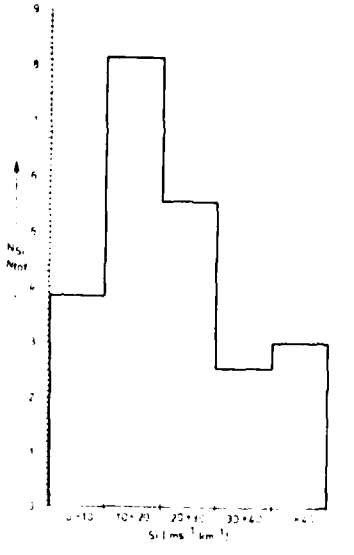

Fig. 19: Abundance of wind shears of different strength in the D-region (75-95 km) determined from foil cloud measurements.

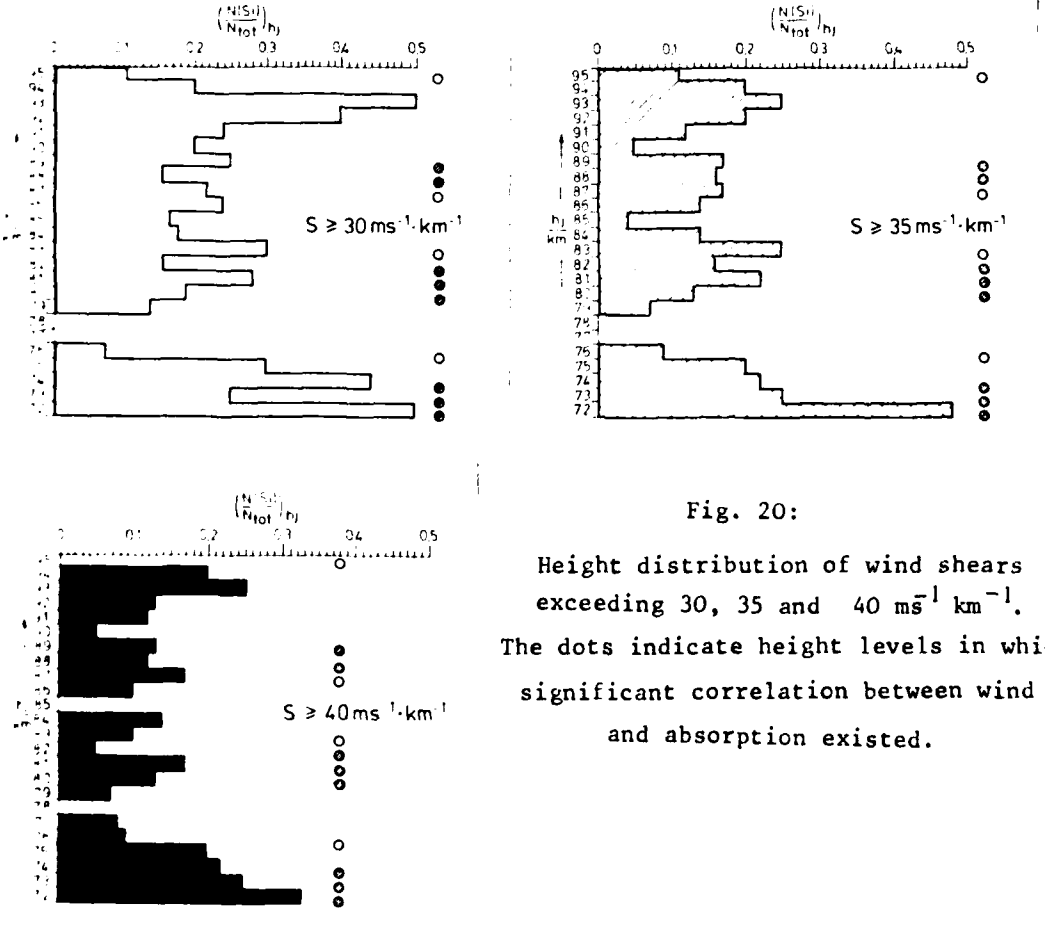

Fig. 20:

Height distribution of wind shears exceeding 30, 35 and 40 ms^{-1} km^{-1}. The dots indicate height levels in which a significant correlation between wind and absorption existed.

the most abundant strength of shears present in the D-region was between 10-20 m s^{-1} km^{-1}. Such shears are certainly not turbulent, but probability for being turbulent increases with increasing shear strength. Because no temperature data were available, (temperature data would allow to decide if a certain shear was probably turbulent or not) several height distributions of shears exceeding a certain value were investigated. Fig. 20 shows the height distribution of abundance of shears exceeding 30 $m \cdot s^{-1} \cdot km^{-1}$, 35 $m \cdot s^{-1} \cdot km^{-1}$ and 40 $m \cdot s^{-1} \cdot km^{-1}$. The probability that shears above 35 $m \cdot s^{-1}$ are turbulent at temperatures found in the D-region is rather high. The levels for which significant correlations between wind and absorption were found were marked in the diagrams with dots. Filled dots indicate a significance of the correlation coefficients between wind and absorption of greater than 99 %, light dots those of above 95 %. The levels are located at or near the height of strong wind shears, especially at the lower and the lowest level. The strong shears of wind found between 93 and 94 km seem not to correlate with absorption. This might have two reasons. A first reason is that the density at these heights is low and that the temperature is fairly high. This means an increased viscosity which prevents break-up into turbulence. Results of vapour trail experiments support this interpretation. A second reason might be that this level is already fairly close to the reflection height of the probing wave used for the absorption measurements and that the contribution of "non-deviative" absorption is much smaller at these heights than in lower ones, for which the probing wave of 2830 KHz and the A3 method used for the relevant absorption measurements is more sensitive. In conclusion, the result obtained so far suggests that the observed correlations between wind and absorption might mirror more the turbulence and mixing processes which are present "locally" in the D-region of the ionosphere rather than transport phenomena which affect a larger area.

Under this aspect, the very significant correlation between wind and absorption which was found for the lowest level (near 72 km) deserves some particular interest. At first sight, this correlation is hard to understand because the contribution to absorption is fairly low from this height level compared to that delivered from greater heights. The picture however changes if one considers that a strong source of nitric oxyde exists at lower heights which originates from ionization by cosmic rays. The absolute number density of nitric oxyde in that source exceeds the number density of nitric oxyde produced in the D-region. Vertical

transport by turbulent mixing can therefore well increase the number density of nitric oxyde in the D-region. But, besides nitric oxyde, other constituents like water are present in quantities at lower heights also. Water affects the electron loss rate considerably. Further, it is a powerful quenching agent for excited states of molecules. One manifestation of presence of water vapour in the D-region is a "ledge" in the electron density profile. This ledge is mostly found near 82-86 km. (The actual height depends upon season and time of day.) The height in which this ledge is found coincides with the height up to which positively-charged water cluster ions are found. The photolytic lifetime of water is however much smaller (of order of a day) than that of nitric oxyde (of order seven days). This means that if water vapour and nitric oxyde are transported into the D-region in which both constituents can affect the equilibrium electron density and if this transport is not quasi-continuous, water vapour would be photolyzed while nitric oxyde remains fairly unaffected. If such a process really plays a role, one has to deal with the uncomfortable aspect that the source and location were this injection into the D-region occurs remains a posteriori almost undetectable. For several reasons water is rather difficult to measure, but a sensitive check for the absence of water in the D-region would be the disappearance of the ledge in electron density and an increase of excited states of oxygen molecules at lower levels of the D-region of the ionosphere, for example $O_2\Delta^1$ g. Results of mass spectrometer measurements (25) and of optical measurements (26) (27) performed during the Western European Winter Anomaly Campaign 1976 seem to indicate that this might well be the case. However, much more measurements of this kind are necessary for a confirmation. An indication that the height distribution of electron density may be altered by wind shears can be obtained if one looks onto electron density profiles, or, better suited, profiles of the contribution of electron density to the integral value of absorption measured during the flight on which the wind measurements were made. Because the electron density is measured during ascent of the rocket while the wind measurement takes place a little later, a perfect agreement cannot be expected because the life history of the vertical movement supposed to cause a "wiggle" in the electron density profile resp. absorption contribution profile is not known. Further, the location of wind measurement and that of the electron density profile does not necessarily coincide.

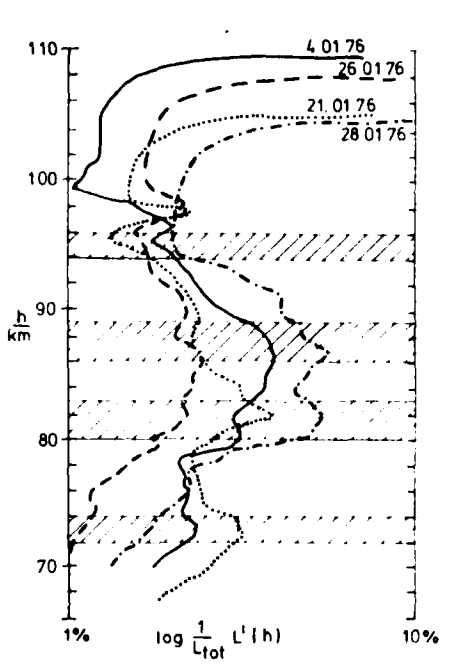

Fig. 21: Relation between absorption contribution (electron density weighted with electron collision frequency) and location of wind shears in the D-region. Relative maxima of absorption contribution are located in or near windshears.

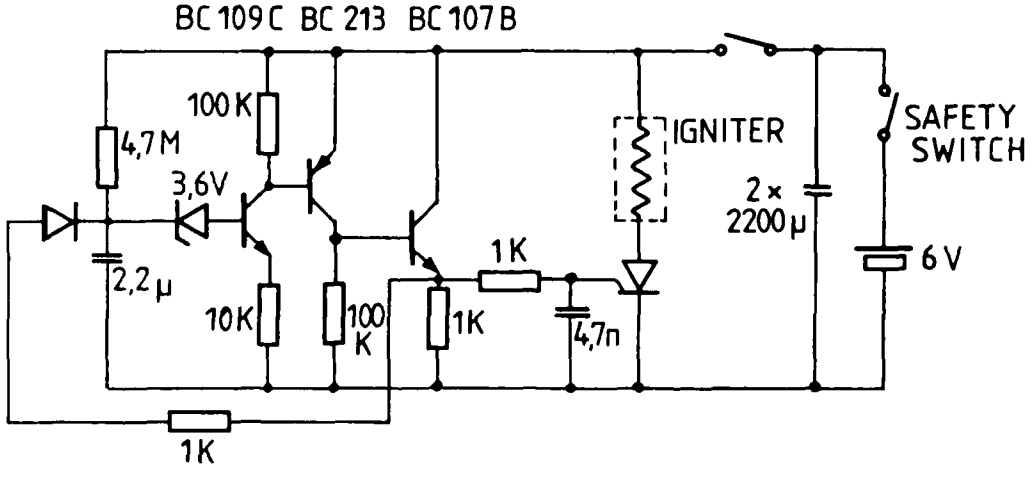

Fig. 22: Electric circuit of timer used to activate the pyrotechnic valves of gas vessels.

A check was made with profiles obtained during the Western European Winter Anomaly Campaign. The profiles do indeed show increases of electron density resp. increases of absorption contribution at or near height levels for which significant correlations between wind and absorptions were found, and were strong wind shears were observed. The levels of strong wind shears coincide quite well with the levels for which significant correlations between absorption and wind were obtained, but a difference was noted for the highest level near 95 km. The absorption contribution profile had a minimum at the height were strong wind shears were found (Fig. 21). The question if this result mirrors different physical processes or if it is caused by a difference in response of the foil cloud winds cannot be decided from these measurements.

Relation between wind shears and partial echoes.

Vertical incidence sounding of the ionosphere with short wave transmitters yield quite often transient echoes from height levels below 90 km (so-called 'deep echoes'). It was claimed that these deep echoes are present during winter only but it was later found that "deep echoes" can be observed during other seasons also, but they seem to be then less intense and less frequent. Investigations performed in the northern and in the southern hemisphere have shown that certain prevailing echo heights do exist which have a distance from each other of about 3 and 6 km. The heights from which these "prevailing echoes" were observed by radio methods coincide with the heights in which strong wind shears were observed. It is therefore suggestive to assume that these deep echoes are caused by gradients of electron density which are caused by vertical movements induced by wind shears. Unfortunately, there was no possibility to move a sensitive vertical sounding equipment to the launch site to try for a direct comparison and proof. The question if "deep echoes" are caused by wind shears remains therefore open.

Technical realization of the wind finding experiment.

Because the foil cloud experiment is technically fairly simple it is comparatively easy to put it into several shapes to fit various kinds of payloads and rocket vehicles.

The experiment was flown on European rockets (Bristol Aerojet Ltd. "Skua") on "ARCAS" vehicles and also on Super Loki "Darts". The latter however is only possible when sensitive radars are available because only a small number of foils can be stored in the payload compartment of such a small rocket. The number of foils required to produce a target depends upon the sensitivity of the tracking radar. The radar return cross section of a cloud which consists of n elements is given by: $G_C = n \cdot G_D$. G_D is the radar return cross section of a single foil element. This cross section can be measured in an appropriate non-echo chamber and depends upon the orientation of the foil dipole to the electric field of the wave. For dipoles $\lambda/2$ long the maximum of the radar return cross section is obtained when the dipole axis is orientated parallel to the electric field of the wave. The maximum return cross section can be calculated in this case and turns out to be:

$$G_{Dmax} = 0.86 \cdot \lambda^2$$

λ is the wave length of the tracking radar. This optimum case is however never achieved because the foil elements may have any orientation in respect to the electric field of the radar wave. An experimental "rule of thumb" says that reality is described to a good approximation when 1/5 of the maximum return cross section is used. Therefore, the effective radar return cross section is given by:

$$G_{Deff} = 0,17\ \lambda^2$$

If the effective return cross section G_R of a target is known which can be detected by the radar at a certain distance, the minimum number of foil elements can be estimated by:

$$n_{min} = \frac{G_R}{G_{Deff}} = \frac{G_R}{0.17\lambda^2} = \frac{5G_R}{\lambda^2}$$

During the first experiments, a radar was used which allowed to detect a target of 1 m² radar return cross section at a distance comparable to that expected for the foil cloud during tracking. The wavelength of the radar was 10 cm. Therefore, one one should expect that about 600 foil elements in the volume covered by the pulse length of the radar (150 m) should be detectable. This was indeed the case, but it turned out that it is advisable to increase the number of foils per experiment when greater height coverage of measurement is desired, because the effects of diffusion and of wind shears cannot be fully compensated by the means described

in this report. But if a very sensitive radar is available for tracking, only very few foils are sufficient. This reduction results in a considerable improvement of tracking data, and the way in which the foils are expelled can much be simplified.

For tracking by less sensitive radars, the foils were packed into a canister which was part of the rocket payload shell. Though the payload shell of a small sounding rocket becomes quite hot during ascend due to aerodynamic heating, no effects were observed which could be traced to effects of heat. Therefore, thermal insulation of the canister for the foil clouds was not necessary. For storage of expulsion gas, pressurized vessels known as "Eagerpeaks" were used. Two, later three of them (type CONAX 1811) were used in each payload. Each vessel contains 0.89 cubic inches of pure N_2 at a pressure of 1500 psi. These vessels are opened by pyrotechnic valves. The charges of the valves are ignited electrically. When the canister was separated from the rocket, two microswitches closed. These microswitches connect the batteries to the timers which then start to operate. Because only a short delay (1.8 - 2.2 sec) between separation and foil cloud generation is required, a simple capacity - charge timer was used. Its circuit is shown in Fig. 22. It has turned out to be advisable to put a large capacitor parallel to the timer input. This capacitor is charged by the battery when the battery is connected to the timer. This capacitor serves then as the energy reservoir for the igniter current which has to flow only for a few milliseconds. This safety measure helps to avoid failures and relieves demands upon battery capacity and of battery self-discharge which might become critical at elevated temperatures or when the rocket has to sit on the launch pad for a longer period of time. Nickel cadmium rechargable cells (Nicads) with 150 mA capacity were used, but an experimental set-up which used 6 V silveroxyde photoflash batteries and a capacitor of 4700 μF as storage capacitor turned out to be at least as reliable as the Nicad device. The setup which used silveroxyde nonrechargable batteries has the advantage that it is much smaller and has much less weight. Further, it requires no maintenance or attention.

The first versions of the experiment used individual discharge throttle plates on each valve of the "Eagerpeak" storage vessel. This solution however is not fail-proof because the storage vessels have to be assigned to different, separate, duties. If one of the vessels fails, the jet system becomes unbalanced. This has some negative influence upon the proper formation of the foil cloud.

The design was therefore changed in that all vessels discharge into a common plenum chamber. This plenum chamber is tapped by proper orifices for the dispersion jets and for canister overpressure generation. This design assures that if one vessel does not function the pressure distribution of the jets remain equal.

Quite a few experiments have proven (what was anticipated) that it is not recommended to produce the foil cloud above about 95 km because the weight-to-area ratio is too high to yield useful wind or fall rate data and the cloud becomes fairly dispersed. This causes a reduced quality of tracking data.

When two foil clouds designed for different heights are to be used, it is advisable to eject the second foil cloud on the downleg of the rocket's trajectory. It is then recommended to use two canisters. One canister is fixed to the payload nose section which is separated at apogee in order to produce the first foil cloud. The second canister should remain with the motor and the second foil cloud should be ejected upwards. It is further advisable to induce a large coning angle of the motor after payload separation because some advantages of the "backward" ejection of the foil cloud can then be retained. This is fairly easy to do by a built - in, intentional, unbalance of the canister/motor system which is balanced out in the payload section when the payload is completely assembled, and becomes effective after payload separation only.

When a very sensitive radar is used, the payload can be designed much more simpler. Experience has shown that the replacement of the "Robin" balloon in the standard payload of a Super Loki "Dart" by a handful of foils yields reasonably good tracking data, provided that the cloud is not exposed in a height too large for proper function as was the case during trial experiments performed with this arrangement.

The guardring probe experiment

The payload capacity of small sounding rockets is by no means exhausted by the relatively simple and light-weight foil cloud experiment. Wind and density data, though important are not sufficient to explain all phenomena but should be supplemented by simultaneous measurement of other atmospheric parameters like composition of neutral and of ionized components of the atmosphere. When ionospheric absorption is involved, the need is obvious to measure electron density. Quite a few methods to measure electron density have been developed using wave propagation experiments; but wave propagation experiments have only

a low sensitivity at lower heights. It is therefore suggestive to turn to DC-probes which can measure the difference of electron and ion conductivity at presence of collisions with neutrals. Such a probe must be able to measure the polar conductivity (separate measurement of electrons and ions).

One way to do this is to use a cylindrical capacitor through which the airflow is passing. Measuring the current/voltage characteristics, it is possible to derive carrier mobilities and concentration. From the mobility, carrier size in respect to size of ambient molecules, and by this, (to a certain degree) masses can be derived, while the concentration is given by the saturation current. Such instruments are known as "Gerdien" condensers. An instrument of this type has been developed here (28) (29) and was flown successfully (30) (31) (32) (33). Leaving off the outer electrode of the Gerdien cylindrical condenser and replacing it with the remaining part of the rocket body as the counter electrode, one obtains a configuration which can be considered as an "open" Gerdien system in the height region were collisions between charged carriers and neutrals govern the movement of charged carriers in an electric field. The field lines of the probe leave the surface of the probe at right angle and end at a distance for which the Debye length is a measure. The charged carriers enter this "sheath region" by diffusion and their further fate is determined by the configuration of the electric field and the distribution of charges within the sheath region. The sheath region represents the "collecting volume" of the probe. The size of the collecting volume is determined by the Debye length and by the number density of the charged carriers in the undisturbed plasma. When collisions between charged carriers and neutrals become negligible the probe response can well be described by theory and the probe is called a "Langmuir" probe. A theory which describes satisfactorily the response of the probe when collisions between neutrals and charged carriers occur is not yet developed. Therefore, one has to calibrate the results of such probes against other experiments performed simultaneously and uses "calibration factors" to convert probe currents into ambient electron densities.

Disturbing effects

The current measured with such a probe is not only caused by the number density of the ambient plasma but is affected by several other effects. Some of them are discussed below.

Photo effect

One of these effects is the liberation of free electrons from the surface of the probe electrodes. The amount of photocurrent varies with the work function and with the yield of the surface material. Though small, the photoeffect can considerably alter the result when electron temperature measurements are attempted in the usual manner by determining the slope at the "knee" of the measured current/voltage characteris of the probe. Attempts to produce surfaces which have low photo emission have been made (34). One solution is to cover the probe surfaces with a graphite coating. The graphite coating has a porous structure in which electrons liberated by radiation can be trapped. Another way to reduce the effects of photoemission is to reduce the size of the probe in respect to the volume from which the charged carriers are collected. The photo-current has the largest impact upon measurement when the probe currents are still small. When the probe currents become larger, the effect of photocurrents may become negligible because its contribution comprises then only a few percent of the total current.

Cosmic rays

Another source which might have an influence upon the measured currents is ionization by cosmic rays produced inside the payload section. Because of the large variation of pressure which is present during the short time of flight of a rocket, one cannot assume that the pressure within the payload section equals the ambient pressure. It is not unprobable that a pressure not too different from pressure measured at ground remains in the payload especially when no large vent holes are provided. Particle showers generated in the payload shell can produce ionization which causes currents to flow between differences of potential. By this, a "leak" current can be caused between the payload shell and the lead which connects the probe with the electrometer.

Coning of the rocket.

Another effect which can cause considerable uncertainty of the interpretation of results is the precession of a spinning rocket called "coning". Coning is caused by an unbalance of the rocket. Because the probe works in a regime in which the movement of carriers is determined by their mobilities, the difference in flow velocity at different positions of the precession cone causes a change of probe current. This modulation of the probe current by coning makes

it difficult to decide whether an observed change of probe current was caused by a genuine change of number density of charged carriers in the environment of the probe or was just produced by coning of the rocket.

An obvious way-out is to balance carefully the payload before launch and to use sounding rockets which are less susceptible to coning. Rockets which are less susceptible to coning are those which motors burn out at fairly low altitudes, because the atmospheric drag can then damp out oscillations which may be caused, for example, by spin-yaw resonance.

Electric charges on insulating surfaces

Electric charges which collect on insulating surfaces as the result of different accommodation coefficients can seriously affect the current/voltage characteristics when the probe potential is rapidly changed. The electric field of charges which remain seated on the insulator until they are neutralized by carriers of opposite charge disturb the field of the probe and modifies it. This in turn changes the current/voltage characteristics of the probe from what one should expect. Laboratory experiments performed here at different pressures have shown that this effect is in a rather complicated way dependent of pressure and of ion density. As a consequence, large insulator surfaces should be avoided at the vicinity of the collecting electrode of the probe.

Technical design of the experiment

Mechanical design

The probe was a 7 cm long insulated section of the nose tip of the rocket payload. It was made of steel. No significant difference of probe response was found between probes made of stainless steel and of ordinary mild steel. In order to obtain a clear configuration of the field line geometry and to remove effects which might be caused by distortion of the electric field at the transition between the measuring probe and the reminder of the rockets body, the probe was followed by a fairly long guardring section. This guardring section was kept on the same potential as the probing electrode. The guardring put the disturbance of the electric field lines to a place where it did not affect any more the electric field of the probing electrode. The guardring section further extended up to the point were the lead from the probe entered the current amplifier of the probe. This lead was a steel rod 2 mm thick orientated along the center line of

the payload. This rod carries the same potential as the probing electrode. If the section covered by the guardring would carry a different potential than the probe lead, it would act as a capacitor and if ionization would be present in this volume, the difference of potential would draw a current. Because both electrodes of this potential ionization chamber are at the same potential, no current is drawn.

The guardring arrangement has further advantages. The probe currents range between about 10^{-8} to 10^{-6} Amp. This value is low enough to pay attention to the quality of insulation in order to avoid leak currents which would be indicated by the current meter. When a guardring is used, the demands upon insulation are less because there is no difference of potential between the two electrodes. Further, the current meter is in parallel with the generator for the driving potential. This means that leakages which might occur in the insulation just load the driving potential generator but do not affect the indication of the current meter because its circuit is closed over the ambient plasma.

The guardring increases the capacity of the probe against the environment but this does not become effective because the two electrodes, tip and guardring, are at the same potential. This property can be used to advantage to solve the insulator problem: As was mentioned before, surfaces of insulators can affect the probe current by collection of electric charges. Collection of electric charges can be avoided by recessing the insulator and reducing its thickness. Because the increase of capacity by reduction of insulator thickness becomes neutralized by the guardring arrangement, it was possible to reduce the part of the insulator which is exposed to the open air to 1.5 mm and this was recessed by 5 mm. By this, about no electric charge can collect on the insulator. While it is not much of a problem to produce mechanical rigidness for the connection between measuring tip and guardring (the design is shown in Fig. 23), the fixture between guardring section and remaining part of the payload is a little more difficult to design because it has take up some bending forces and has to be failsafe even in case that the insulator cracks. The solution is shown in Fig. 24. An insulator section is centered in a center hole of the payload section and rests in a mating piece which has a thread. The thread fits into the guardring section. The insulator was fixed with screws alternately to the mating piece and to the payload. For protection against heat, an outer

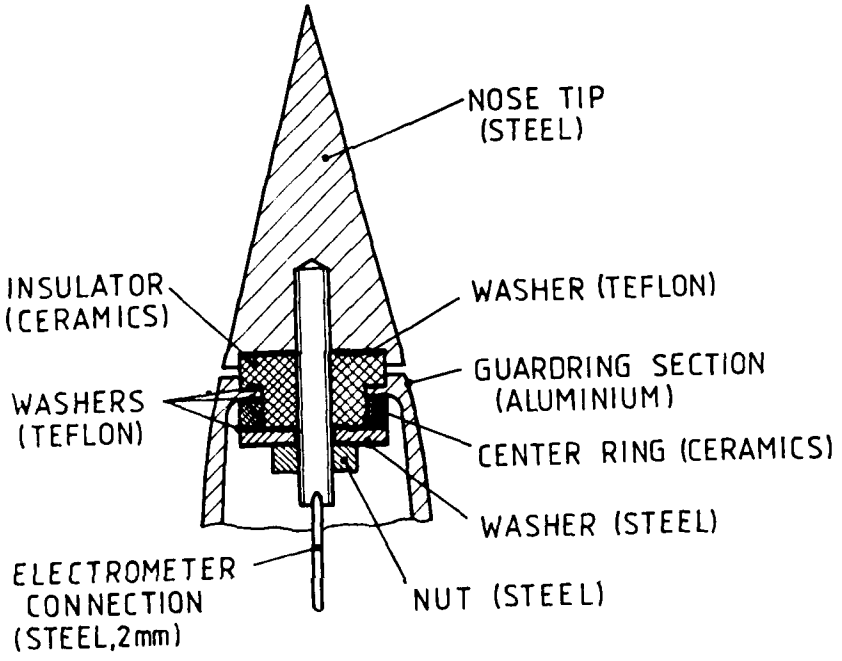

Fig. 23: Design of fixture between nose tip (measuring electrode) and guardring section of the payload.

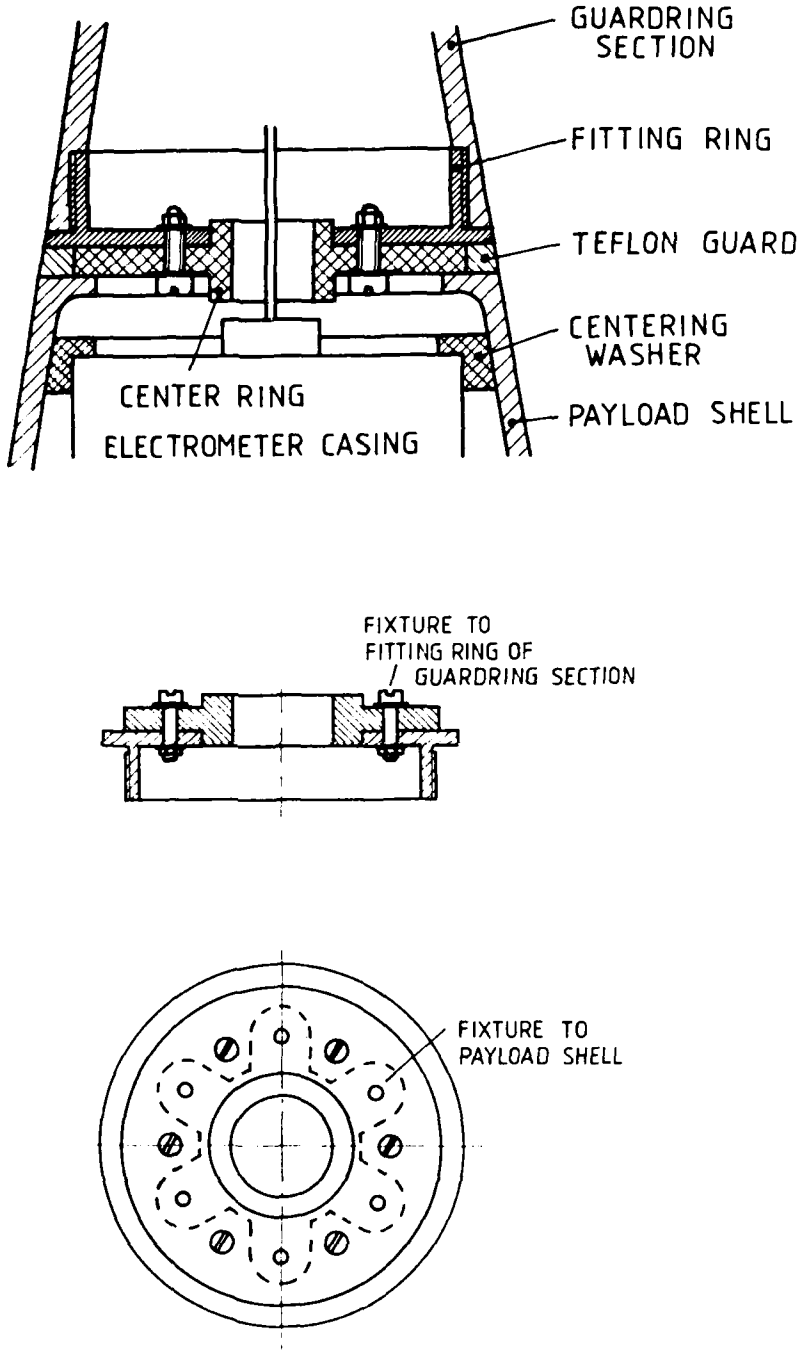

Fig. 24: Design of joint between guardring section of payload and payload ogival shell.

insulating ring made of "Teflon" was used which also confined the movement of parts of the insulator in case it broke under load. It was found in tests that the remaining strength of this joint was more than sufficient to keep the payload together under any conceivable load even when the insulator was completely broken into pieces. Later, this ceramic insulator (which is somewhat difficult to produce) was replaced by a machined piece of resinsoaked fabric ("Novotext"). "Novotext" has insulation properties sufficient for this application. It was protected against aerodynamic heating by the ring of teflon mentioned before which had a thickness of 5 mm.

The electric components of the payload which comprised batteries, telemetry, current meter and probe voltage generator were mounted on a conventionally stacked column-plate arrangement of standard "Duraluminium". In order to reduce weight, holes were drilled into the structure. This additional work could have been saved if the structure would have been made of magnesium alloy, but our workshops were not prepared to work with magnesium. Further, special treatment of magnesium surfaces is necessary in order to protect them from detrimental influences of the atmosphere for which neither "know-how" nor equipment was available. If such facilities are available, their use is highly recommended.

Heat transfer

In order to avoid resp. minimize transfer of heat from the outer payload shell into the payload and to its electronic components, the payload structure was joined to the payload only at its bottom end using a fairly high concentration of mass at this point in order to increase heat capacity. The plates on which the electronic components were mounted had no contact with the payload shell. The effective heat conduction from the warmer bottom section was reduced by the reduction of cross section of the columns which carried the payload bays. To provide mechanical stability against bending forces, a centering ring made of heat-resistant resin was placed at the top of the guardring payload structure. This ring took up bending forces caused by the rotation of the rocket during flight. The most sensitive part of the electronics, the current amplifier and the probe driving voltage waveform generator was housed in a cylindrical box

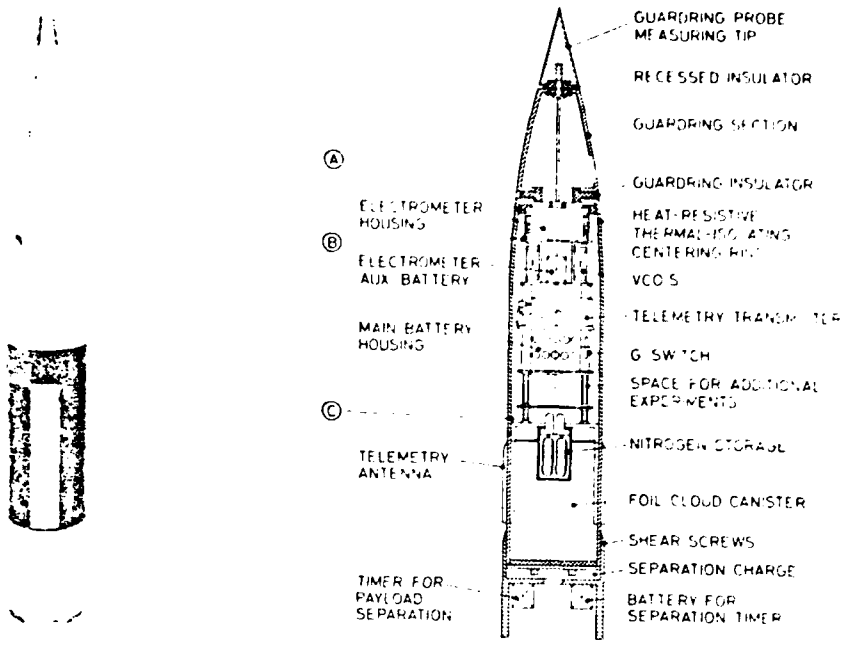

Fig. 25a: Section through payload. (Not to scale). A, B, C indicates locations were temperature sensors were placed on different flights.

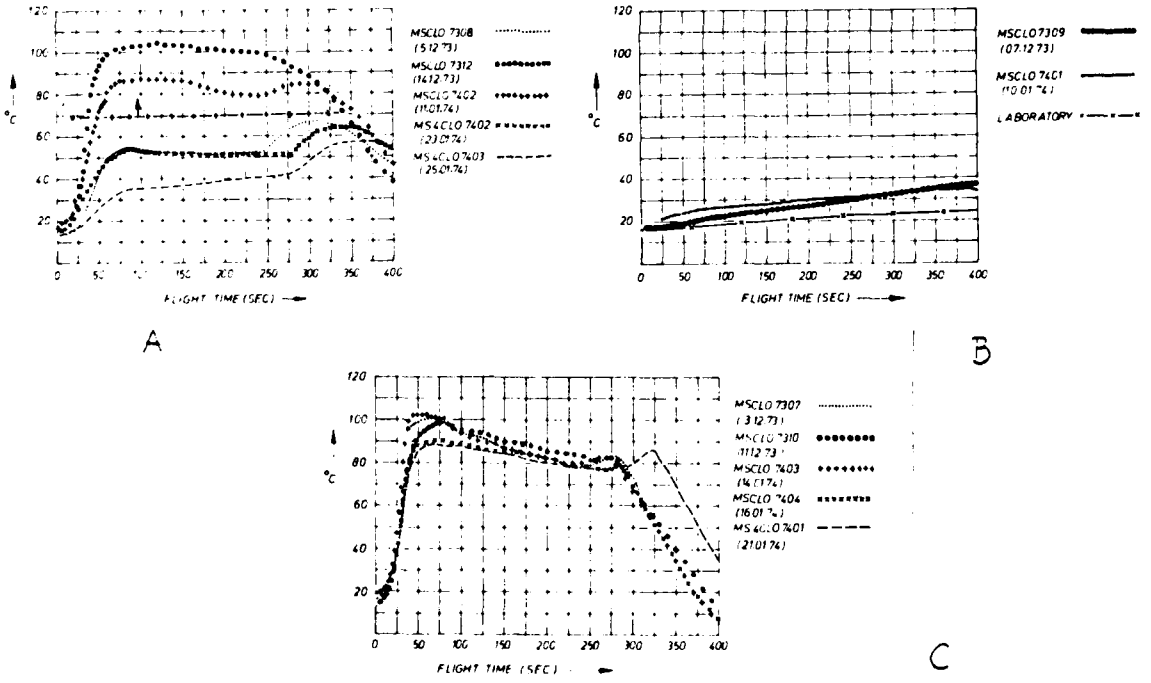

Fig. 25b: Results of temperature measurements: A: Measurements at point A (Spacer, see fig. 25a) during different flights. Radial position of sensor was varied from flight to flight. B: Measurement at the bottom of electrometer case. C: Measurement at the top of telemetry transmitter. D: Measurement on inner surface of a hatch at point (fig. 25a). Apogee was reached after 156-160 see flighttime.

in order to protect it from heat transfer by radiation. The same measures (no contact of the printed plates to the shell of the box) were used to minimize heat transfer. Adequate vent holes near the end of the payload's ogival section were provided to reduce the pressure inside of the payload during ascend. These measures turned out to be sufficient to keep the temperatures within acceptable limits. Liberal use was made of the fact that the rocket does not have to perform a sustained flight over long periods of time but is subjected to heating only over a certain portion of the flight. This allows the application of heat sinks, for example a relatively thick nose cone ogival section.

Results of payload temperature measurements

The effectiveness of the measures mentioned before was proven by temperature measurements made during a number of flights. Only one channel was available for transmission of temperature data. The temperature measurements which are shown in the following figures were made on several selected points (which are indicated in Fig. 25), on different flights. The sensor was a NTC resistor. It size was chosen to be about equal to those of resistors used in the electronic circuits. The reason for this choice was that not the absolute temperature data were of interest but the response of typical electronic components to ambient conditions found in the payload.

One notes that the heating occurs only during the first part of the flight but temperature remained almost constant at the heights which were of most interest.

Mating of the foil cloud experiment

The foil cloud experiment was mated with the guardring experiment by using the cylindrical section of the payload. It was not necessary to provide any heat insulation in this payload section because the temperatures remained within acceptable limits. The gas storage vessels were mounted in a can which protruded into the cylindrical section. By this, the space available for the foil clouds were somewhat reduced. This reduction however turned out not to affect very much the performance. Two gas jets as mentioned before were used to distribute the foils during expulsion.

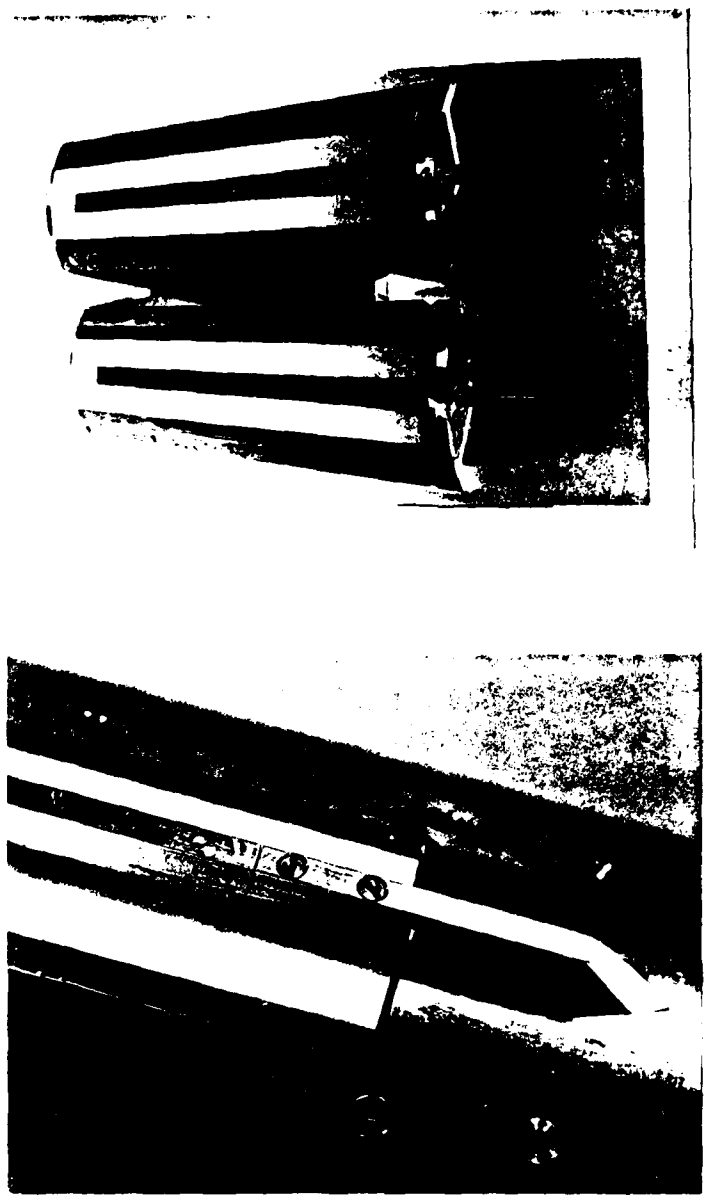

Fig. 25c: Photos of the P-band antenna. a: first version, b: Detail (heat barrier) of final version.

Antenna design

One of the most difficult task was the design of the antennas which are necessary to transmit the data to the ground. P band (230 MHz) telemetry had to be used. This posed problems because the wavelengths of these frequencies are almost comparable to the dimensions of the rocket; and the diameter of the rocket was quite small (13 cm). Further, the rocket had to remain aerodynamically "clean", that is, no protruding elements were allowed to be used which would cause additional drag (which would result in lower apogee) and might destabilize the rocket. Further, the antenna should not consume any appreciable space of the cylindrical section because this space had to be used for the foils. Further, mechanical stability was of prime importance, which meant that the antenna should under no circumstances weaken the structure. The antenna structure should be able to take up all loads and stresses present during flight. The final result was a very flat antenna element of the "travelling wave" type. It was imbedded into teflon which in turn was housed in an aluminium case of about triangular shape. This case was mated flush into a rectangular cut in the cyclindrical payload shell. The antenna case was fastened securely to the payload shell with screws and was, by this, part of the structure which carried the load.

Such type of antennas are rather critically in tuning (tuning was provided by a screw rod at the "hot" end of the antenna which acted as a capacitance). It turned out during the first flights that this antenna design ran out of tuning when heated. This detuning resulted in a degradation of signal strength. This was remedied by a slight change in that the antenna was made to protrude by about 10 mm from the payload skin. To protect the antenna from heat, a heat barrier in front of the antenna separated by a slot from the antenna element was provided. To reduce drag, the front end of the heat barrier was wedge-shaped in two dimensions. The results of flights showed that this protruding antenna had no discernable effects upon apogee. This is possibly due to the fact that the antenna was placed behind the point were boundary layer detachment occurs, resp. it was placed inside the boundary layer. Photos of the antenna are presented by Fig. 25c.

Payload separation

For ejection of the foil cloud experiment, the payload must be separated from the motor in order to expose the rear end of the payload. The joint between payload and motor must however remain rigid during flight, because it is subjected to considerable bending forces during the initial phases of the flight when the

motor is still burning. A reliable and rigid joint was obtained by inserting the payload section into the ejection section (see Fig. 25). This demands that the diameter of the ejection section becomes slightly larger than the diameter of the payload. To avoid jamming, the depth of insertion should be about half the diameter of the payload section. The wall thickness of the ejection section was 4 mm. In order to reduce friction, the surfaces of the joint were treated with molybdenium sulfide. (Other heat-resistant lubrication materials like silicone could be used as well). The payload was fixed to the expulsion section at the upper end of this section with four shear screws made of soft aluminium. These shear screws are standard hardware of the "Skua" rocket system. For adjustment, four further screws were used which touched the rim of the lid of the payload canister at its lowest end. These screws allow to correct tolerances and allow to adjust the payload to be in line with the rotational axis.

Choice of propellant for the expulsion charge

A peculiarity of the Skua rocket system is that the center of the top of the rocket motor is occupied by a thermoswitch. This thermoswitch retracts at motor burnout and activates the timer. This arrangement does not allow to place an expulsion charge at the center but forces one to use a ring-shaped charge. It was found by experiment that propellants used in conventional gas generators are burning too slow when put into a ring-shaped charge. A propellant was needed with a high burning rate. For several reasons a charge made from a stochiometric mixture of potassium permanganate and magnesium powder (total 20 g) was used. This meant that momentum transfer was used instead of gas pressure to expel the payload. This charge, being rather cheap and easy to handle, turned out to be very reliable and safe against temperature shocks. (The mixture did not ignite when exposed to 300 C and can easily be made inert by moisture). The charge was enclosed in a plastic disk which had a circular groove and was protected against moisture by sealing the lid of the disk with epoxy resin. The expulsion section itself was made as airtight as possible in order to preserve an overpressure of order of 1 Bar. This overpressure preloads the shear screws and facilitates separation of the payload.

Cable wrings of the payload

One problem which caused a serious difficulty during the first stages of development was the use of conventional "cable-trees" to interconnect the electric

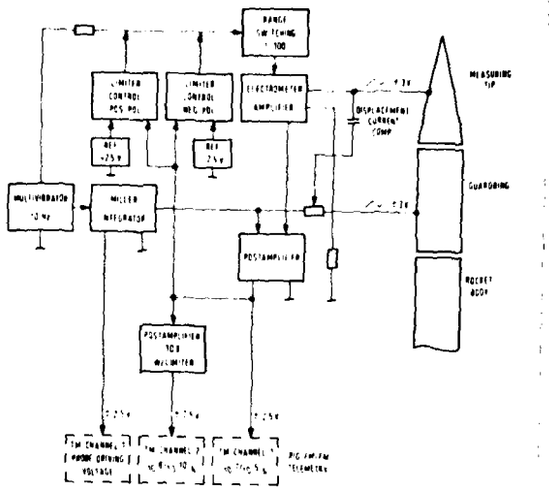

Fig. 26: Block diagram of guardring probe electronics.

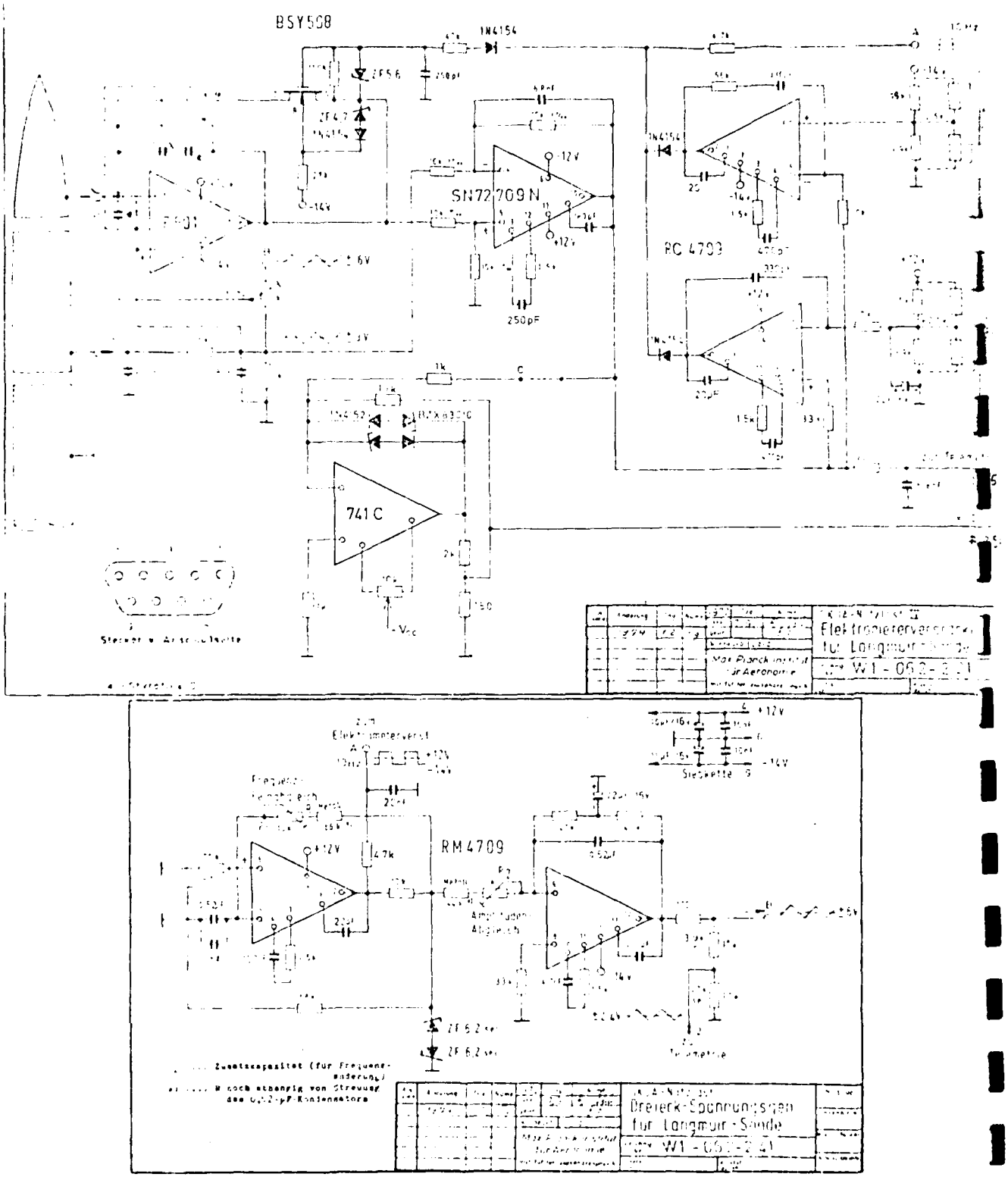

Fig. 27: Circuit diagram of electrometer/waveform generator for guardring probe.

components of the payload. On three test flights two rockets went into flat spin shortlyafter burnout of the rocket motor despite the payload was tested thoroughly before flight. A remaining payload was investigated on a balancing machine in order to find out the cause. Originally, specification for payload acceptance tests was to spin the rocket at average spin frequency for some minutes. During these new tests, the spin frequency was increased to the maximum value observed during flight which is found at time of motor burnout. When this frequency was approached, a large moment of imbalance developed which could be just kept under control by switching off the balancing machine and activating the emergency brake. Inspection of the payload revealed that the cable trees started to deform quite rapidly when the centrifugal forces exceeded a certain value, despite they were carefully fixed with clamps to the structure.

This result illustrates that it is more important for small rocket payloads to test their rigidity and their behaviour under the influence of centrifugal forces rather than to test their resistivity against vibrations, and, further, to balance them carefully by moment and couple for the highest spin frequency to be expected (for the case of the Skua II vehicle, the maximum spin can be as high as 18 rev . sec-1 compared to 10 rev sec-1 as the average).

As a consequence, about all interconnections between payload components were made via printed circuit boards safely fastened to the payload structure. The use of printed circuit boards has the further advantage that printed boards are very easily and cheaply produced and that about no error can occur during wiring. This means that even very unexperienced people can put a payload of this kind together provided they are able to produce good soldering connections. The result was a technical success rate of better than 98 percent out of more than 100 launches.

ELECTRICAL CIRCUIT

Probe circuit and telemetry

The block diagram of the electronics of the guardring probe is shown in Fig. 26. The diagram of the circuit shows Fig. 27. This circuit was a derivative of a current meter developed by Dr. A. Loidl for another experiment which was not flown. The design stems from 1968/1969 and might possibly be improved today by using more modern components. The probe driving voltage generator is in series with the probe current amplifier. The probe driving voltage sweeps linearly between +3 V and -3 V. The wave form is symmetrical. This means that the

displacement currents generated due to the capacitance of the probe are of equal magnitude when the voltage sweeps form +3 V to -3 V and vice versa. The repetition frequency of the waveform is 10 Hz. This means that current/voltage characteristics are measured with a repetition frequency of 20 Hz. This in return provides a fairl large resolution of height (75 m at the highest speed of the rocket (1500 ms^{-1})). The displacement current remains small (10^{-9}A) compared to the conduction currents to be expected in the D-region of the ionosphere and could be neglected but it was decided to compensate them. This was done by deriving a square wave from a symmetrical sawtooth probe driving voltage wave form of opposite phase. A small adjustable capacitor connected to the input of the current amplifier was used for this purpose. The square waveform was also used to activate a FET switch in the feedback circuit of the current amplifier in order to change its sensitivity. Switching of sensitivity of the current amplifier was necessary because it was decided to use a linear scale rather than a logarithmic one to transmit the current/voltage characteristics. A linear response of the amplifier was considered to have an edge over a logarithmic response because any malfunction or non-linearity is immediately recognized in the current/voltage characteristics. Further, a linear characteristic facilitated calibration and evaluation. The large dynamic range of the probe currents to be expected, however, requires switching of the sensitivity of the current amplifier. This was done alternatively by changing the value of the feedback resistor of the current amplifier by activating the already-mentioned FET switch once during one period of the probe driving voltage waveform. The sensitivity of the current amplifier was by this changed by a factor of 1000. In order to cover four decades of current, a second TM channel was added which transmitted the output of a post-amplifier of the current meter. This post-amplifier amplified the current meter output by a factor of ten. The post amplifier had limiter properties to keep the output to $\pm$ 2.5 Volt. $\pm$ 2.5 V is the standard input voltage swing of standard IRIG FM/FM VCO's. By this, adequate coverage of current readings was obtained for the range 10^{-9} A ... 10^{-5} A.

Telemetry

For transmission of data, standard IRIG FM/FM telemetry was used. Transmitter output power was 2,5 Watt. The telemetry transmitter was a standard crystal-controlled phase-modulated transmitter of the same type as used on satellites. In one case, a modification of this transmitter which had an output frequency of 1830 MHz was used on ARCAS rockets. The voltage-controlled subcarrier oscillators

made by the same manufacturer however turned out to be less satisfactorily because of drift and should be replaced by a better design.

Data recording was made on UV sensitive paper using a high speed light recorder. For backup, recording was made on magnetic tape. Analog recording on paper has the advantage that the data are available immediately after flight, that the data are easily and quickly evaluated by hand or by semi-automatic devices and that even a certain amount of noise can be tolerated before the data have to be considered as useless. Digital transmission of data even in its simplest forms of technical realization requires a much better signal to noise ratio than analog transmission and causes an increase of payload complexity (with associated increase of costs) with all its inherent sources of errors and malfunctions. Of cause, the advantages of simplicity and of low band with requirement for data transmission has to be traded against accuracy, but an overall accuracy of 5-10 % was tolerable for this application.

Activation of payload electronics

Standard practice is to turn on electric power in the payload short before launch by using an umbilical connector which operates a latching relay. The umbilical connection allows testing of the payload up to the last moment. The umbilical connector is either pulled off short before launch by remote control (sometimes also by hand) or just torn off during launch. This is a procedure which can be easily done on rockets launched from rails but is somewhat difficult to execute when the rocket is launched out of a tube. A hatch in the tube is needed in most cases, and a check if the umbilical was retracted correctly is somewhat difficult. On small rockets, the umbilical socket might spoil the aerodynamical properties. On a larger vehicle this effect can be considered as unimportant. If, for some reason or the other, the plug of the umbilical remains on the rocket, the change of aerodynamics can seriously affect the flight performance of a small vehicle. (It was, however, found that the Skua rocket can be flown with fairly large holes (diameter 15-20 mm) in the nose cone ogival without serious detoriation of flight performance but this should not be recommended because apogee becomes reduced). Further, a telemetry transmitter operating on a live rocket inside of a steel tube should be considered as a hazard and should therefore be avoided. During ignition, a shock wave travels through the motor which is transmitted to the payload followed by launch acceleration. The ignition shock can be quite severe (several thousand g). The ignition shock might cause transient shorts in electric components which are easily survived by a "dead"

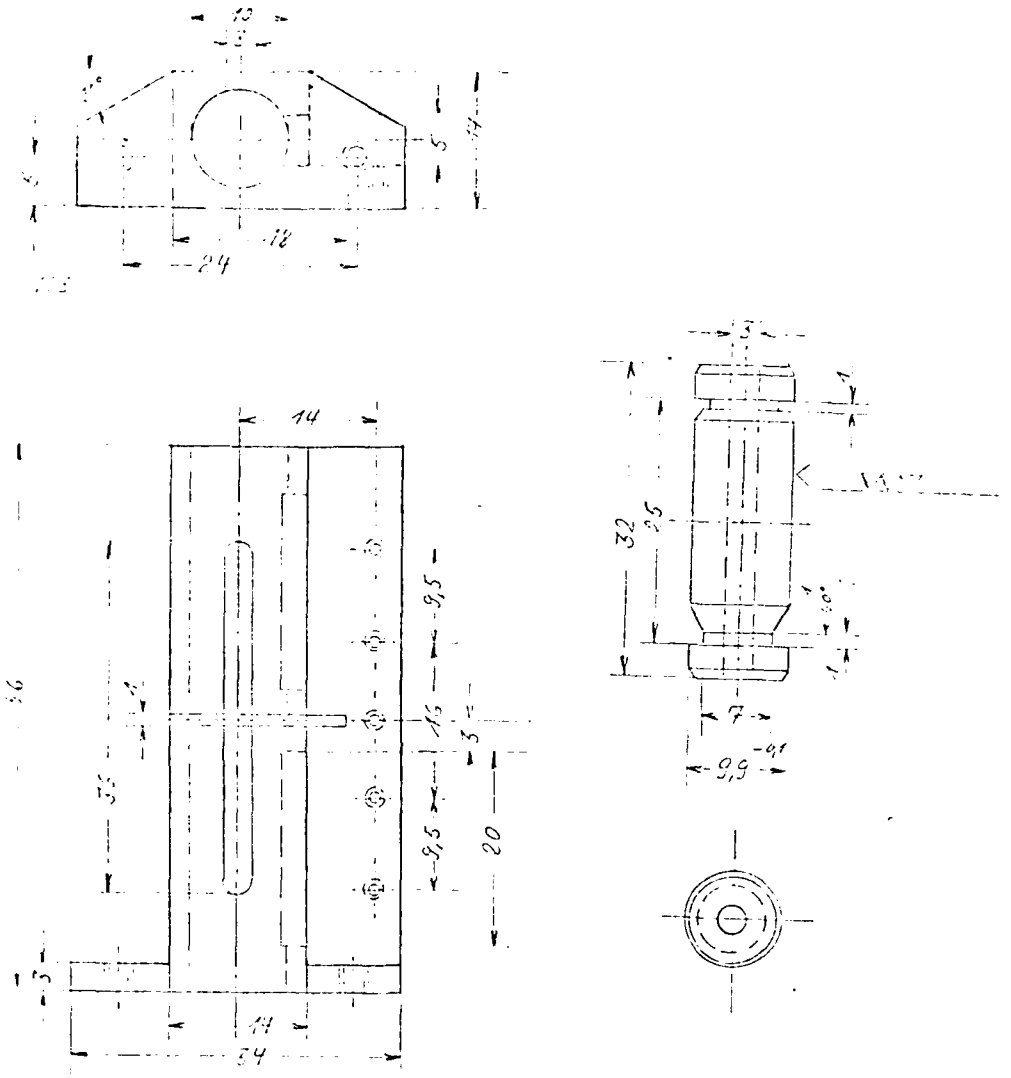

Fig. 28: Design of G-Switch used to activate payload electronics by launch shock.

circuit but can turn out to be disastrous when power is applied. The obvious way-out is then to apply power after ignition and after the initial acceleration phase. This can be done by a g-switch but calls for a careful design of the payload electronics. The electronics must stabilize within a few seconds. Stabilization of an electronic circuit is a matter of proper choice of components. In our case meaningful measurements could be expected after a flight time of 50-60 sec. Our payload electronics was designed to stabilize within less than a second. This allowed to perform already some measurements even in the troposphere. Cirrus clouds could be detected as well as the electric field near the surface of the sea which is caused by ions. Final testing of the payload on the launch pad was considered not necessary because each payload was tested thoroughly during preparation. (This included spinning at maximum spin rate before delivery.) It was known to withstand severe shocks and was designed in a way that any damage during rocket preparation work was impossible. A payload which would not stand normal handling procedures during rocket preparation work would not survive the launch shock and should therefore be considered as unsuitable.

It offers itself to use the launch shock to activate the payload electronics by a g-switch. The requirements for this g-switch are low: It should be inoperative when subjected to normal handling, should be sensitive only when the force acts in the direction of the longitudinal axis of the rocket and should operate when the g-load exceeds 50 g. The time lag between application of the acceleration and closing of the switch is unimportant as is the actual amount of accelerations. This allowed to use a rather simple design. This design is shown in Fig. 28. A brass block is held in a tube by a hairpin-shaped spring on its lower, conical end. The block starts to move downwards under the influence of inertia forces and passes two microswitches. These microswitches are then closed. Two microswitches were used in order to provide redundancy. The block is held in place on its lower resting point by the same hairpin spring which was used to keep the block in place during normal handling. The hairpin spring jumps into a groove at the rear end of the block and keeps it firmly in place. A slot is provided in the g-switch casing which allows visual respection of the state of the g-switch. Because the block has to travel a certain path on its way downwards until the microswitches close, (the length of this path depends upon the length of the block and upon the position of the microswitches) a time lag between application of the acceleration and closing of the switches is present which is

desired. The actual time delay depends upon the amount of acceleration but is sufficiently long to keep the ignition shock away from the payload electronics. This kind of switch is easy to build, relatively inexpense, and has never failed. It can be built in almost any shape. By principle, one could use also a spin-sensitive device. This idea was however abandoned because the spin of the Skua builds up too slowly and is not as constant as is the acceleration at launch.

Power supply

Three silver sinc-batteries (SZ6) were used as main battery to supply electric power. Its voltage was controlled by an appropriate circuit. Auxillilary voltages needed for the electronics of the probe current amplifier were supplied by standard dry batteries cast into resin. Casting into resin was used to render the batteries shock-proof.

Method of conversion of probe currents into ambient electron densities

"Langmuir" probes have been used quite extensively since the early attempts of in-situ measurements of electron density in the ionosphere. While such probes seem to yield consistent results for heights well above 90-95 km for which a theory has been developed which seems to describe reality quite satisfactorily, the conditions found at lower heights in which collisions between particles and and neutrals play a role for resp. dominate the movement of charged carriers in the electric field of a probe are much more complex. As a result of this complexity a theory of operation of such DC probes has not yet been developed. Empirical conversion factors have been derived instead by comparing the measured probe current with the results of in-situ measurements of electron densities which were obtained with wave propagation experiments. It turned out that the calibration factors of the probes derived by comparisons with results obtained with wave propagation experiments may vary up to a factor of 4-5. This seems to exclude their use as a measuring device. But because wave propagation experiments have only a limited resolution of height, they are not suitable to investigate fine structures of the ionosphere for which the "Langmuir" probe is then used after proper calibration by the wave propagation experiment flown on the same payload.

In our case certain constraints did not permit to develop an in-situ experiment based upon radio frequency wave propagation, but ground-based wave propagation experiments were used to measure radio wave absorption on an absolute scale. (See part I of this report.) Further, an ionosonde was available to measure

critical frequency and reflection height of the probing wave. Therefore, the numerical value of the integral: $\int_0^h (N_e \cdot \nu_{en})\, dh$

(ν_{en}: electron-neutral collision frequency, N_e: electron density) which corresponds to the amount of radio wave absorption was known with quite a high accuracy, and the propagation path over which this integral extended was also known because it was in all cases the 1XE-hop mode. The latter was assured by the choice of the operational frequency of the circuits, its path length and by the choice of antennas. Assuming that the ionospheric conditions do not vary very much over the path of wave propagation, the ionosonde data yield the reflection height of the probing wave, and by this, the propagation path of the wave is known. The guard-ring experiment shows that the electron currents are proportional to applied probe driving voltage up to a certain height which corresponds to the height in which the mean free path corresponds to the mean diameter of the probe. The mean free path depends upon pressure. As Phelps and Pack (35) have shown, the collision frequency of electrons depends upon pressure. Therefore, pressure data are required. These can either be obtained by independent in-situ measurements (for example, from the fall rates of the chaff cloud) or can be taken from Standard Atmosphere data which may be considered for this purpose to be sufficiently accurate. Up to the height where the mean free path is small against the dimensions of the probe, the ambient electron density can be put as Ne = C.I (I = probe current). Above this height, a correction is applied of the form C.I.exp.$(\alpha \cdot (h-ho))$, ho being the height in which the probe dimensions become comparable to the mean free path of the electrons. The well-known transmission curve technique is used to derive the angle of departure and the angle of arrival of the probing wave from ionograms taken before, during and after the flight. For simple analytic treatment, the magnetic field is neglected near the reflection point of the wave but is re-introduced when absorption is calculated for upleg and downleg of the wave. (This approximation is well-known and accepted.) The constants C and α which relate the probe currents to the ambient electron densities are then computed in the following way: Starting with the angle of incidence obtained from the ionograms by the transmission curve method, a pair of C and α are chosen and a ray tracing is performed by adjusting C and α until the ray is "homed in"

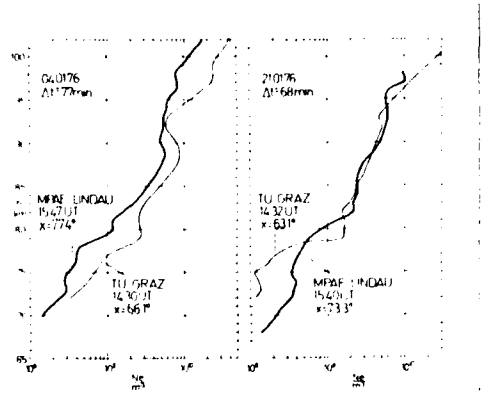

Fig. 29: Comparison between electron density profiles derived from guardring probes current measurements using the method outlined in the text and those for which a wave propagation experiment was used.

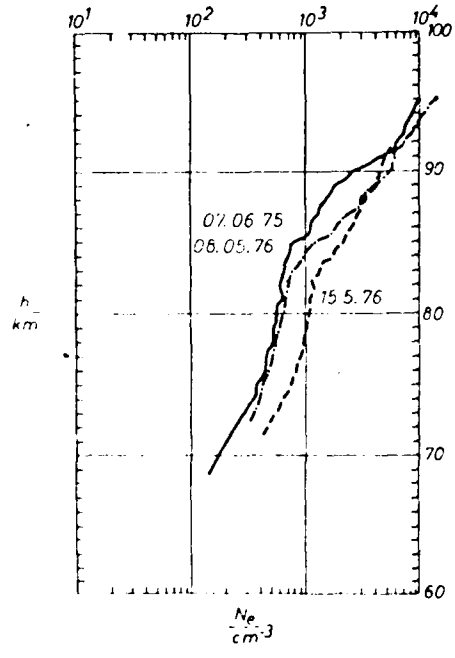

Fig. 30 Electron density profiles measured during Spring/early Summer.

that is, the ray meets the receiving point at the right angle of arrival. Taking into account the magnetic field of the earth, the full Senn-Wyller formalism is then used to calculate the absorption of the ordinary ray using electron collision frequencies derived from the air pressure. At first, α is varied. If the calculated absorption does not fully fit the observed value, the constant C is changed a little in the desired direction and the calculation is repeated from the very beginning. This procedure will be repeated until calculated and observed absorption coincide within a certain margin ($\sim$ 3 dB). In order to facilitate calculation, the electron density profile was approximated in the immediate vicinity of the reflection level of the wave by an exponential in order to render the problem analytically treatable. The error introduced by these approximations can however not be very large because a reasonably good agreement was found between electron profiles derived this way from probe current profiles and with those measured with wave propagation experiments, especially if one takes into account the difference of time when these measurements were made (see Fig. 29).

A further indication that the method described above yields reasonable results was that the approach fails if a reflection height is assumed (or determined from the ionograms) which does not meet reality. This was proven by model calculations in which the reflection height was intentionally changed, and by cases in which a sporadic E-layer was present over parts of the propagation path which was lower than the reflection height determined from the ionograms taken at the launch site were this E-layer was not seen. This sporadic E-layer was then seen in the ionograms taken over another location close to the receiving site located at the range. The method then failed until the proper height (that of the E-layer) was chosen.

A further result was that the constant C varied by the same amount which was found for conversion factors derived from comparisons between probe measurements and in-situ wave propagation experiments. A possible reason for this variation of the conversion factor shall be discussed later.

RESULTS OF GUARDRING PROBE MEASUREMENTS

Electron density

A fair amount of individual flights have been performed between 1972 and 1976. Most of these flights were launched near noon for reasons outlined before: The temporal variation of absorption is in most cases smallest at this time of the day and its amount is in most cases the highest. (This however, holds only true for the summer season) but some flights were also launched during afternoon (Winter 1975/76). The results of all these measurements allow to synthesize a

picture of phenomenological changes of electron density and admits some speculation about possible causes.

Electron density during Spring and Autumn

Relatively few measurements of electron density have been made during this season. At first sight, they seem to have nothing in peculiar different from profiles observed over other locations. A "ledge" or "shelf" is well pronounced near 85 km which is common to most profiles ever measured, but the ledge seems to be often less sharp than observed on profiles obtained at higher latitudes, for example, at South Uist (58° N). This feature of the El Arenosillo profiles could, by principle, be an artifact caused by the evaluation process, but this interpretation seems to be not valid because some electron density profiles do have a very sharp and pronounced ledge.

In general, the probe current profiles measured over El Arenosillo show an increase with height which is close to exponential. The conversion factors for the electron current vary very little during these seasons. Some difference was observed for Autumn profiles in that the "ledge" seemed to be more pronounced and that the electron density near 90 km was somewhat higher. This held true also for profiles measured during early winter, but the number of measurements were too small to decide if this observation was accidental or not.

Electron density profiles measured during winter: "normal" conditions

Salient feature of winter radio wave absorption is its tremendous variability of both, amount and of shape of diurnal variation. The amount of absorption can by far exceed summer values on certain days, (this condition is therefore called winter-anomalous) and can be very low next day after. This variability renders it at first rather difficult to define what should be termed "normal". An obvious definition would be to say that a day is "normal" when the amount of absorption corresponds to that what should be expected from the seasonal variation of the sun's zenith angle. This clear definition is however hard to use in practice unless one has a reliable reference (which could be supplied when the measurements are made on an absolute scale) and a parameter which eliminates the seasonal variation of the sun's zenith angle. The parameter $L_D = L_o/n+1$ has

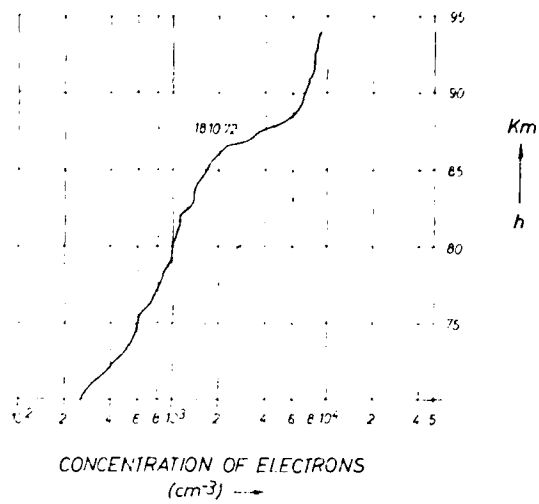

Fig. 31: Electron density profile measured in Autumn.

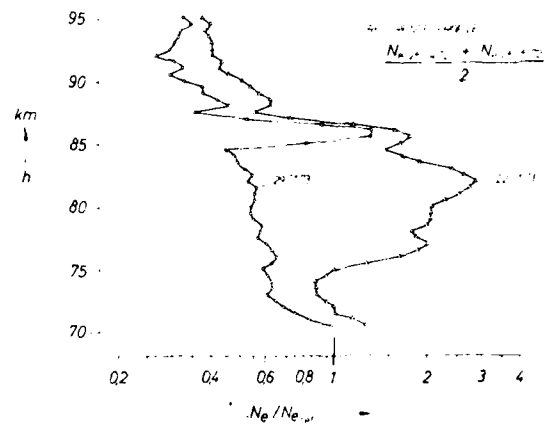

Fig. 32: Enhancement of electron density during a winter-anomalous day in reference to conditions found on a "normal" winter day and during Spring/early Summer.

this property. (This was outlined in part I of this report.) L_D was therefore used to distinguish if a day should be considered as "normal" or "winter-anomalous". Considering "normal" days, one notes that the electron density profiles retain some of the features observed during Spring resp. during Autumn in that a ledge is still present, but display at the same time an unexpected peculiarity: The height level above which electrons can be distinguished from ions as a change of slope of the current/voltage characteristics when the driving potential of the probe is crossing zero volts is much lower than was found in Spring/early Summer electron density profiles. Considering the seasonal variation of the zenith angle of the sun, one might expect the reverse. Further, the ledge was often much less pronounced in winter profiles than it was in summer. The electron density profile was "more exponential" during winter even under "normal" conditions.

Winter-anomalous conditions

Electron density profiles obtained when radio wave absorption was winter-anomalous had about the same shape as was observed over other locations. A fairly large increase of electron density was found at heights were the "ledge" was seen when conditions were more or less "normal". The enhancement of electron density was about of same amount as was reported by other authors if one takes the difference of latitude into account. In this respect, nothing new was found if the electron density profiles obtained under winter-anomalous conditions were considered solely. The bu.. of electron density enhancement is quite well seen when the profiles of a "normal day" and that of a winter anomaly are normalized to an average profile which was measured under undisturbed conditions during Spring/early Summer. An example is shown in Fig. 32 (36). One notes that the relative enhancement of electron density on a winter-anomalous day was confined to heights between about 87 to 75 km. This bulge was superimposed to a slope of electron density which was about the same like that found for a reference day on which absorption was, according to the $L_o/n+1$ criterion, normal. It turned out that this criterion means very low absorption. The peak superimposed to the profile found for the 29.01.73 is however not real but an artifact. It is just caused by the fact that the ledge was by about 3 km lower when the winter measurement was made. This result can be taken as an indication that the physical processes which produce ionization in the D-region of the ionosphere under normal conditions during winter are essentially the same than those present during the other seasons and that the enhancement of electron density must definitely be caused by a trace constituent which is not present in numbers when conditions are normal.

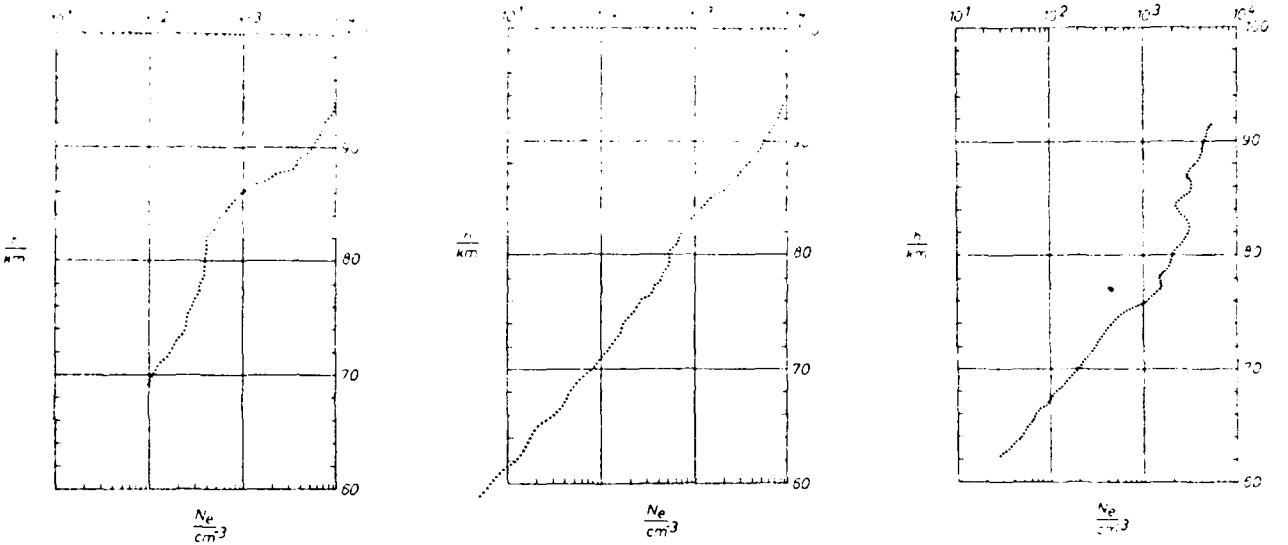

Fig. 33: Electron density profiles measured during winter. Transition from "normal" to winter-anomalous conditions.

Time development of winter-anomaly electron density profiles in the D-region of the ionosphere

Due to the relatively low cost of the experiments and rockets, a fairly dense sequence of in-situ measurements of electron density could be made near noon, and, in a later program, during afternoon in several winter seasons. This high density of measurements allowed to follow the development of the winter-anomaly electron density profile rather closely. A final discussion is however hampered by the fact that the diurnal variation of absorption is in the majority of all cases everything else but regular (this question was discussed at some length in part I of this report) but a few profiles were obtained under absorption conditions regular enough to allow a synthesis of the development. This development might however follow different time scales not synchronized with the variation of the sun's zenith angle. It may need several days, but also may happen in the course of a day. This fact complicates considerably an analysis of data.

If one compares a winter-anomaly electron density profile with a profile measured under Summer conditions, one notes (as was mentioned before) that the ledge found in a summer profile (as well as in a "normal" winter profile) is replaced by a "bulge" at approximately the same height. Looking closer, one may note on several profiles that their "lower end" and their "upper end" seem to follow fairly closely an exponential while the "ledge" or the "bulge" seems to be caused by a reduction or increase of electron density. (See Fig. 33).

This causes one to suspect that a pre-stage may exist in which the "ledge" caused by a depletion of electron density is filled up so that the electron density profile becomes more or less exponential with height. The decrease may be caused by an increase of electron loss rate caused by some minor constituent which is common to normal D-region atmospheric composition. One might expect such exponential profiles when the amount of absorption becomes quite close to winter-anomalous. Such profiles were found but, surprisingly, not when absorption was close to winter-anomalous but when it was rather low, or very low, and as far as can be judged from the set of data, were found most frequently at the beginning of winter (during December), when the transition from "summer" to "winter" conditions occurs but the data gathered during the Western European Aeronomy program (Winter 1975/76) in which the launches took place during January indicate similar results. However, the launches had to take place then during afternoon. This renders a direct comparison with the earlier results somewhat difficult.

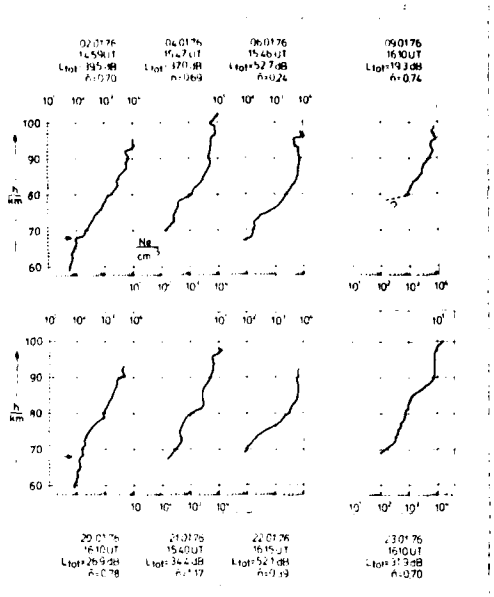

Fig. 34: Development of winter-anomalous absorption observed at time of launch (afternoon) during Winter 1975/76 over El Arenosillo (South-West Spain): Electron density profiles.

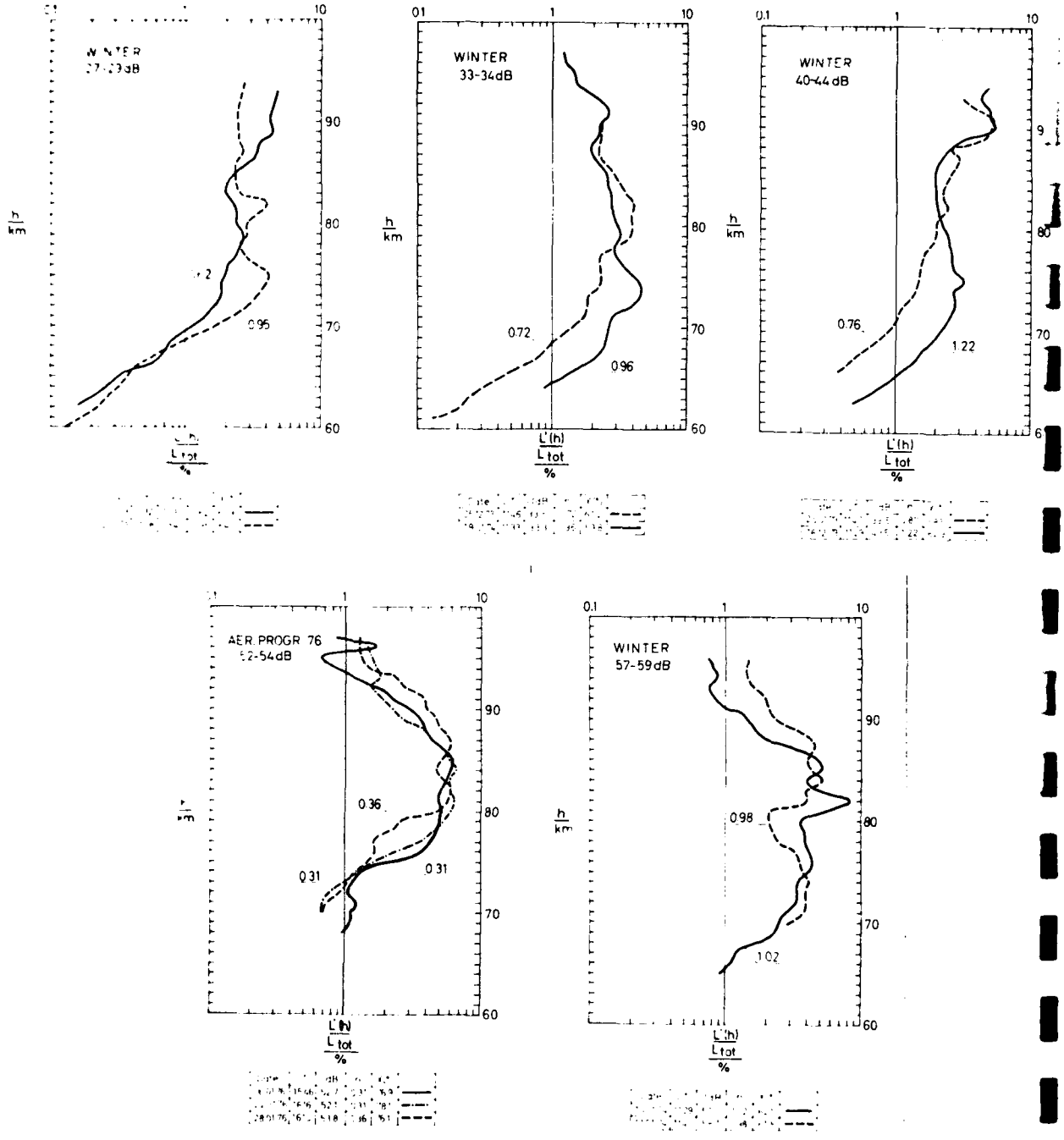

Fig. 35: Relation between shape of diurnal variation of absorption (described by $(L(X) = L_o \cos^n X)$ and height distribution of electron density: If "n" is large (of order 1) the electron density is enlarged below about 80 km, as is the relative contribution to absorption $L'(h) = \frac{dL}{dn} \cdot \frac{1}{L_{tot}}$

But on three occasions a similar development of winter anomaly as described was observed during this campaign: About two days before a winter anomaly day, electrons could be distinguished from ions at a rather low height already. Absorption was then fairly low. The electron density profile did not show a pronounced "bulge". The now well-known winter anomaly bulge developed during the next days and the winter anomaly condition ended when a well-pronounced "ledge" appeared again near 80 km (37) (38). The sequence of electron density profiles obtained during this program is shown in Fig. 34. The matter shall be discussed later.

Electron density distribution and shape of diurnal variation

The fairly large number of individual measurements made at the same time of the day performed under different absorption conditions allowed to compare electron density profiles observed under similar conditions of absorption. This comparison yielded the time history of development of winter anomaly radio wave absorption which was mentioned in the preceding paragraph but revealed also a relation between the shape of the diurnal variation of absorption and the height distribution of electron density. (The problems which one encounters if one considers the shape of the diurnal variation of absorption were outlined in detail in part I of this report.) For description of the diurnal variation of absorption, the exponent "n" of the cos $n\chi$-law was used. It was found that the electron density was slightly higher below about 80 km when the cos χ-exponent "n" was large ($n \sim 0.9...1$) than it was the case when n was "low" ($n \sim 0.5$). Considering that the radio wave absorption at a certain height h is determined by the product: electron collision frequency times electron density, a more appropriate parameter for eludication of differences is the specific absorption $L'(h) = dL/dh \cdot 1/L_{tot}$, that is the contribution to total absorption of a slab of thickness dh normalized to the total amount of absorption observed during the flight of the rocket. Fig. 35 shows, that the relation: "high n, more electrons below 80 m" was found for all cases for which comparable observations were available, low, medium and winter anomaly absorption. This seems to hold true also for spring and early summer conditions as Fig. 36 shows but the number of measurements were quite

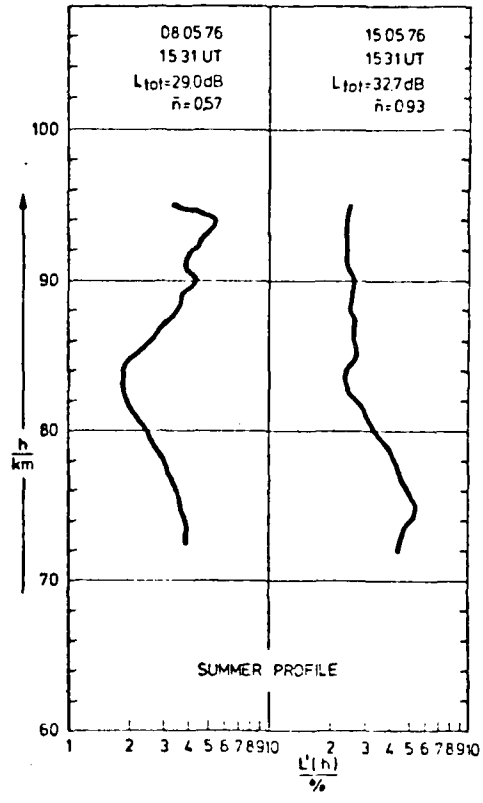

Fig. 36: The relation between n and height distribution of electron density holds also during Summer/Spring.

small and, further, it is a priori difficult to obtain measurements under widely - varying absorption conditions because the day-to-day variation is much smaller during summer than during winter. (See part I of this report) A relation between an increase of electron density at lower heights and the shape of diurnal variation can be expected because the electron loss rate which determines the equilibrium electron density at low elevation angles of the sun is much higher at lower altitudes. The question however remains open how a change of the relation between electron density above 80 km and below 80 km can occur when the ionizing radiation of the sun remains essentially constant. (This was proven by satellite measurements of ultra-violet, extreme ultraviolet and X-ray radiation.) Either we have to take into account another source of ionization which has not been identified yet but is effective during winter only, or we have to deal with a change of the λ-ratio (the number density of negative ions and that of free ions) at lower heights. This means that the effective electron loss rate changes. The latter may be easily caused by a change of composition of minor constituents either in nature or by quantity. Because the guard ring probe responds to both polarities of carriers, the results obtained with this device may yield some qualitative limits when the launches are performed at different times of the day.

Negative ions and effective electron production and loss

As is well known, negative ions dominate over electrons in number density at heights below about 70 km. The result that electrons can be distinguished from negative ions in the current/voltage characteristics of the guardring probe during winter at lower heights than in summer does indicate already that a change of the λ-ratio takes place from summer to winter. The formation of negative ions requires the presence of minor constituents which have a large affinity to electrons. Negative ions are easily destroyed by radiation of relatively large wave lengths. This radiation should be expected to be stronger during summer than during winter. From this consideration one should expect that the lower limit of height above which free electrons can be distinguished from negative ions is higher during winter than during summer. The observations tell, however, that the reverse seems to be the case. This experimental result can be tentatively taken as an argument that a change of composition of atmospheric constituents does take place at the lower part of the D-region of the ionosphere.

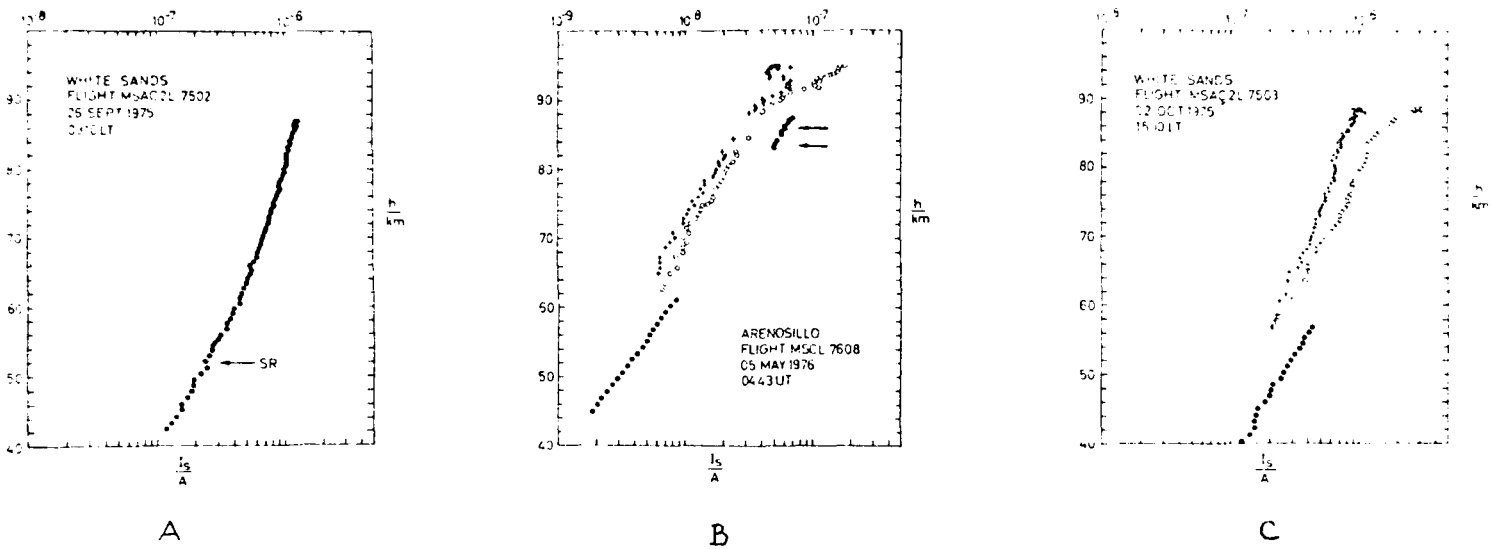

Fig. 37: Indications for presence of negative ions in the D-region at nighttime: The first flight (A) was launched during nighttime with sunrise at about 50 km. No free electrons were observed but positive and negative ions only. The second flight (B) was launched somewhat later. It shows negative ions, free electrons and again a (double?) layer of negative ions near 88 km. Flight C was launched near noon. No negative ions are present above about 70 km.

Some results of guardring probe measurements (35) (37) obtained during the Western European Winter anomaly campaign have shown that the lower limit of height above which electrons could be distinguished from ions were quite high, and the profiles suggest that a strong gradient of electron density must have been present then at the transition height from dominance of negative ions to dominance of free electrons. These launches took place during afternoon, while all other launches which were discussed so far were performed near noon. Further, the cases in which the transition from negative ions to electrons were observed at greater heights were cases which can be assigned to the ending of the winter-anomaly state of the D-region atmosphere. This result suggests that the electron loss at sunset is caused in the lower D-region not by a direct recombination of positive ions and free electrons but by an attachment of electrons to some trace constituent forming negative ions. These negative ions recombine than with positive ions. This was confirmed by some experiments. Some of them were performed in a cooperative program at White Sands Missile Range in which ARCAS vehicles were used. The physical dimensions of the "ARCAS" are not too different from the "Skua". This feature permitted to use the same geometry of the probe and, by this, allowed a direct comparison between results obtained over "El Arenosillo" and over White Sands. These results are shown in Fig. 37.

One rocket was launched before sunrise at ground, with the ionosphere already sunlit above about 50 km. Surprisingly, an ion current was found which corresponded to that seen over the day, up to apogee of the rocket which, however, was less than 90 km. In contrast to this, a second rocket launched near noon showed normal current/voltage characteristics in the sense that electrons could be distinguished from ions above a certain height. Obviously, the primary electrons produced by ionization through radiation from the raising sun convert to negative ions by attachment to some unidentified trace constituent, and these negative ions are then destroyed later by radiation of another wave length which is screened off at low solar elevation angles. This destruction of negative ions should happen shortly after the sun has elevated over the screening atmospheric layer. For a check, one rocket was launched at El Arenosillo in later spring at a time when the solar angle was slightly higher than that present during the morning launch at White Sands. The result was at first somewhat surprising: free electrons could be distinguished from

negative ions at a fairly low height already but no electrons were found between 83 and 85 km and between 88 and 89 km. This effect could possibly be explained as a shading effect of a thin layer present at lower heights which is transparent for ionizing radiation but is fairly opaque for longer infrared wave lengths which destroy the negative ions by detachment. The height in which these negative ions were found coincides with the height in which Narcisi et al (39) saw negative ions of high mass numbers during an eclipse. The results of Narcisi however suggest that these negative ions might have been not the result of a shading effect of a thin layer of certain absorption properties but comprise a species which is more resistant against photolysis than normal negative ions. Such species are, for example, higher-order clusters of water. Whatever the real cause for the formation of negative ions in that height level might be, a minor constituent which has a large affinity to electrons must be present there in certain numbers, at least during the morning hours. If this constituent is absent, one might expect a fairly rapid increase of electron density in the D-region short before sunrise. Such an absence of minor constituents should manifest itself as an increase of absorption which will not be found in the normal case. Such an effect is well known in the D-region as the "November effect": It was observed that attenuation of medium waves starts already shortly before sunrise when the winter season begins. This is not the case during the summer months. Further, it was found that the build-up of absorption during summer follows the sun's zenith angle somewhat retarded while the decay of absorption follows in most cases the variation of the sun's zenith angle quite closely. The November effect is commonly explained by the assumption that a minor constituent which has a low ionizing potential (for example nitric oxyde) is present in larger numbers in the D-region during winter than it is the case during summer. But this assumption does not explain the retardation which the two-stage ionization process mentioned before does. The issue becomes more complicated in detail because one has to take into account the build-up and the decay of the reflecting ionospheric E-layer. The normal E_1 layer, however, seems to follow quite closely the variation of the sun's zenith angle but this normal E-layer is often masked by other layers like sporadic E. Nevertheless, the idea that a layer of minor constituents of certain absorption properties for radiation which affects the effective electron production and loss rate might be worth an experimental verification.

Variations of ion density below 60 km.

In the preceding paragraphs enough experimental material was presented which seems to allow to formulate tentatively a model which explains qualitatively the phenomenological aspects of winter anomaly of radio wave absorption. The phenomena described so far can be understood if one assumes that a minor constituent exists in the D-region which has a large affinity to electrons. Its number density varies with season as the result of changes of general atmospheric circulation and of decreased input of radiation from the sun. Considering the fact that the height up to which water cluster ions are observed with mass epctrometers varies with season and that this height coincides with the height above which the well-known ledge of electron density is found, one might suspect that water vapour is a probable candidate for the role of this minor constituent sought for. It has all the properties required: It has a high affinity to electrons, forms stable cluster ions with many constituents of the atmosphere and is fairly abundant. It has also strong quenching properties for excited states and can destroy species like $0_2\Delta^1$ g which could otherwise supply free electrons through ionization by comparatively long wave lengths. Further, it is fairly abundant but, unfortunately, is rather difficult to measure quantitatively mainly because of contamination problems of sensors and of their slow response and of their low sensitivity. But it is known from laboratory experiments that traces of water vapour can change appreciably the properties of gas discharges. The source of water vapour should be sought at altitudes well below the D-region of the ionosphere, be it water transported from the troposphere into the stratosphere or be it the oxydation product of methane in the stratosphere. One might therefore expect that a change of water vapour affects also the amount of ionization at heights below 60 km, and that this change is related to temperature and to changes of electron density at least in the lower part of the D-region.

Such changes were indeed observed, but their relation to changes of electron density in the D-region and, by this, absorption remains unresolved (40). It was found that free electrons existed in appreciable numbers at heights below 39 km one or two days before winter anomaly develops. When this occurs the ion density is increased by a factor of about 20 at a height of 40 km when compared to the normal case. (See Fig. 38). This increase of ion density was not only observed by the guardring probe (the increase of probe current could

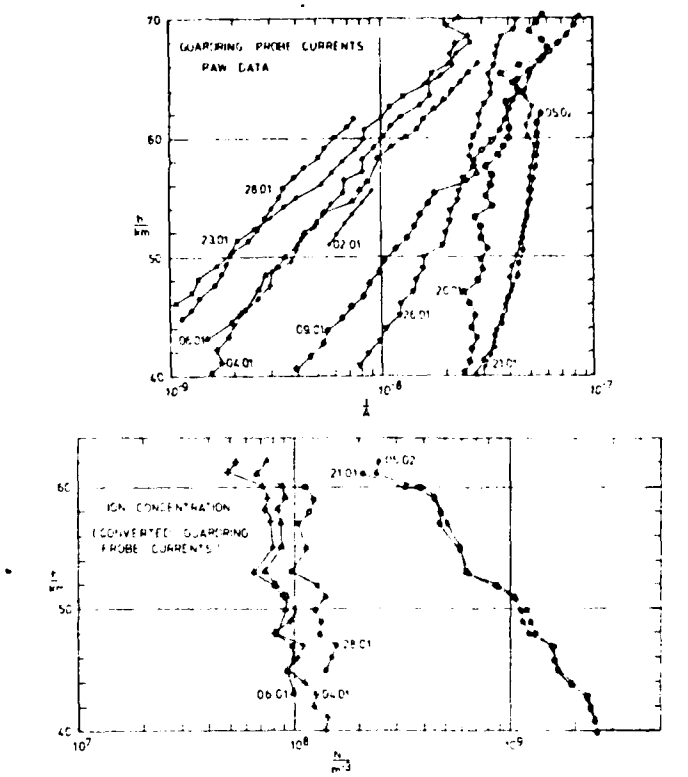

Fig. 38: Increase of positive ion density at heights below 40 km during winter. No relation ambient air temperature was found. (El Arenosillo, Winter 1979/76).

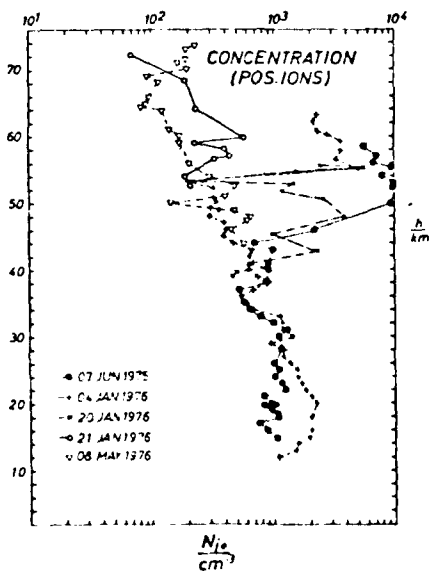

Fig. 39: A result which shows that transient increases of ion conductivity can be observed also during Summer. Again no relations to other phenomena could be established.

principally be caused also by an increase of ion mobility) but was seen also by an aspiration condenser Gerdien experiment which was flown shortly after the launch of the guardring probe. Because Cipriano et al (42) derived a temperature dependence of ion conductivity of 5% K^{-1} from comparisons of simultaneous conductivity and neutral air temperatures, one might expect that the observed increase of ion density was caused by an increase of air temperature in the relevant height region. After the launch of the guardring probes, in-situ temperature measurements were made with standard NASA thermistor devices flown in "Loki Dart" rockets. These temperature measurements revealed that the observed increase of conductivity caused by an increase of ion density could not be caused by temperature changes unless one assumes that the temperature coefficient of conductivity is very (unreasonably) high in this height level. The temperature varied by about 2-5 K while the probe current varied by about a factor of 20. No corresponding change of the intensity of cosmic rays could be inferred from available data. Cosmic rays are believed to be the main source of ionization in that height region. Further, a malfunction of the probe's electronics can also be excluded with a high degree of certainty. A possible explanation might be found by assuming that a change of the ion loss rate has occurred then. A change of ion loss rate could be caused by a transient change of composition which included the temporal reduction of certain trace constituents. Transient changes of ionization of this kind at heights well below the D-region of the ionosphere which cannot be detected by ground-based means seem not only to occur during the winter season but can also happen in other seasons too (37) (40). In one case, a large change of conductivity was observed over "El Arenosillo" in early summer. Again the two independent instruments were used to measure ionization, a Gerdien condenser system and a guardring probe. The instruments were flown on different rockets. The increase of conductivity at 40 km in reference to the normal case was found to be of same order as was found for some winter anomaly precursors, and a further flight indicated an increase of conductivity near 50 km. The results are shown in Fig. 39. Nothing peculiar did happen in the D-region to be recognized as a change of absorption and no conclusions could be drawn from the data about frequency of occurrence or time scale of the event. By personal communication (L.C. Hale) it was found out that similar effects were seen also over White Sands on certain but apparently rare occasions. A temporal change of number density of a minor constituent which has a high affinity to electrons and causes a large loss rate for ions might explain the observations. One possible candidate for this role is again water.

Temperatures derived from guardring probe measurements

A result which was not expected was obtained when the guardring data were examined more closely. As was outlined earlier, the probe currents were converted into ambient electron densities by deriving calibration factors from comparisons with results obtained by wave propagation experiments. In our case, (as was mentioned earlier) the wave propagation experiments were not made in-situ but from the ground. It could be shown (as was outlined before) by comparisons with results obtained by in-situ wave propagation experiments flown nearly simultaneously that this approach is applicable.

Looking at the calibration factors so obtained it was noted that they varied with conditions of the D-region and with height. The variation was of same order of magnitude (roughly a factor of four) than is reported in the literature. This result can be taken as a further hint that the conversion method which we used yields meaningful results.

Empirically it was found that the calibration factors vary much less when the current caused by positive ions is used as a measure of electron density. Some authors (e.g. 43) disregard therefore the electron current as a measure of ambient electron density and refer to the current caused by positive ions. This difference of behaviour of the two probe currents must have a deeper reason, because the experiment shows that the probe currents are proportional to applied probe voltage provided that the probe voltage remains sufficiently small. (The current caused by electrons deviates from linearity at higher probe voltages, but only by a small amount (of order 10% of the total current) and a range in which the probe current remains proportional to applied probe voltage can always be found). Because the air density is still comparatively high in the D-region, one cannot expect that the collision-free Langmuir theory describes satisfactorily the current/voltage characteristics of the probe. A more appropriate approach would be to assume that of both carriers, electrons and positive ions, are affected by collisions with neutrals. This means that the carrier drift velocity v is governed by mobilities and that the probe current is described

by:

$$i = n.e.v.F = n.e.k.F.E$$

(n: carrier density, e: electric charge, k: mobility, F: effective surface of the probe, E: electric field strength). The carrier mobility varies inversely with carrier mass and may increase proportional to the square roof of the temperature.

Experimental results

If both carriers, electrons and positive ions would behave in the same manner when moving under the influence of an electric field, which is the same for both polarities, one would expect that the ratio between electron and ion current is given by the ratio of their mobilities. This should turn out to be:

$$\frac{ie}{ii} = \frac{ke}{ki} = \frac{mi}{me}$$

(k: relevant mobilities, m: mass of charged particles.) This ratio should be constant and independent of height because the variation of k with density cancels. Taking for mi mass number 32 (this assumes that the dominant positive ion is O_2^+. This holds true for heights above about 84-87 km) one should observe a current ratio ie/ii of about 240. Such large current ratios were never found. The ones actually observed were about 50-100 times smaller, were dependent of height and varied with season. They were smallest during Summer and Autumn and were largest during winter. The height-dependence was relatively small in Spring and during early Summer but was very strong when the conditions in the D-region were winter-anomalous. Rather large current ratios were then observed in the height region between 83 and 86 km. This is just the range of height in which a bulge of electron density is observed when the D-region becomes winter-anomalous. In total, the probe current ratio varied by roughly a factor of four between Summer and Winter in that height range and for "normal" and "winter anomaly" conditions. This is the same amount of variation reported in the literature for the conversion factors of probe current into ambient electron density derived from comparisons between in-situ measurements of electron density by wave propagation experiments and probe currents,

and the same amount of variation of the conversion factor was obtained when our conversion method was applied which relied upon ground-based propagation experiments. Malfunction of the experiment which might have caused this variation of probe current ratio can be excluded. For an explanation, one could think of a dramatic change of ion composition in the relevant height range. Such changes were indeed observed by mass spectrometer measurements (Arnold and Krankowsky, Kopp, Narcisi etc) but a variation of current ratio was observed also at heights (above 86 km) were such a change was not seen by mass spectrometer measurements performed when the ionospheric conditions were different. In those heights, O_2^+ remains the dominant positive ions, and one has to look for another reason for the observed variations other than change of composition.

Qualitative explanation

The height profiles of probe current ratio resumble strongly to temperature profiles reported in the literature and to seasonal variations of them. One should therefore look for a physical process other than change of composition which causes a temperature dependence of the current ratio. The experimental result that the conversion factors for currents caused by positive ions vary much less than the conversion factors for electron currents suggests that the cause might be found in certain peculiarities of electrons moving under the influence of the probe's electric field. The considerations which follow are based on facts summarized in (44) and (45).

The movement of charged carriers under the influence of the electric field of the probe is governed by the electric field and by collisions. The range in which this occurs is defined by the distance at which the electric field ends. In a plasma, a measure for this screening distance is the Debye length

$$\lambda_D = \sqrt{\frac{\varepsilon_o \cdot k \cdot T}{e^2 \cdot n \cdot 4\pi}}$$ (n: number density of charged particles)

The Debye length defines the "sheath region" of the probe. Assuming that the electric field of the probe really ends at a distance equivalent to the Debye length (this is possibly a rather crude approximation) the electric field of the probe is given by $\frac{V}{\lambda_D}$. V is the probe driving potential. The experimental results justified to put for V the voltage applied between rocket and probe. Outside of the sheath region, the plasma remains undisturbed. By this we have to consider only effects which occur within the sheath. This means that we have to compare

free path lengths for different collision processes with the size of the Debye length. We further assume that the charged particles do not gain much kinetic energy when moving in the electric field of the probe. This means that the concept of constant mobility remains valid. For ions, the momentum exchange between ions and neutral particles is the most important collision process. This means that the drift velocity of the ions (and, by this, the ion current) is proportional to $\frac{\text{const}}{m_i \nu_{in}} \cdot E$ (ν_{in}: ion neutral collision frequency), provided that the mobility concept is still valid. This is the case for small fields and when the mean free path between collisions is smaller than or comparable with the Debye length. Assuming that the temperature is 200k (this is a typical figure for Summer and even for "normal" Winter conditions), the probable velocity of nitrogen molecules (the most abundant constituent of the D-region atmosphere) is 345 ms-1. For a height of 85 km, the mean free path of the nitrogen molecules will be then 1.2cm. The Debye length is independent of height and varies with electron density as follows:

(T = 200k)

Ne	100	500	1000	5000	e ℓ/cm³
λ_D	9.76	4.36	3	1.38	cm
λ_{in}/λ_D	0.12	0.28	0.4	0.87	

The ratio between mean free path of ion-neutral collision and Debye length turns out to be smaller than 1 for this height even for larger ion densities. This consideration holds true for a probe being at rest. Because proportionality between probe driving voltage and current was seen to be maintained at even greater heights, it seems that either the electric field of the probe extends to a somewhat larger distance than the Debye length yields or that some effect related to the supersonic speed of the probe causes an apparent increase of air density.

The mobility of ions increases with temperatures proportional to $\sqrt{T}$. The electric field E of the probe turns out to vary inversely proportional $\sqrt{T}$ because E is defined as voltage across a distance D. D is in our case the Debye length. This means that the two dependencies cancel each other. The ion current becomes therefore essentially independent of temperature and depends upon neutral air density only.

For electrons, matters are different. The cross section for collisions between electrons and neutrals becomes very small, which means that the mean free path of electron becomes much larger than the mean free path of ions when they collide with neutrals. But the electrons move always under the influence of the Coulomb field of positive ions which are present in the ion sheath and in the plasma. This influence causes a deflection (change of path) of the path of the electron travelling in the field of the probe. This change of path is considered to be equivalent to a collision. The cross section for this electron-ion collision turns out to be very large. (This is due to the long range of the Coulomb forces) and strongly dependent of temperature. The ion-electron collision frequency is proportional to $T^{-3/2}$. Inserting this temperature dependence into the Langmuir relation for the drift velocity, $v = \varkappa \cdot E = \frac{e \cdot \lambda}{m \bar{v}} \cdot E$ with $\bar{v} = \sqrt{\frac{8 k T}{\pi m}}$, $\lambda = \frac{\bar{v}}{\nu_{ie}}$

and $\nu_{ie} = \frac{4 \cdot \sqrt{2\pi}}{3} \cdot \frac{e^4}{\sqrt{m_e}} \cdot \frac{\ln \Lambda}{(kT)^{3/2}} \cdot N_i$ one obtains for $v = \varkappa_i E = \frac{3 (kT)^{3/2}}{4 \sqrt{m_e} \sqrt{2\pi}} \cdot \frac{E}{e^3 \ln \Lambda} \cdot \frac{1}{N_i}$

$v = \varkappa \cdot E = \frac{3 (kT)^{3/2}}{4 \sqrt{2\pi} \sqrt{m_e}} \cdot \frac{E}{e^3}$, and, eventually, for the ratio between electron and ion mobilities: $\frac{\varkappa_e}{\varkappa_i} = \frac{3}{\sqrt{2}} \frac{(kT)^2}{e^4 \ln \Lambda} \cdot \sqrt{\frac{m_i}{m_e}} \cdot \frac{N D^2}{N_i}$

At first sight it seems to be not very plausible why the electron-ion collision should play such an important role for probes when it takes no effort to prove convincingly that the electron-ion collision does not play any significant role in the D-region when considering wave propagation experiments because the plasma density is so low. (The collision cross section for collisions between electrons and neutrals is of order $10^{-20} m^2$. The cross section for electron-ion collision is of order 10^{-13} m^2, indeed very large but the degree of ionization in the D-region is about 10^{-11} near 80-85 km or even less. The ratio between the two collision frequencies which determines the ratio of losses is therefore of order 10^{-4}. This result seems to exclude that electron-ion collision may play a significant role in the D-region of the ionosphere).

An at least partial answer is found when the difference between wave propagation experiments and probe experiments is considered. Wave propagation experiments affect a large volume.

Therefore, the time elapsed between collisions determines the loss of wave energy which was put into the movement of the electron in the electromagnetic field as superposition to its random motion. Because the affected volume is large, the (mean) free path of the electron does not enter directly the consideration because there is no physical confinement. The issue is different for DC-probes. All directed movement of charged particles under the influence of a field takes place in the confined volume of the sheath given by Debye length and by the surface of the probe. For this case, the probability for a collision during the time in which the electron travels through the sheet comes into play. The ratio between mean free path length for electron-neutral collision and Debye length is a measure for this. The following table shows the ratio between electron free path length (collision electron-neutral) and Debye length. The mean free path λel was estimated from $\bar{v}el/\nu_{en}$ ($\bar{v}_{el}$: mean velocity of electrons, ν_{en}: electron collision frequency). In the following table, the mean velocity of the electrons was taken as $10^5 ms^{-1}$. The collision frequencies were obtained from (43).

The figures are:

height (km)	ν_{el} (sec^{-1})	λ_{el} (cm)
78	$2.1.10^6$	5 (4.76)
80	$1.5.10^6$	7 (6.67)
85	$6.t.10^5$	15 (15)
88	$3.8.10^5$	26 (26)

From this, one obtains the following ratios of $\lambda el/\lambda_D$ for 100, 500, 1000 and 5000 el cm^{-3}

height (km)	λ_{el}/λ_D (100 cm^{-3})	λ_{el}/λ_D (500 cm^{-3})	λ_{el}/λ_D (1000 cm^{-3})	λ_{el}/λ_D (5000 cm^{-3}
78	0.49	1.1	1.58	3.44
80	0.68	1.52	2.22	4.8
85	1.53	3.44	5	10.86
88	2.66	5.96	8.66	18.8

Measured electron densities were of order 5oo - 1000el cm^{-3} at 75 km (dependent upon season) and raised to some 10^3 at 88 - 90 km. The figures show that the mean

free path of electrons was in most cases larger than the Debye length. This means that the friction term in the equation of motion $\nu_{en} \cdot v_e$ becomes small and can be neglected.

For comparison, the ratio between mean free path length of ions and Debye length and the ratio between mean free path length of electron for collisions with neutrals are summarized in the following table for a height of 85 km:

N_e	100	500	1000
$\frac{\lambda_{in}}{\lambda_D}$	0.12	0.28	0.87
$\frac{\lambda_{en}}{\lambda_D}$	1.53	3.44	10.06

This table shows that the chance that an electron collides with a neutral within the sheath is fairly remote. This means that the movement of electrons within the sheath is not very much affected by neutrals but is influenced by the Coulomb field of the positive ions present within the sheath. This influence is described as electron-ion-collision.

The next question to be answered is how the electron might enter the sheath. If the electrons (and ions) would have no temperature, they would be screened off by the ion sheath which develops in the Coulomb field of probe, and no electron current could flow.

Consequently, they must enter the sheath by diffusion. This means that an additional temperature dependence for the electron current comes into play which is proportional to T in addition to the T^2 law mentioned before. This leads to a temperature dependence of the current ratio proportional to $T^{5/2}$ and to a relation inversely proportional to ion mass. This means that the probe current ratio is dependent of both, temperature and ion mass.

Calibration

A satisfying theoretical description of the problem could not yet be developed. The formulation of an appropriate theory seems to be rather complex. Resort was therefore made to calibration by comparing measured probe current ratios with neutral air temperatures measured almost simultaneously with other

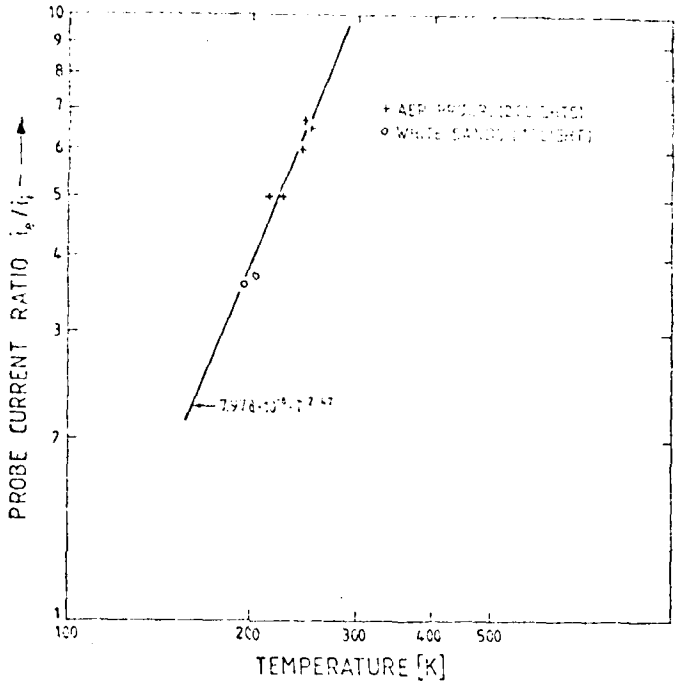

Fig. 40: Temperature calibration of the electron to ion current ratio of guardring probes derived by comparisons with in-situ measurements of neutral air temperature (falling spheres and mass spectrometers).

AD-A106 770 MAX-PLANCK-INST FUER AERONOMIE LINDAU-UEBER-NORTHEIM --ETC F/G 20/14
HIGH ALTITUDE ATMOSPHERIC INVESTIGATIONS, PART II. DEVELOPMENT --ETC(U)
JUN 81 H WIDDEL
DA-ERO-75-G-076

UNCLASSIFIED

NL

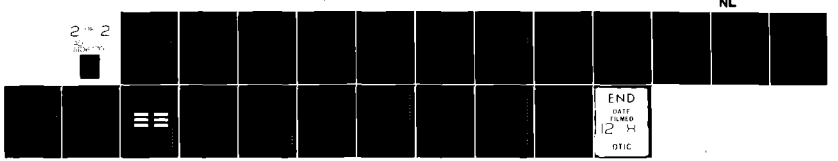

experiments. The time difference between guardring probe measurement and temperature measurement varied between about 30 min to about 2 hours. Temperature was measured by falling spheres over White Sands and by Pitot tubes and mass spectrometers over El Arenosillo (Southern Spain). The latter derived temperatures from the measured ratio of water cluster ions using known reaction rates.

The result was the empirical relation shown in Fig. 40. The data points represent averages of several individual measurements of temperature and of current ratio. Least square fit was used to derive the empirical temperature function. The scatter of individual data was quite high. This means that the overall accuracy of the temperature function is not too great. Assuming that ie/ii = const. T^n, a temperature dependence proportional to $T^{2.47}$ was obtained. This value is close to $T^{2.5}$. but the data would allow also to fit a temperature dependence proportional to T^3. This temperature dependence proportional to T^3 would yield somewhat lower temperatures for high current ratios and elevate temperatures a little bit for low probe current ratios. For the evaluation to follow, the empirical temperature dependence derived by least square fit was used throughout.

Evaluation of data

Spring conditions

The conversion was first tested on two profiles measured over El Arenosillo during spring (08.05.76 and 15.05.76) ground-based absorption was nearly the same on both days during launch, 29.dB and 32.7 dB). The only but slight difference was seen in the shape of diurnal variation. This difference might be attributed to a change of the effective loss rate of electrons near 8o km. It was expected that the temperature profiles derived from the two current ratio profiles would fit rather closely to Standard Atmosphere data for heights above about 86 km, because this is the height were the water cluster ion regime normally ends. Water cluster ions have a higher mass than O_2^+ and are dominant below about 86 km.

The results are shown in Fig. 41 and Fig. 42. The results meet expectations in that the derived temperatures agree quite well with the reference data taken from Cole and Kantor (46) for heights above about 85 km. Below that height, fairly large deviations from the reference temperatures were found. The reference to Standard Atmosphere data is justified by the fact that those two days were normal days, and there is no sound reason to assume that large deviations from average temperature are present on a normal day. The deviations from standard temperature observed below 85 km are to be expected because the

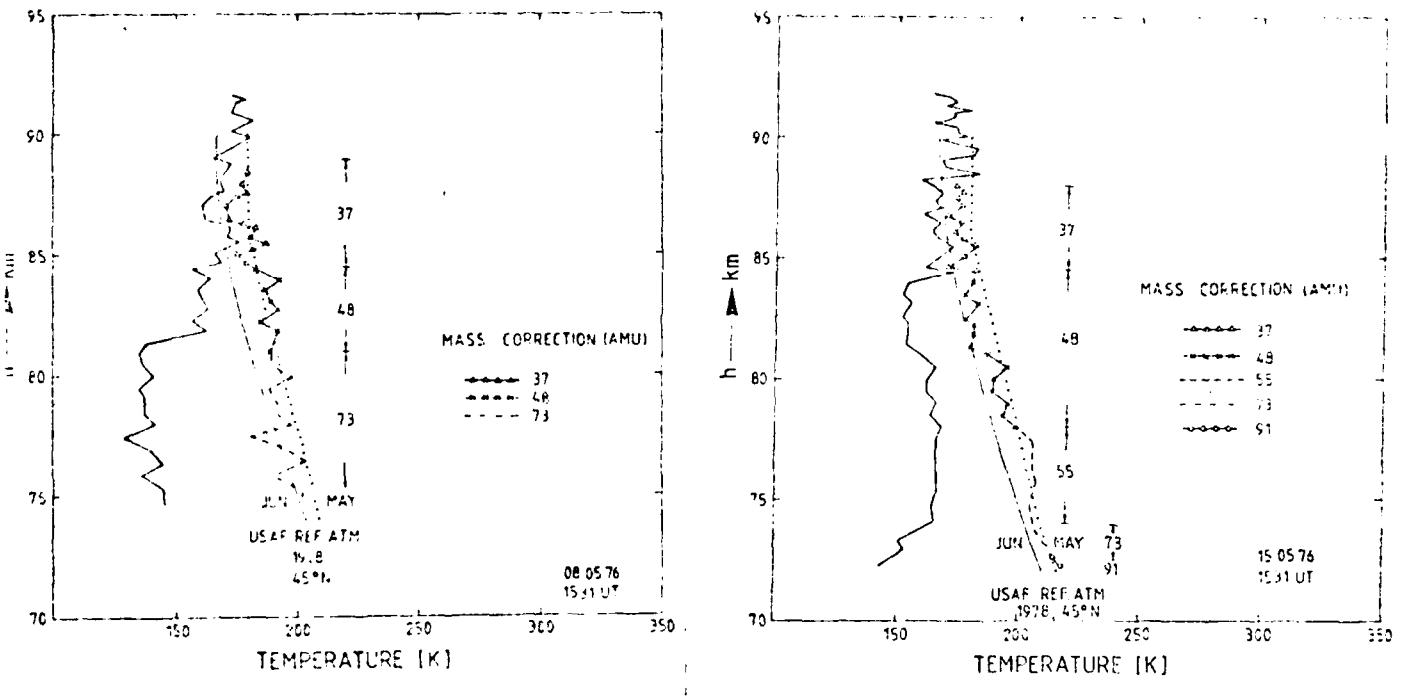

Fig. 41, 42: Temperatures derived from guardring probe measurements during early Spring/Summer.

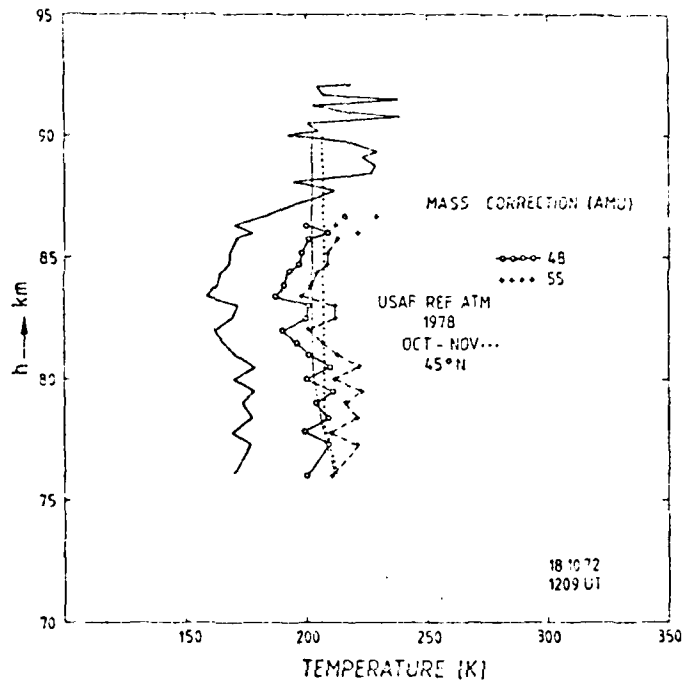

Fig. 43: Temperatures derived from guardring probe measurements performed in Autumn.

composition of the positive ion population changes there. The "ledges" found in the probe current ratio can therefore be explained as being caused by a change of the dominant positive ion population. As was mentioned before, the empirical temperature function was derived for heights in which O_2^+ is in all seasons the dominant positive ion. (Mass number 32). Eliminating this mass number from the empirically derived constant C of the relation $ie/ii = C.T^n$, a residual constant was obtained. This residual constant allows to calculate the mass number of the positive ion required to shift the temperatures below the ledge which are obviously too low compared to values of the standard atmosphere. A mass number very close to 37 was obtained. This mass number belongs to a well-known water cluster ion of the type H_3o^+ (H_2o) known to be found in this height region as the dominant ion as mass spectrometer measurements have shown. The correction needed for the next ledges yielded mass number 48 and then 73 resp. 55. Those mass numbers are again well-known water cluster ions known to be dominant in the relevant height regions if the mass spectrometer measurements are correct.

This result, though in a certain way satisfying (in both cases an almost identical result was obtained when the D-region conditions are similar) shows clearly a problem and, by this, a limitation of the method: Disregarding other effects which might play a role, temperatures can only be derived from the probe current ratio when the composition of the positive ions is known. This calls for the need for a simultaneous measurement of ion composition. Further, as was mentioned earlier, the number density of negative ions must be much smaller than the number density of free electrons.

Autumn

Unfortunately, not many launches took place during autumn. One example is shown in Fig. 43. One notes that, in essence, the same type of corrections had to be applied (with mass numbers 48 resp. 55 in about the same height region as in spring) to shift the ledges into the range of the standard temperature. The range in which mass number 37 should be used for corrections is in this case rather small and the data were not entered into this diagram. The deviation towards higher temperatures at heights near 90 km was found in about all winter profiles which were obtained on non-winter-anomalous days. Assuming that the measurements are correct, these temperatures could be real but might also be caused by a change of ion composition in that the number density of light ions like O^+ and metallic ions increases in relation to the number

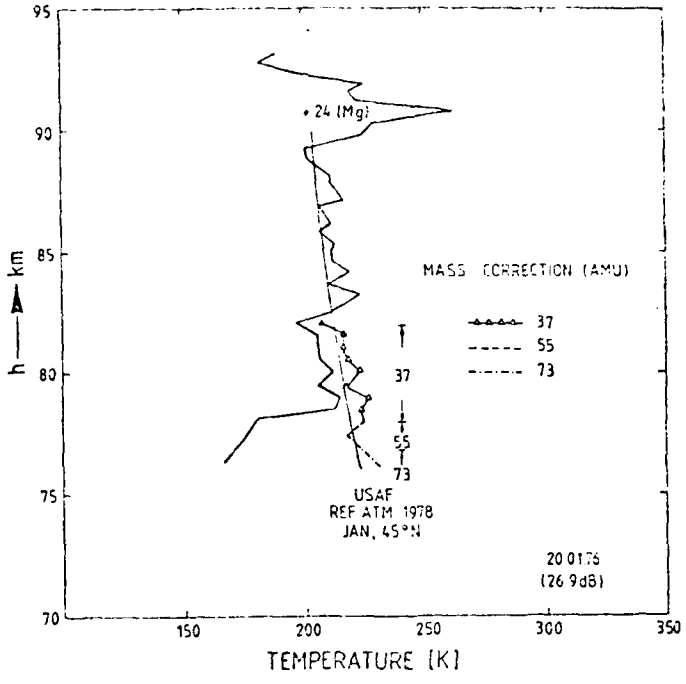

Fig. 44: Derived temperatures for a normal winter day.

density of O_2^+ ions. Because the Reference temperatures were derived from results of the falling sphere, (this experiment which has a tendency of smoothing out local fluctuations) and that the Reference temperatures represent means of a large number of individual measurements, the observed variations of temperatures might at least be partly real and not be fully caused by inaccuracy of measurement.

Normal winter day

As was outlined in part I of this report, "normal" winter days in the sense defined there are somewhat scarce. The $L_D = \frac{L_o}{n+1}$ parameter indicates that absorption is rather low on such days and the diurnal variation of absorption follows closely the variation of the sun's zenith angle zenith angle. The results obtained for such a "normal" day (20.01.76) is shown in Fig. 44. This day immediately preceded winter anomaly. (See Fig. 45 which shows the results of radio wave absorption measurements obtained during the relevant winter (1975/76)). It is well known from results of mass spectrometer measurements that the height in which water cluster ions dominate are shifted to lower levels when the state of the D-region atmosphere becomes winter-anomalous. This measurement seems to indicate that the cluster ion regime shifts downward before winter anomaly starts which manifests itself as an increase of absorption of radio waves. The "shelves" observed in the original data near 82 km and 78 km can be removed by inserting mass numbers 37, 55 and73. The temperature peak near 91 km is believed to be only partial real because the electron density profile derived from the guardring probe data of this flight had a ledge near 90 km. This ledge of electron density was seen in the ionograms taken before, during and after the flight as a sporadic E-layer in the same height range. Therefore, one might assume that this peak of temperature might be caused by a change of ion composition in that a thin layer of metallic ions existed then. Therefore, a correction with smaller mass numbers was attempted•A correction with mass number 24 reduced the peak of temperature to temperatures rather close to Reference Atmosphere Temperature.

Winter anomaly

One can distinguish phenomenologically between two types of winter anomaly which represent extremes. One case is the "regular" winter anomaly, regular in

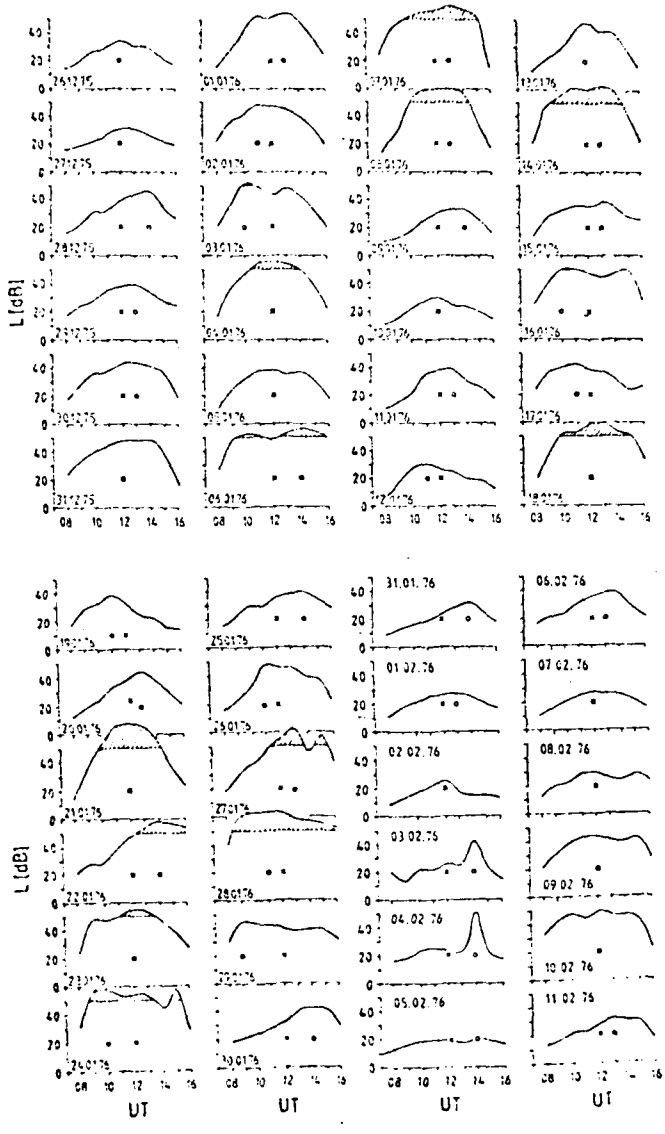

Fig. 45: Diurnal variations of radio wave absorption measured during winter 1975/76.

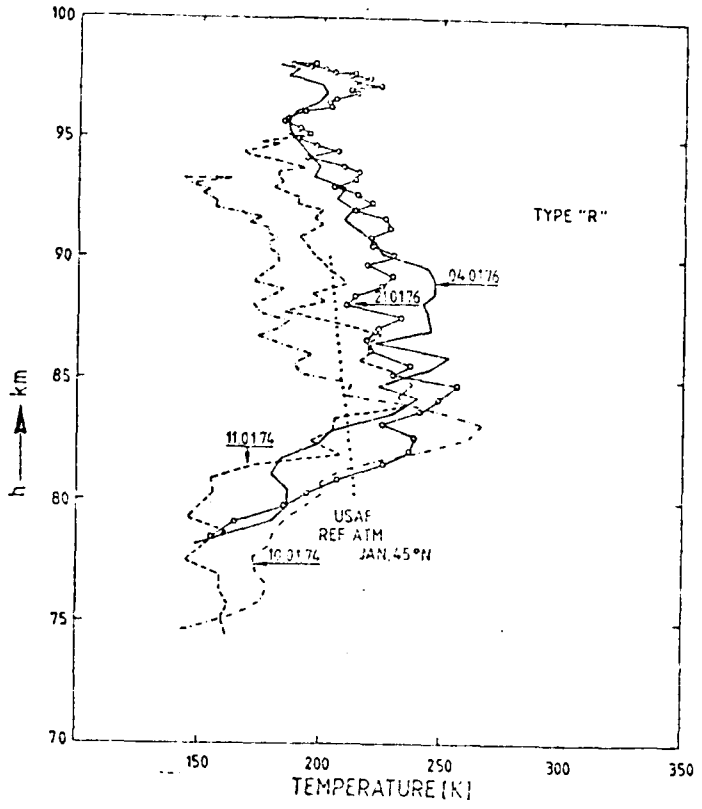

Fig. 46: Derived temperatures from guardring probe measurements performed on 04. and 21. January supplemented by data from days which had a similar diurnal variation of absorption.

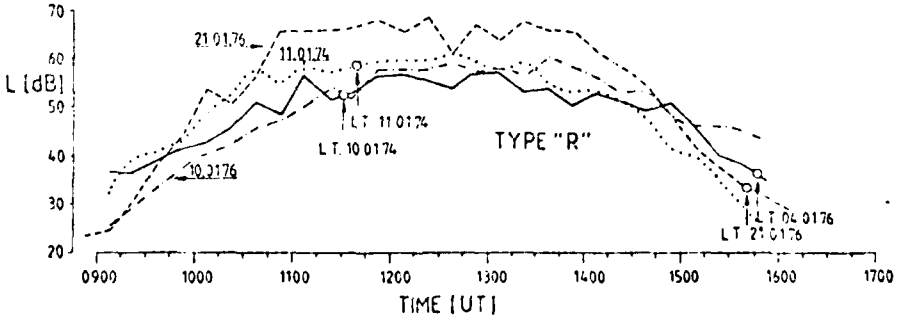

Fig. 47: Diurnal variation of absorption observed on the days for which Fig. 46 shows the derived temperatures.

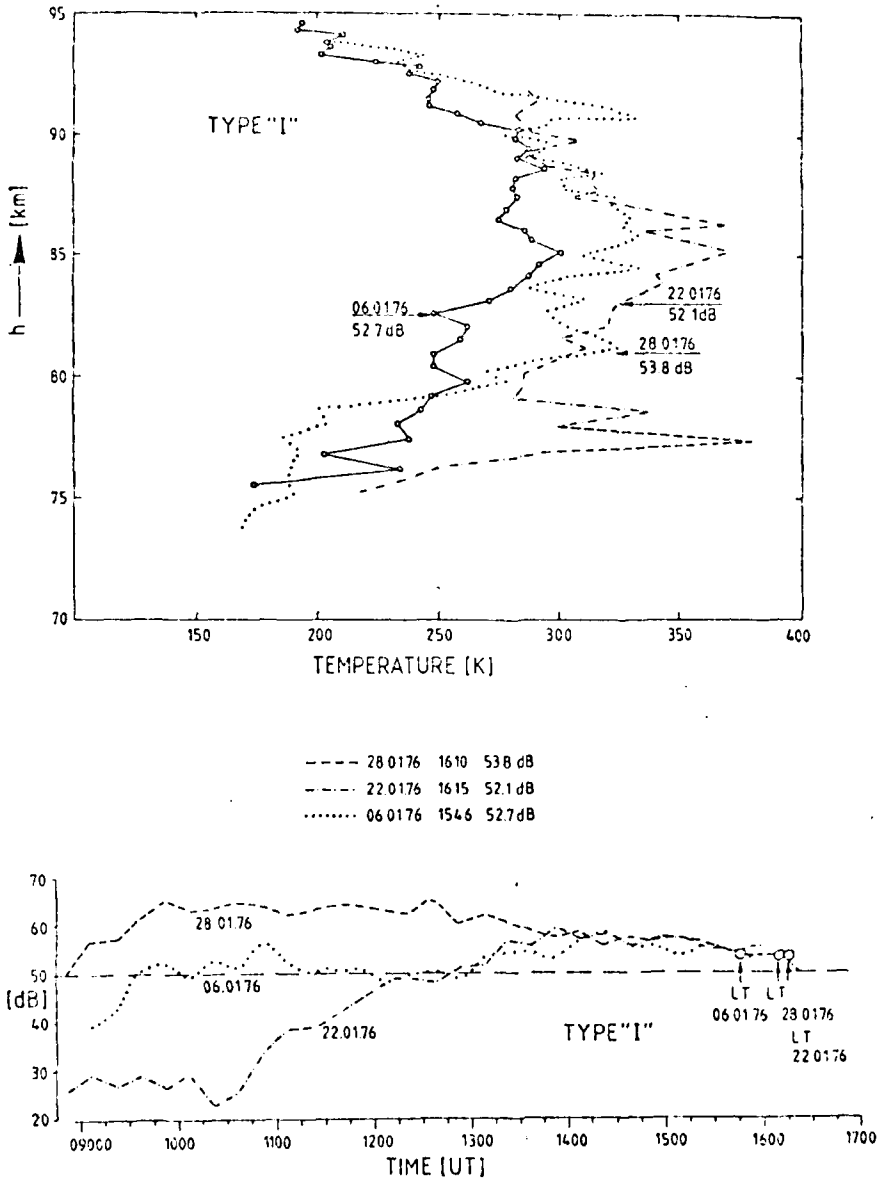

Fig. 48: Temperatures derived from guardring probe measurements under conditions of "irregular" winter anomaly. Bottom: Diurnal variation of absorption observed on the relevant days.

the sense that the diurnal variation of absorption follows quite nicely the variation of th solar zenith angle. The other is the "irregular" case in which absorption does not follow at all the diurnal variation of the solar zenith angle. Examples for both types can be found in Fig. 45 which shows the diurnal variation of absorption observed at El Arenosillo during the Western European Winter Anomaly Campaign 1975/76. "Regular" winter anomaly was present on 04. January, 08. January and 21. January 1976, "irregular" winter anomaly occurred on 6, 22, 23, 23, 27 and 28 January 1976. "Mixed cases" are the remaining days on which the absolute absorption exceeded 50 dB.

Regular winter anomaly

Fig. 46 shows the derived temperatures for 04 and 21 January supplemented by results obtained during an earlier campaign in which the experiments were launched about one hour before local noon. At this time the maximum of absorption had not yet been reached. No cluster ion corrections were applied to these data because of uncertainty if they were valid. The four profiles are, in general, quite similar and the supposition that "the higher the absorption at time of launch, the higher is the temperature in certain parts of the D-region" seems to be confirmed. This is illustrated by Fig. 47 (upper part) which shows the diurnal variation of absorption for the four days. The time at which the rocket were launched is marked.

Irregular winter anomaly

Irregular winter anomaly is characterized by a diurnal variation of absorption which is not related in an easily recognizable way to the diurnal variation of the solar zenith angle. It may be present in the forenoon hours already, may rather suddenly appear near noon, or develop in the afternoon. A rather high absorption which corresponds to noon-time values is then observed when the solar zenith angle is already quite low. A higher temperature in the D-region might be expected when this occurs, but one cannot exclude that a change of abundance of minor constituents which causes winter anomaly contributes to this together with advection.

The derived temperature shown in Fig. 48 confirm that temperatures were indeed higher than those shown in Fig. 46 which were obtained during "regular" winter anomaly. Absorption at time of launch was about the same in all three cases (6 January 1976, 52.7 dB, 22 January 1976: 52.1 dB, 28 January 1976: 53.8 dB)

but the diurnal variation differed as is shown in Fig. 47 (bottom). The derived temperatures were highest on 22 January 1976 when winter anomaly started to develop after 1100 UT. It was present in the morning hours already on the remaining two days, but absorption was higher on 28 January than on 6 January 1976.

If temperatures controls the amount of winter anomaly, one would expect that the temperatures at time of launch were higher on 28 January than on 6 January and would be probably highest on 22 January 1976. This was the case but the derived temperatures for 22 January were very high (350 K). This high temperature will be reduced by about 10% if the calibration data used to produce Fig. 40 are fitted to a relation proportional to T^3, but this kind of correction was not used here. The empirical relation was applied to all data presented in this report.

Difference between "regular" and "irregular" winter anomaly:

Caused by different nature of positive ions?

Another way to reduce the unreasonably high temperatures which the empirical relation between probe current ratio and temperature yielded when D-region winter anomaly was "irregular" is to try with a lower ion mass. Putting a mass lower than 32, for example, 28-30, one obtains then temperatures which are well within the limits reported by other sources. To assume a change of mass of positive ions seems to be not unreasonable physically when results of ion composition measurements obtained under winter anomalous condition are considered. A large increase of nitric oxygen was observed by one source when the D-region atmosphere was winter-anomalous. During the Western European Winter Anomaly Campaign 1975/76 a large increase of $O_2\Delta g$ was observed and by this, a dominance of O_2^+ over nitric oxyde. Because nitrc oxyde has a much longer photolytic lifetime than the excited stage of oxygen it seems quite feasible that the "regular" tpye of winter anomaly might be produced mainly by $O_2{}^1\Delta g$ while the irregular type of winter anomaly might be caused mainly by NO which is, in addition, insensitive to quenching of excited states. Further in-situ measurements of ion composition are necessary to support this supposition. In both cases the development of an appreciable increase of either NO or $O_2{}^1\Delta$ requires that water be absent or reduced considerably in number density. The disappearance of winter anomaly absorption should therefore go parallel with the re-apperance of water and, by this, with the re-appearance of water cluster ions in the D-region.

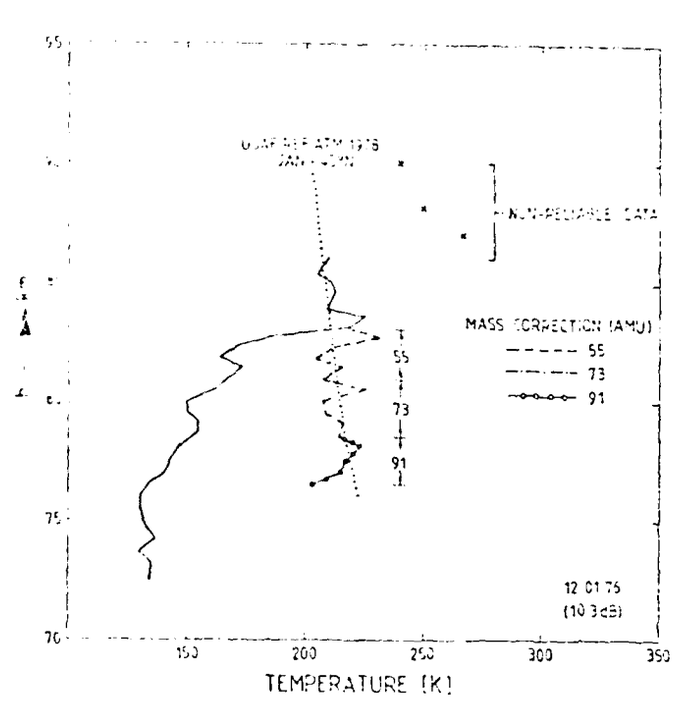

Fig. 49: Winter anomaly decay: (12. January 1976): Re-apperance of cluster ions.

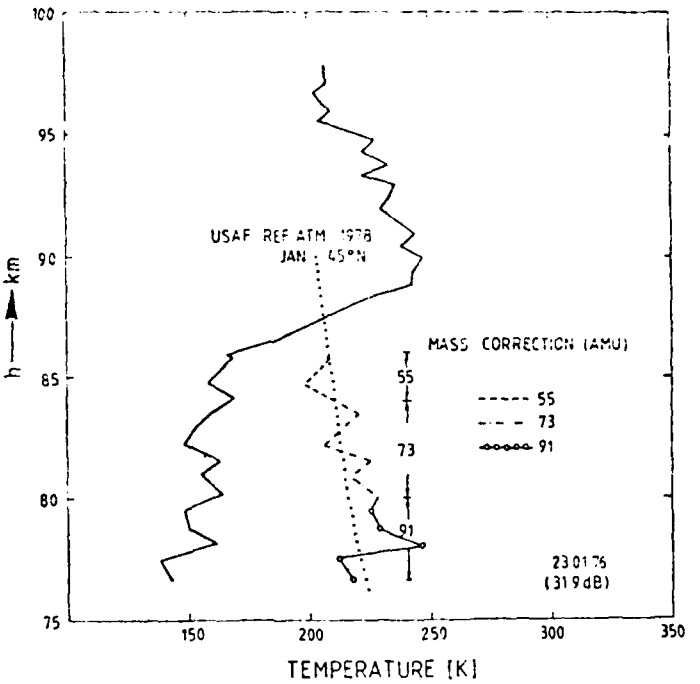

Fig. 50: Winter anomaly decay: 23. January 1976.

Winter anomaly decay

Electron density profiles, measured when D-region conditions are not winter-anomalous, have often a reduction of electron density (a "shelf") near 84-87 km, similar to that found during Summer which is thought to be at least partially caused by the presence of water cluster ions. Such a non-winter-anomalous day was 12 January 1976. The derived temperatures followed closely the Reference Atmosphere between about 83 to 86 km (Fig.49). Unfortunately, the data above 86 km were unreliable because the positive ion current was very noisy. The derived temperature profile had a "shelf" between 82 and 83 km and the temperatures were very low below that height. Correction with mass numbers 55 (the most abundant cluster ion during the winter season), 73 and 91 put into temperatures near to Standard Atmosphere values.

A further example is shown in Fig. 50 (23 January 1976). The noon absorption was about 55 dB but decayed fairly rapid in the afternoon. Winter anomaly was present again during the forenoon hours of the next day. The electron density profile had a ledge in about the same height were the derived temperatures had a "shelf." Assuming that the temperatures returned to about normal values in lower heights, a correction was attempted with the same numbers 55, 73 and 91 as were used for the derived temperatures close to Standard Atmosphere temperatures.

Other cases: Winter

Temperatures derived from probe data obtained on days which can neither be considered as "winter-anomalous" nor as "normal" are very hard to interpret because there is no way to distinguish if an observed low "temperature" is real or was just caused by a change of the effective mass of positive ions. It looks, however, as if the temperature above the 90 km level remains elevated all through the winter season when D-region conditions are not winter-anomalous. This has, however, still to be established by other reliable means of temperature measurements for which techniques still have to be developed.

S.I.D conditions

Good fortune allowed us to launch one rocket into an SID event on 25.10.72. Four events of different intensities were observed on this day, as is

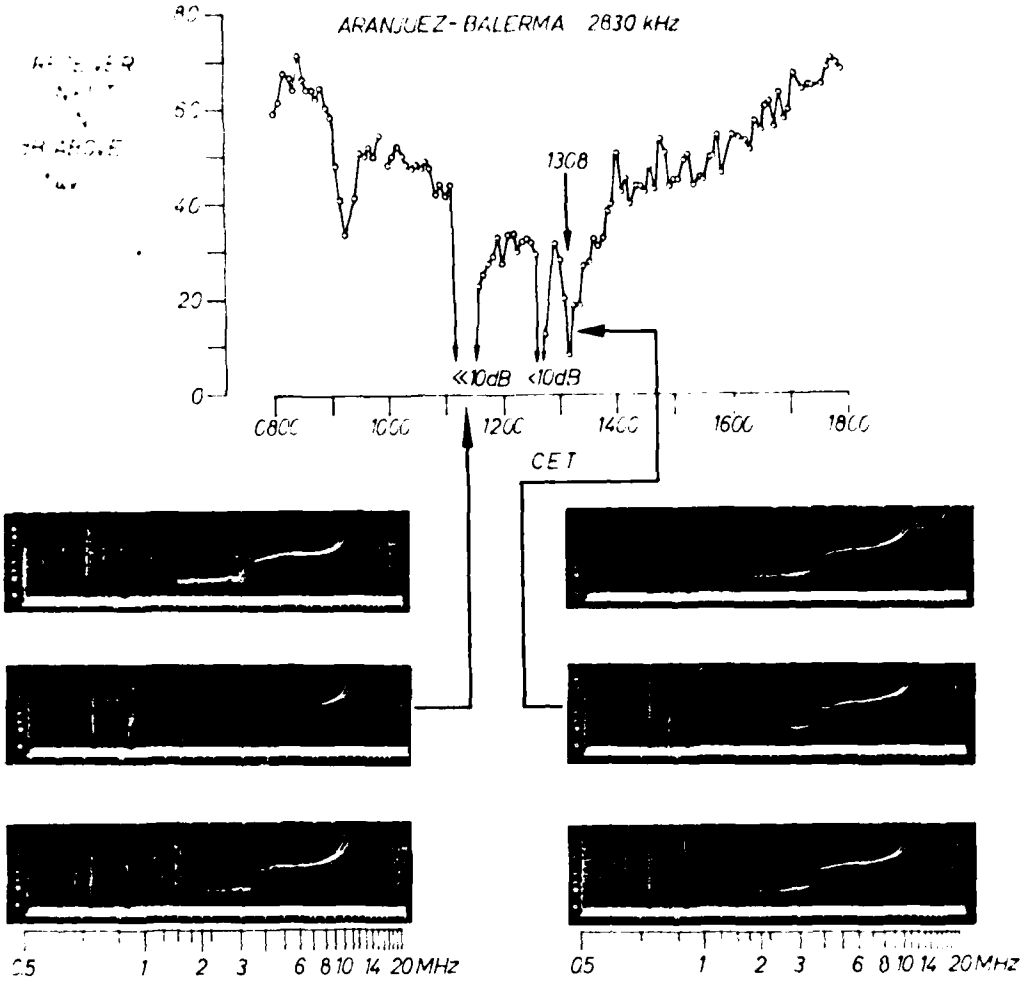

Fig. 51: SID events on 25.10.1972; lauch time of rocket indicated.

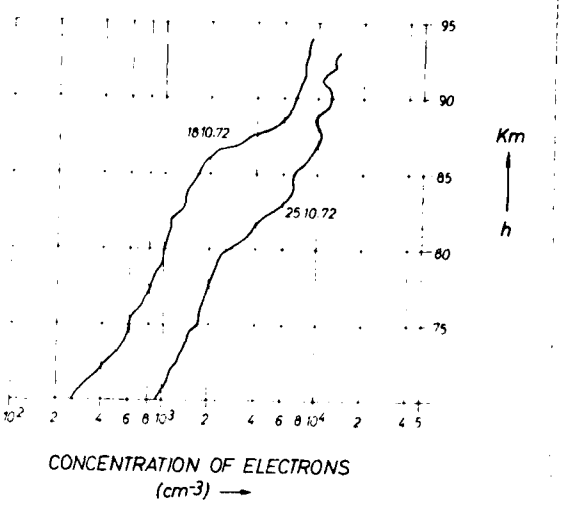

Fig. 52: Electron density profile during SID. This profile has some similarity to a winter-anomaly electron density profile.

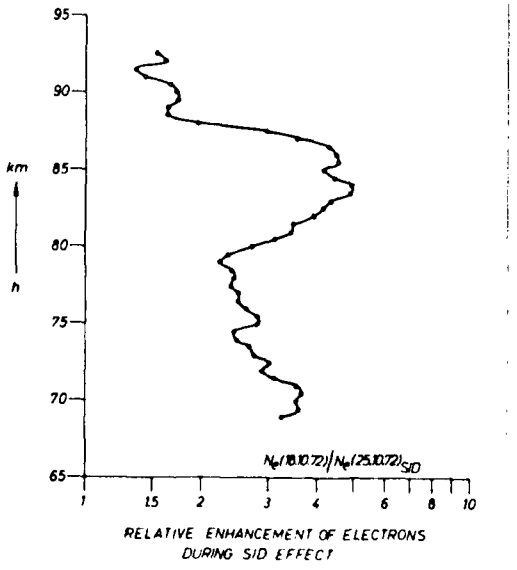

Fig. 53: Relative increase of electron density during SID. (Reference: "Normal day", 18.10.72.)

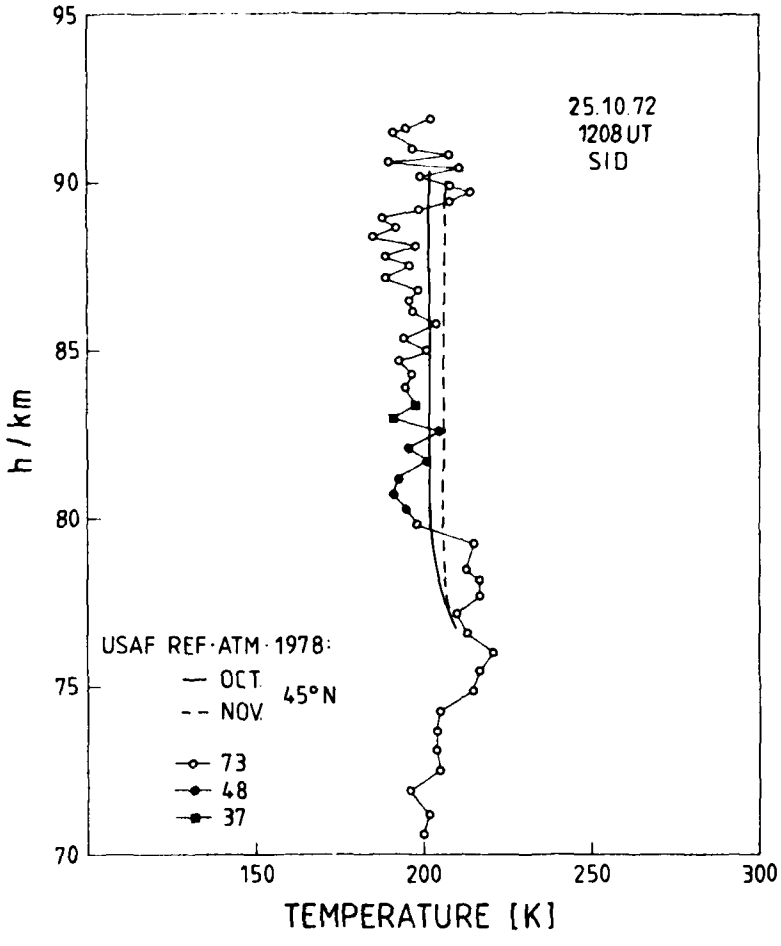

Fig. 54: Derived temperatures for 25.10.72

shown in Fig. 51. The rocket was launched into the last and smallest event of this day. This event was barely discernible in the ionogram records but was well recognized by the absorption measurement. A large increase of electron density was observed between 90 and 79 km. The ledge of electron density observed on a previous flight (18.10.72) has disappeared (Fig. 52). In so far the electron density profile resembled quite closely to a winter anomaly profile. The relative enhancement of electron density (reference: flight of 18.10.72) is shown in Fig. 53. It indicates that a "soft" and "hard" component of radiation was present. The "soft" component was absorbed between 80 and 90 km. The hard component caused an increase ionization below 80 km by up to a factor of 4 compared to the "normal" state (18.10.72).

Looking at the temperatures derived from the probe current ratio, one notes that there is no significant difference between the reference day (18.10.72) and the SID effect (Fig. 54). In fact, the temperatures derived for the 25.10.72 appear to be somewhat lower. Such a result can be expected because the additional energy input into the atmosphere during an SID lasts only for a short time and it is not expected that the neutral air temperature reacts immediately upon this energy input. On the other hand the accuracy of the method is too low to detect small increases of temperature which might accompany an SID effect. The result confirms the conclusion that the high temperatures found when the state of the atmosphere becomes winteranomalous must have another cause than a change of energy input by change of incoming radiation. A possible cause might be the change of abundance of a minor constituent which consists of more than three atoms in a molecule. Such molecules can store plenty of latent heat and by this, can prevent an increase of kinetic temperature which is the temperature which is measured. It was suggested that water vapour could be a candidate for this role, but similar properties have CO_2 and O_3. A change of abundance of such constituents would in all cases be a change of composition of minor constituents in favour of NO and excited states of oxygen.

REFERENCES

1 Widdel H.U.: High altitude atmosphere investigations Part I: Results of ground-based radio wave absorption measurements performed between 1968 and 1976 in South-West-Europe (Spain): Phenomenology Final Report DAERO 75-G-076

2 Sato T.: J. Geophys. Res., 85, 197, 1980.

3 Rose G., and H.U. Widdel: J. Geophys. Res., 44, (1977), 15.

4 Rose G., and H.U. Widdel: J. Geophys. Res., 44, (1977), No. 1/2

5 Rose G., and H.U. Widdel: Journ. Atm. Terr. Phys. 41, (1979)

6 George P.L.: Journ. Atm. Terr. Phys. 33, (1971), 1893

7 Rose G., and H.U. Widdel: Zeits. f. Geophys. 35, (1969), 211.

8 Rose G., H.U. Widdel, A. Azcarraga, L. Sanchez: Phil. Trans. Roy. Soc. Lond (A) 271, (1972), 509.

9 Rose G., H.U. Widdel, A. Azcarraga, L. Sanchez: Phil. Trans. Roy. Soc. Lond (A) 271, (1972), 529.

10 Widdel H.U.: Höhenforschungsraketenprogramm Aeronomie: Ein Experiment zur in-situ-Messung von Wind, Luftdichte und mittlerer Temperatur in Höhenbereich zwischen 96 und 80 km. Entwicklung und Ergebnisse. Final Report BMFT-FBW-W-78-23 (Nov. 1978) Bundesministerium für Forschung und Technologie.

11 Rees D., A.F.D. Scott, J.M. Cisneros, J.M. Satrustegui, H.U. Widdel and G. Rose: J. Atm. Terr. Phys. 41 (1979.

12 Sidi C.and H. Teitelbaum: COSPAR XX, (June 1977).

13 Teitelbaum H., and C. Sidi: J. Atmos. Terr. Phys. 38, ( ), 413.

14 Rose G., and H.U. Widdel: Zeits. f. Geophys. 35, (1969), 211.

15 Rose G., and H.U. Widdel: Planet. Space Sci. 20, (1972), 877.

16 Hoerner : Fluid dynamic drag, Hoerner Publ. P.O. Box 432, Brick Town, N.J. 0908723.

17 Rose G., and H.U. Widdel: Planet. Space Sci. 21, (1973), 1131.

18 Bernard R., M. Massebeuf, H.G. Müller, S.P. Kingsley, G. Rose, H.U. Widdel, H. Schwentek, M. Friedrich, K.N. Torker, J.M. Cisneros: COSPAR, Tel Aviv (1977).

19 Rose G., and H.U. Widdel: Zeits. f. Geophys. (1969).

20 Meek C.E. and A.H. Manson: Journ. Atm. Terr. Phys. 40, (1978), 1267.

21 Delabondiniere J.P., R.R. Donnely, H.E. Hinteregger, G. Schmidtke and P.C. Simon: Intercomparison/compilation of relevant solar flux data related to Aeronomy (Solar Cycle 20), COSPAR Technique manual Series, Manual No. 7, (Febr. 1978).

22 Sanchez Muniosguren, L.V.: Estructura de la alta Mesosfera, Publicacion A-68, Servicio Meteorologico Nacional, Madrid (1977).

23 Becker W.: Personal communication

24 Rose G., and H.U. Widdel: Kleinheubacher Berichte 16, (1971), 247.

25 Arnold F., D. Krankowsky, K.H. Marien, W. Joos: J. Geophys. Res., 44, (1977), 125.

26 Bangert W., and V. Amann: J. Gephys. 44, (1977), 165.

27 Beran D., and W. Bangert: J. Atm. Terr. Phys., 41, (1979), 1091.

28 Borchers R.: Ein Gerdienkondensator für Messungen am Fallschirm im Bereich der unteren D-Schicht, Diplom Thesis, University Göttingen (1968).

29 Borchers R.: BMFT Research Report BMBW FBW 71-39, (1971), Bundesminister für Bildung und Wissenschaft.

30 Borchers R., G. Rose, and H.U. Widdel: Kleinheubacher Berichte 14 (1970), 255.

31 Rose G., and H.U. Widdel: J. Geophys. Res., 44, (1977), 65.

32 Widdel H.U., G. Rose, and R. Borchers: Pageoph. 84, (1971), 154.

33 Widdel H.U., G. Rose and R. Borchers: J. Atm. Terr. Phys. 41, (1979).

34 Schutz S.R., and L.G. Smith: Journ. Atm. Terr. Phys. 37, (1975), 1615.

35 Phelps A.V., and J.L. Pack: Phys. Rev. Letters 3, (1959), 240.

36 Dieminger W., G. Rose, H.U. Widdel in: COSPAR Methods of measurements and results of lower ionosphere structure, ed. K. Rawer, Akademie-Verlag, Berlin, (1974).

37 Widdel H.U., G. Rose, K. Spenner, M. Friedrich, K.M. Torkar: J. Atm. Terr. Phys., 41, (1979), 1105.

38 Friedrich M., K.M. Torkar, K. Spenner, G. Rose, and H.U. Widdel: J. Atm. Terr. Phys. 41, (1979), 1121.

39 Narcisi R.S., A.D. Bailey, L.E. Wlodyka, C.R. Philbrick: J. Atm. Terr. Phys., 34, (1972), 647.

40 Widdel H.U., G. Rose, and R. Borchers: J. Geophys. Res., 81, (1976), 6217.

41 (see 22)

42 Cipriano J.P., L.G. Hale, H.D. Mitchell: J. Geophys. Res., 79, (1974), 2260.

43 Folkestad K.: Ionospheric Studies by in-situ-measurements in sounding rockets, NDRE Report No. 59, Norwegian Defence Research Establishment P.O. Box 25, N-2007 Kjeller, Norway.

44 Banks P,M., and G. Kockarts: Aeronomy Part A, Akademic Press, New York, (1973).

45 Loeb L.B., Basic processes of gaseous electronics, Univ. of California, Press, Berkely, 1961.

46 Cole A.E., and A.J. Kantor: Air Force Reference Atmospheres Report AFGL-TR-78-0051 Air Force Surveys in Geophys., No. 382, Air Force Geophysics Laboratory, Hanscom, AFB, Massachusetts 01731.

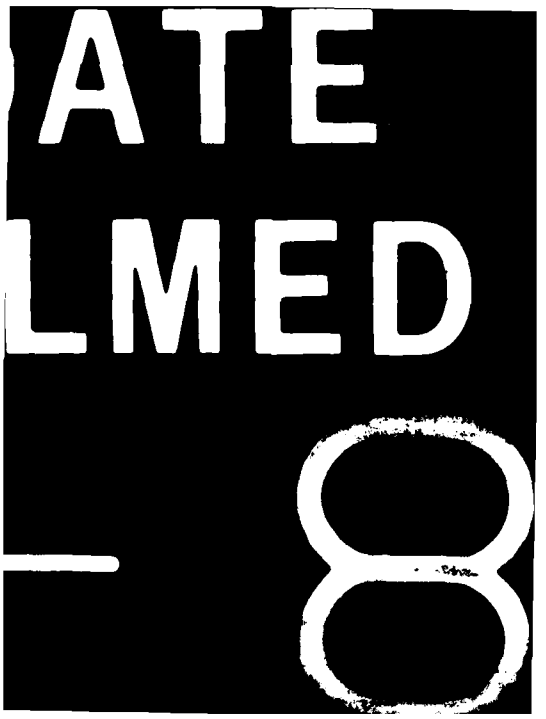
ATE
LMED
8